

THESIS

THE ROLE OF FERREDOXIN 3 IN HYDROGEN METABOLISM IN THE
HYPERTHERMOPHILIC ARCHAEON *THERMOCOCCUS KODAKARENSIS*

Submitted by

Meghan Stettler

Department of Biochemistry and Molecular Biology

In partial fulfillment of the requirements

For the Degree of Master of Science

Colorado State University

Summer 2022

Master's Committee:

Advisor: Thomas Santangelo

Jeffrey Hansen

Graham Peers

Copyright by Meghan Elizabeth Stettler 2022

All Rights Reserved

ABSTRACT

THE ROLE OF FERREDOXIN 3 IN HYDROGEN METABOLISM IN THE HYPERTHERMOPHILIC ARCHAEON *THERMOCOCCUS KODAKARENSIS*

Life faces innumerable challenges to cellular maintenance and reproduction, including access to sufficient energy. As such, all domains of life ubiquitously utilize energetically conservative mechanisms to maximize energy gains from the environment. Use of proteinaceous electron carriers, like ferredoxins, allows cells to harness energy from catabolic reactions that would otherwise be lost to the system as entropy or enthalpy. The hyperthermophilic, anaerobic archaeon *Thermococcus kodakarensis* is of particular interest as a target for bioengineering to maximize total energy gains, as it natively produces hydrogen gas resulting from terminal electron transport through a Membrane Bound Hydrogenase. *T. kodakarensis* encodes for three physiologically distinct ferredoxins. Prior to this thesis, only the sequence and molecular weight of the *T. kodakarensis* ferredoxins were known.

Efforts in this thesis laid the groundwork for the biophysical characterization of each ferredoxin isoform via protein-film voltammetry and x-ray crystallography by the development of a reliable recombinant expression and purification scheme. Preliminary biophysical assay trials resulted in a Ferredoxin 1 crystal capable of diffracting to 1.1 Ångstroms, and midpoint reduction potentials for Ferredoxin 1 and Ferredoxin 3 confirming the predicted redox center geometry, demonstrating the efficacy of the developed protein expression and purification scheme for producing high-quality samples. Further investigation into the activity of the ferredoxins resulted in the generation of *T. kodakarensis* strains encoding for a tether protein

between Ferredoxin 3 and its presumed sole electron acceptor Membrane Bound Hydrogenase at two respective locations. The parent strain includes a deletion of Ferredoxin 3, resulting in a deficient phenotype during sulfur-independent growth. The tethered strains of *T. kodakarensis* demonstrates a full recovery of sulfur-independent growth. Additionally, western-blotting revealed retention of the tethered protein *in-vivo*, and headspace measurements demonstrated restoration of hydrogen gas production compared to the parent deletion strain, and a reduction in total hydrogen gas output per cell compared to the lab parent strain.

These findings implicate the importance of Ferredoxin 3 in hydrogen metabolism in *T. kodakarensis* and indicate Ferredoxin 3 as a potential target for bioengineering. Furthermore, this thesis is the foundation for further characterization of the *T. kodakarensis* ferredoxins as proteinaceous electron carriers with potential applications outside of this model organism.

ACKNOWLEDGEMENTS

This was one of the last sections to be completed in this work; not because I felt as though I had no-one to thank but because I struggled to find language adequate to communicate the depth of my gratitude and appreciation for everyone who has helped me along the way. I don't think I will ever be able to truly do justice to how invaluable each of these people were to my time at CSU and my work on this project.

First and foremost, thank you to Tom Santangelo. When we first met in your office during my sophomore year, you told me to seriously consider the time, toil, and torture of lab work before I joined your lab as an undergraduate trainee. At the time, I thought I knew what you were talking about—what hubris naiveté brings. For the last four years you have been an exemplary mentor, patiently guiding me through my journey as a young scientist and young person, never hesitating to tell me when you thought I was making a mistake and always there to help pick me back up when I'd pushed too far. You were there for me at the lowest points of my personal and professional life, non-judgmental, generous, and understanding. Each challenge you put in front of me made me a better scientist and person, each push taught me a new lesson. You took a chance on me more than once, and for that I will always be grateful. I am honored to say that you were my mentor.

Next, Bree Wenck. I never thought one of my best friends in university would be old enough to be my parent, but here we are. You are so important to me and without our breakroom discussions or after work drinks, I don't think I would have kept my sanity. You took me into your family and were there when I needed help. Your experience working with *Thermococcus* and capability as a scientist are nearly unmatched. You are a lifelong friend.

Brett Burkhart: there's really no words for you. When you first started training me in the lab, we essentially communicated in a terse set of grunts. My debt to you in McChickens is almost certainly greater than the national debt. I would not be where I am today without you, and I can only hope to match the style with which you do your science.

As a self-proclaimed non-scientist, Atley Weems, you sure did manage to help me do a lot of science. You were the first person to see through my gruff exterior at age 14, and ever since all you have ever done is offer unconditional support. You are a well-needed respite, beloved confidante, fun as hell, and someone who will always have a place in my life no matter the distance. I hope I'm as cool as you when I grow up.

This leads me to Maia Zoller. In many ways, you are a surprise to me. Not that I am surprised to be appreciative you, but that I never thought that graduate school could be so fun. You are one of the most dedicated researchers I know, and every day you challenge me to be a better human. You bring so much joy into my life. Thank you for sharing this last year with me.

Finally, everyone in the Santangelo lab. If I were to individually name and thank each of you, this section would be longer than my actual research. As a group, you are the closest to a family I've come in a long time. Thank you so, so much for all your insights, complaints, arguments, compliments, and everything in-between. I wish the best for all of you.

TABLE OF CONTENTS

ABSTRACT.....	ii
ACKNOWLEDGEMENTS.....	iv
LIST OF TABLES.....	vii
LIST OF FIGURES.....	viii
INTRODUCTION.....	1
REFERENCES.....	24
CHAPTER 1: CLONING, EXPRESSION AND PURIFICATION OF THE THREE FERREDOXIN ISOFORMS IN <i>T. KODAKARENSIS</i>	30
RESULTS.....	32
DISCUSSION.....	40
MATERIALS AND METHODS.....	44
REFERENCES.....	52
CHAPTER 2: BIOPHYSICAL ANALYSIS OF THE <i>T. KODAKARENSIS</i> FERREDOXINS ..	53
RESULTS.....	55
DISCUSSION.....	61
MATERIALS AND METHODS.....	65
REFERENCES.....	77
CHAPTER 3: TETHERING OF FERREDOXIN 3 TO THE MEMBRANE BOUND HYDROGENASE IMPACTS HYDROGEN METABOLISM.....	80
RESULTS.....	85
DISCUSSION.....	104
MATERIALS AND METHODS.....	108
REFERENCES.....	122

LIST OF TABLES

1: Primers used for pQE-80L colony PCR	49
2: pQE-80L expression vectors	50
3: List of <i>E. coli</i> strains	50
4: pETSUMO expression vectors	72
5: List of primers used in pETSUMO vector construction	73
6: pQE-80L expression vectors	75
7: List of <i>E. coli</i> strains	75
8: List of <i>T. kodakarensis</i> strains	115
9: List of primers used in pTS700 vector construction	116
10: List of primers used in Tether I strain construction	118
11: List of primers used in Tether II strain construction	119

LIST OF FIGURES

1: Metabolism as a cellular process	2
2: Metabolism as a diverse process.....	3
3: Biological conservation of energy	6
4: Substrate-level phosphorylation.....	8
5: Electron-transfer mediated phosphorylation.....	11
6: Reduction potential as a measure of energetic differences.....	13
7: MBH and MBS as respiratory complexes.....	14
8: Electron carriers.....	16
9: Fd-type iron/sulfur clusters.....	17
10: Interactome of the <i>T. kodakarensis</i> Fds.....	20
11: <i>T. kodakarensis</i> encodes for three Fds.....	21
12: Expression of the <i>T. kodakarensis</i> Fds in BL-21 <i>E. coli</i> cells.....	33
13: Expression of the <i>T. kodakarensis</i> Fds in BI-21 Δ <i>iscR</i> <i>E. coli</i> cells.....	34
14: The purified <i>T. kodakarensis</i> Fds.....	35
15: Total iron content of purified <i>T. kodakarensis</i> Fds.....	36
16: Summary of prosthetic group coordination optimization.....	37
17: Summary of purification trials.....	38
18: Diagram of purification scheme.....	42
19: Cloning of the pETSUMO-Fd crystallography expression vectors.....	55
20: Expression of the pETSUMO-Fd crystallography expression vectors.....	56
21: 1.1 Angstrom structure of Fd1.....	57
22: Alphafold2 predicted models of Fd2 and Fd3.....	58
23: Midpoint reduction potentials of Fd1 and Fd3.....	59
24: Diagram of protein film voltammetry.....	63
25: Desired structure of Fd3:MBH tether proteins.....	82
26: Desired locus structure of Fd3:MBH tether proteins.....	83
27: Cloning diagram for Fd3:MBH vectors.....	85
28: Colony PCR for Fd3:MBH clones.....	87

29: Genome recombination for introduction of Fd3:MBH-J tether into <i>T. kodakarensis</i>	88
30: Intermediate PCR results for <i>T. kodakarensis</i> encoding Fd3:MBH-J tether.....	89
31: Final PCR results for <i>T. kodakarensis</i> encoding Fd3:MBH-J tether:.....	90
32: Whole genome sequencing confirming construction of Fd3:MBH-J <i>T. kodakarensis</i> strain ...	91
33: Genome recombination for introduction of Fd3:MBH-N tether into <i>T. kodakarensis</i>	93
34: Intermediate PCR results for <i>T. kodakarensis</i> encoding Fd3:MBH-N tether.....	94
35: Final PCR results for <i>T. kodakarensis</i> encoding Fd3:MBH-N tether:.....	95
36: Whole genome sequencing confirming construction of Fd3:MBH-N <i>T. kodakarensis</i> strain...	96
37: SDS-PAGE of Fd3:MBH tethers whole cell lysates for western blotting.....	98
38: Western blot of Fd3:MBH whole cell lysates.....	99
39: Growth characterization of the Fd3:MBH tethers.....	101
40: Total hydrogen output of the Fd3:MBH tethers.....	102

INTRODUCTION

Cells have tremendous energetic requirements--they are intrinsically complex thermodynamic and kinetic systems that demand substantial energy contributions to persist¹. The demand for continuous energy production poses the question: how do cells harvest the energy required for life? In short, this is done through metabolism, a process as diverse as life itself.

All domains of life follow the same general scheme for metabolism: uptake of high-energy substrates, stepwise cleavage of those substrates, and utilization of the products of that cleavage (in the form of ATP, an energetic currency; high-energy electrons, and small molecules) for biosynthesis (**Fig. 1**). Cellular metabolism is the delicate balance between energy investment in breaking covalent bonds, energy harvest from bond cleavage (catabolism), and energy utilization in making covalent bonds (anabolism). The cycle of breaking and making bonds in cells is electron flux: the energy of electron transfer is how the energy of biological reactions is quantified--first as reduction potentials and finally as free energy (ΔG). These yields are not always reciprocal: Single-step reactions can have substantial energy investment compared to energy yields, or multi-step reactions can be bottlenecked by one or more high-investment steps (**Fig. 2**). In all cases, this scheme is based on the thermodynamic and oxidative/reductive (redox) limits of cells, as well as the redox limits of their terminal electron acceptors². Aerobic metabolism and respiration benefits from generous overall differences in midpoint reduction potential between substrate and terminal electron acceptor³, leading to some of the greatest energetic gains—demonstrated most clearly in eukaryotes—where per unit glucose, complete catabolism through the electron transport chain to proton gradient-mediated phosphorylation generates ~36-38 ATP equivalents⁴.

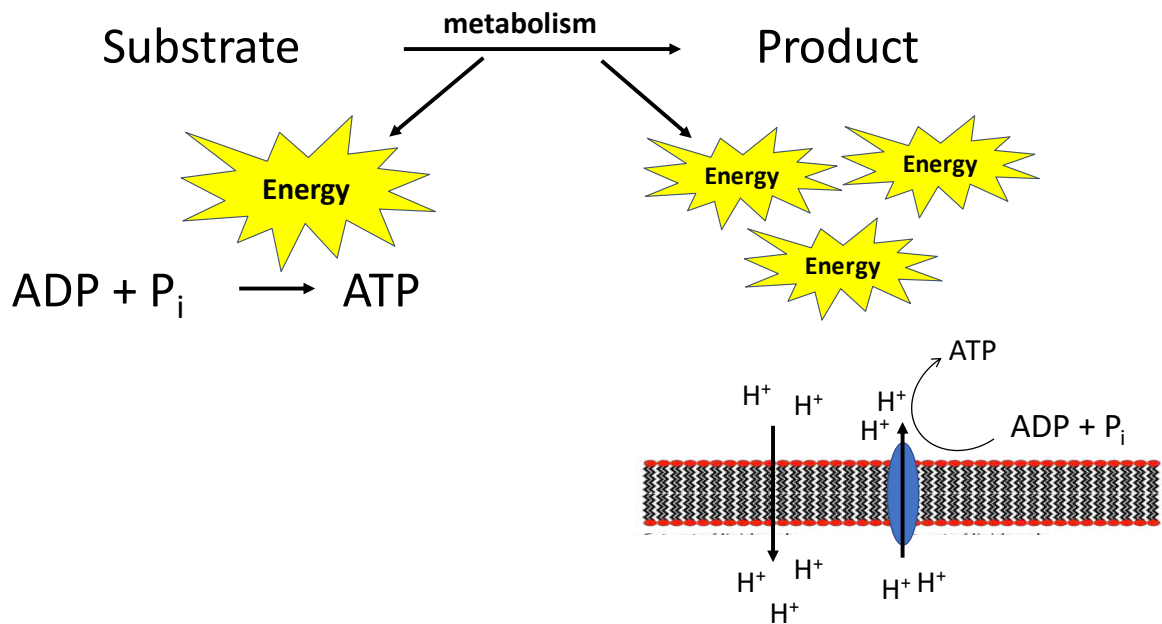


Figure 1

Metabolism is the cellular process of harvesting energy from the breakdown of substrates into products. Sometimes this breakdown yields enough energy to facilitate the direct phosphorylation of ADP to ATP. More often, the energy from individual breakdown reactions is banked as cross-membrane ion gradients that can build up to powering the conversion of ADP to ATP.

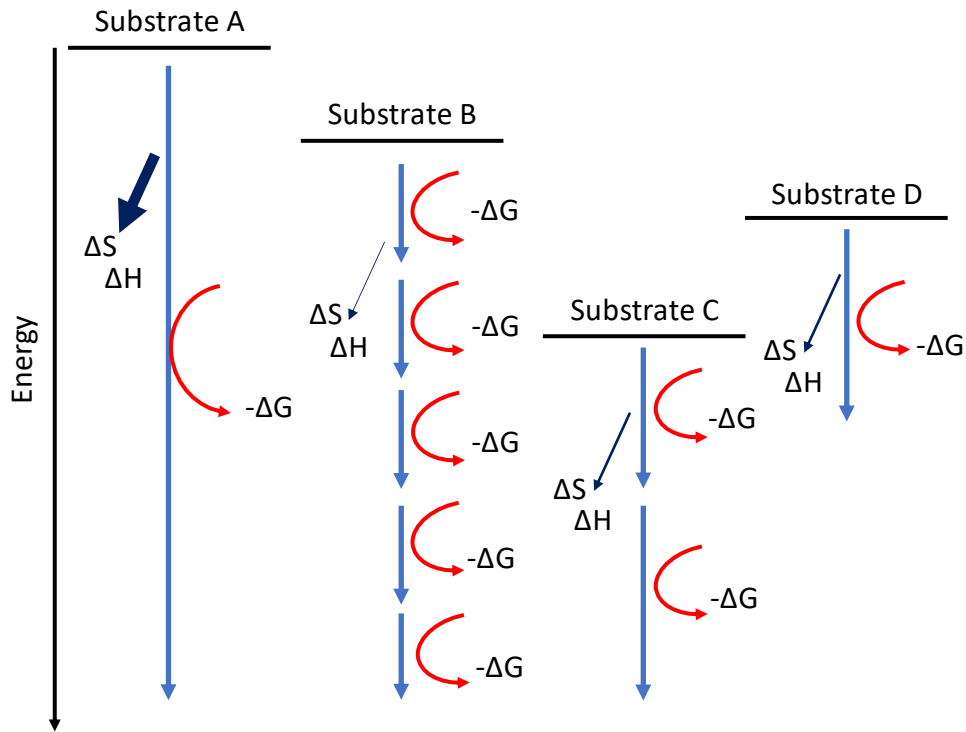


Figure 2

Substrates can differ in starting energy, overall reaction efficiency, and final product energy. Substrate A is cleaved in a single-step reaction with substantial energy investment (ΔH , ΔS) and some energy yield ($-\Delta G$). Substrate B is cleaved in a multi-step reaction, with minimal energy investment and substantial energy yields from each intermediate step. Substrate C is cleaved in a two-step reaction with moderate energy investment and moderate energy yield from each intermediate step. Substrate D is cleaved in a single-step reactions with moderate investment and yield.

In contrast, energetic gains from anaerobic respiration are severely limited by the redox capabilities of non-oxygen terminal electron acceptors (the difference in energy gained from reducing protons compared to reducing O₂ is approximately 5-fold less)⁵. Anaerobic extremophiles are further limited, having restricted access to high-energy substrates, and undergoing extreme thermodynamic and kinetic stressors⁶.

Nonetheless, life continues to proliferate in challenging conditions. Metabolic strategies (trophism) are grouped by an organism's access to substrates and the mechanisms by which the organism garners energy from those substrates. Common in caves, chemolithoautotrophs (literally "stone-eaters") demonstrate the simplicity of metabolism⁷. These organisms garner high-energy electrons from the oxidation inorganic (carbon-lacking) compounds such as hydrogen or elemental sulfur and use carbon dioxide as a carbon source. Together, these two components are broken down in catabolic reactions and their integral parts are utilized in anabolic reactions producing organic (carbon-containing) compounds necessary for life. In effect: metabolism is the shuttling of high energy electrons and carbon from source compounds for use in biologically useful reactions (biosynthesis)⁸. This organization of metabolism as flow from energy investment to energy utilization presents conflicting needs within the cell: energy is required to cleave compounds, yielding high-energy electrons; the energy for cleavage comes from the high-energy electrons associated with cleavage; the energy from cleavage must also be used to generate useful cellular products. This delicate balance between energy investment and energy expenditure demands cells develop conservative mechanisms for metabolism⁹.

Biological conservation of energy

Viewing life through the lens of metabolism paints a picture of the cell as a chaotic environment, locked in a Sisyphean struggle against the demands of external damage, cellular replication, and cellular growth. Regardless of the efficiency of terminal electron transfer, cells must optimize metabolic gains to best match the demands of sustaining life¹⁰. Biological conservation of energy describes the capability of a mechanism to harness the energy of catabolism into an energy currency for use elsewhere in the system. Biological conservation of energy is found in all domains, taking on three general forms¹¹: (1) substrate-level phosphorylation, (2) electron-bifurcation, a likely-ancient, but only recently described mechanism of energy conservation and (3) electron transfer-mediated phosphorylation¹². In all cases, these conservative mechanisms allow cells to store the energy associated with low-yield catabolic reactions until the stored energy is great enough to facilitate cellular work (**Fig. 3**).

Substrate-Level Phosphorylation

Substrate-level phosphorylation (SLP) is restricted to seven known biological reactions¹³. The energy required to directly phosphorylate ADP to ATP ($\Delta G^\circ = +31.8 \text{ kJ/mol}$)¹³ is great enough that most catabolic reactions do not meet this threshold, nor are most enzymes efficient enough to couple catabolism to phosphorylation without significant losses to enthalpy and entropy¹. When energetic releases are insufficient to directly permit SLP, conservation of energy is relegated to the two, electron transfer-mediated conservative mechanisms. Of the seven SLP reactions, two occur in glycolysis. Aerobic oxidation of glucose to CO_2 and H_2O is ($\Delta G^\circ = -2,870 \text{ kJ/mol glucose}$) but to do so in a single step would result in substantial energy losses.

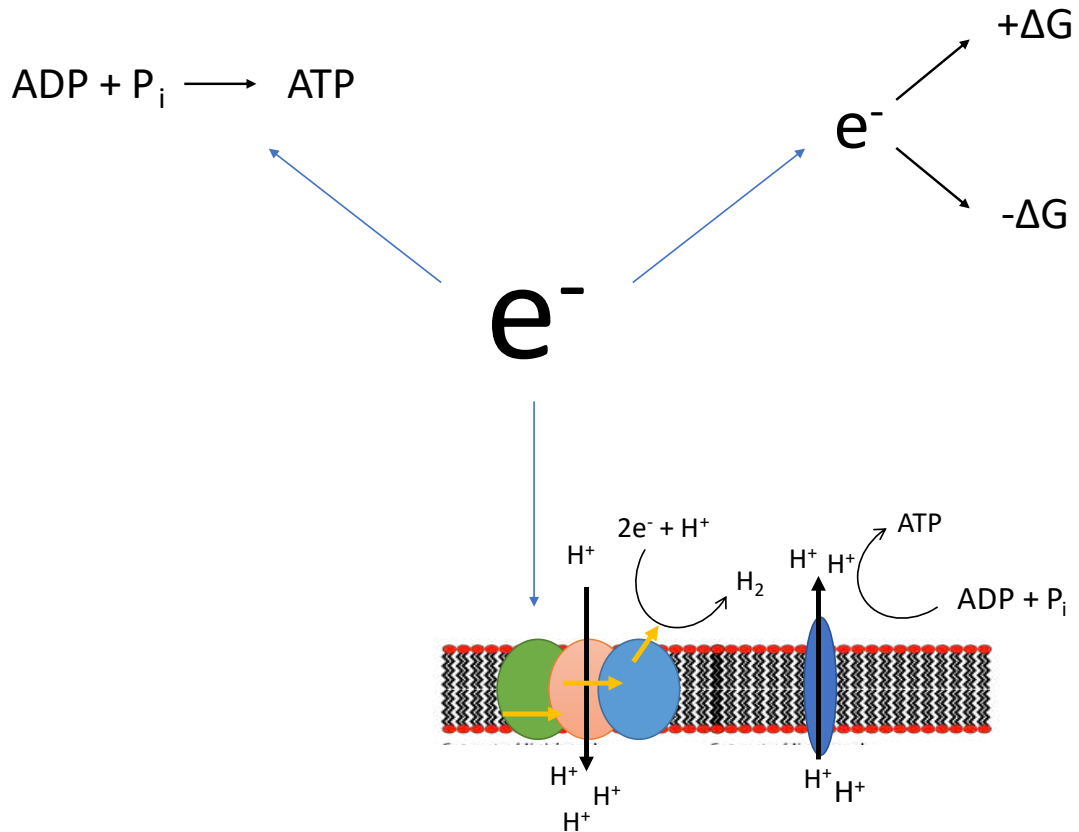


Figure 3

There are three forms of biological conservation of energy: Substrate level phosphorylation (upper right), electron bifurcation (upper right), and electron transfer-mediate phosphorylation (lower center). Substrate-level phosphorylation is restricted to seven high-energy biological reactions. Electron bifurcation and electron-mediated phosphorylation are involved in lower energy reactions. Both mechanisms utilize the energy of electron transfer to facilitate otherwise energetically impossible reactions.

Famously, glycolysis generates enough energy to produce four ATP but requires two ATP invested, yielding two ATP overall¹⁰. This is accomplished by pairing exergonic hydrolytic reactions with endergonic phosphorylation reactions, allowing for the stepwise garnering of energy from catabolism. Hydrolysis of glyceraldehyde-3-phosphate (G3P) by phosphoglycerate kinase yields ($\Delta G^\circ = -51.6\text{kJ/mol}$)¹³, which is sufficiently great to phosphorylate ADP to ATP. Similarly, hydrolysis of phosphoenolpyruvate by pyruvate kinase is exergonic enough to power ADP phosphorylation¹¹. In both cases, these substrates are uniquely high-energy and uncoupling hydrolysis from SLP would substantially decrease net energy from hydrolysis. The energy of electron transfer between substrates and products would be lost to the system. This would have drastic repercussions, especially in fermentative systems where most energy comes from anaerobic glycolysis¹⁴.

Albeit rare, SLP is a conservative pathway for high-energy reactions that would otherwise be paired to conservative mechanisms that are unfit for large energy changes. The majority of SLP reactions occur during fermentation where the terminal electron acceptor is not O₂. Anaerobic conditions strongly restrict the total energy that can be reclaimed from high energy catabolic reactions like those of glycolysis¹. Total energy gain from directing electrons from the cleavage of G3P to the generation of a cross-membrane ion gradient or coupling G3P oxidation to the reduction of an electron carrier would be substantially less than SLP, largely due to the fundamental energetic difference between hydrolysis and redox reactions¹⁵. Furthermore, banking what little energy is gained from a redox-coupled mechanism in a cross-membrane ion gradient would still be substantially less than SLP based on the relative energy of non-O₂ terminal electron acceptors¹⁴ (**Fig. 4**).

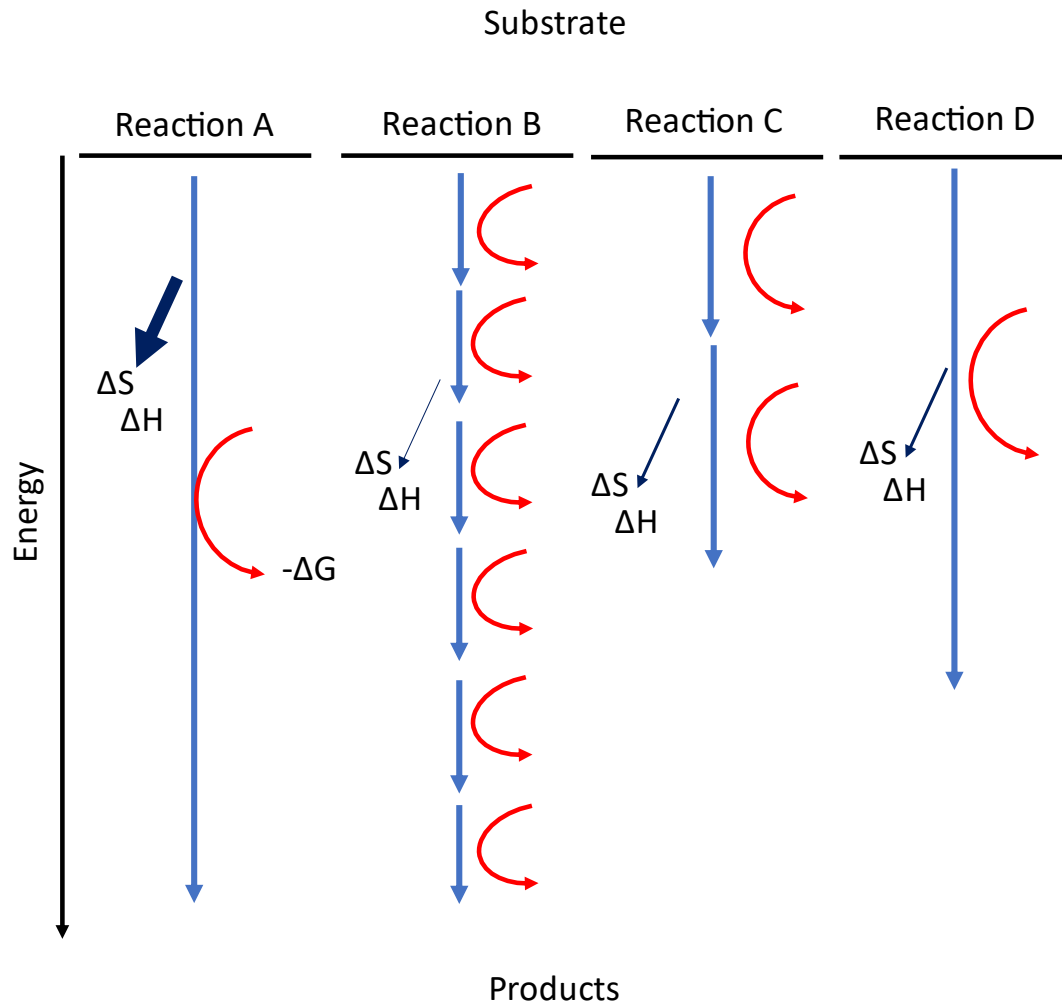


Figure 4

Cells can break down a substrate using a variety of pathways, each having its own investment, yield, and losses. SLP requires substantial investment but allows for significant yields over losses in few steps when compared to multi-step electron transfer-mediated mechanisms. Pictured is an energy map for the hypothetical catabolic pathways a substrate could undergo with the associated yield (ΔG) and losses (ΔS , ΔH).

The remaining mechanisms of biological conservation of energy both rely on electron transfer in redox reactions as a primary means of energy conservation. These mechanisms can be viewed as functioning in-tandem, where the reducing equivalents produced via bifurcation pass electrons through electron transport-mediated phosphorylation furthering energy gains, though both can occur independently ¹¹.

Electron bifurcation

Electron bifurcation is a newly understood mechanism of energy conservation: two high-energy electrons are donated to a bifurcating complex, where one electron is directed to an exergonic (energy gained) redox reaction, while the other electron is directed to an endergonic reaction (energy given)¹⁶. These reactions are coupled, allowing for cells to perform challenging redox reactions that would otherwise be impossible. Bifurcating electrons enables cells to increase metabolic efficiency without compromising the overall redox balance of the cell^{11,17}. Bifurcation is facilitated by soluble complexes coordinating flavins capable of transitioning between quinone, meta-quinone, and semi-quinone states allowing for the drastic changes in reduction potential required for transition between the exergonic and endergonic reactions¹⁶.

Flavin-based electron bifurcation is common in prokaryotes, particularly anaerobes^{1,14} where exergonic reduction of $\text{NAD}^+/\text{NADP}^+$ is coupled with endergonic reduction of a ferredoxin (Fd)³ which can then either participate in the generation of an electron transfer-mediated chemiosmotic gradient or be exergonically oxidized in anabolism¹⁸. Effectively, bifurcation passes electrons to strongly reductive electron carriers like Fds, enabling cells to increase net energy by extending electron flux beyond catabolism¹⁷. In the absence of electron

bifurcation, the remaining low-energy reducing equivalents are shunted into anabolism of low-energy, low-value cellular products.

Electron Transfer-Mediated Phosphorylation

Electron transfer-mediated phosphorylation (EMP) is similar to electron bifurcation in the sense that both utilize reducing equivalents produced during catabolism^{10,13,16,17}. While bifurcation relies on the passage of an electron down an energy gradient to facilitate the passage of a partner electron up an energy gradient, EMP relies on the passage of electrons down an energy gradient to facilitate the passage of a partner ion up a chemiosmotic gradient¹⁹. This is a phenomenon well documented in all domains, typically represented by the eukaryotic mitochondrial respiratory complexes but is utilized by eukaryotes, prokaryotes, aerobes and anaerobes alike.^{10,12,13,16}

In its simplest form, EMP is facilitated by an electron carrier shuttling electrons to a membrane-bound complex which, via a series of electron transfer reactions, generates a chemiosmotic ion gradient (**Fig. 5**). This ion gradient is then used to generate ATP from ADP and P_i by a membrane-bound ATP synthase. The electrons used for ion transfer are passaged to a terminal electron acceptor^{12,17}. This metabolic strategy sets a distinct advantage: complete aerobic catabolism of glucose to CO₂ and H₂O via EMP nets sufficient energy to generate 36-38 ATP equivalents. In contrast, anaerobic catabolism of glucose via lactic acid fermentation can at most produce 2 ATP equivalents.

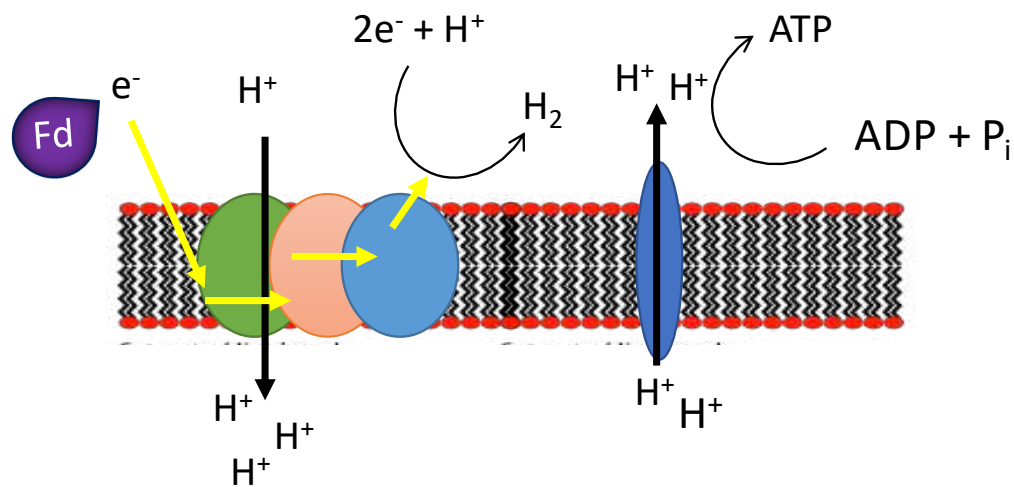


Figure 5

The general scheme of electron transfer-mediated phosphorylation involves an electron carrier donating electrons (shown as Fd) to a membrane-bound complex that utilizes the energy of electron transfer to generate a chemiosmotic gradient (in this case, H^+). The membrane-bound complex then passes the electrons to a terminal electron acceptor (also H^+). The transported ions will pass back down the chemiosmotic gradient via a nearby ATPase which will phosphorylate ADP to ATP.

The two limiting parameters of EMP are the reduction potential of the electron carrier and the reduction potential of the terminal electron acceptor¹³. The greater the difference in reduction potentials, the greater the total energy gain from EMP in the form of the chemiosmotic gradient⁵ (**Fig. 6**). Given its strongly positive reduction potential, O₂ is an ideal terminal electron acceptor, which is shown by the tremendous energy yields associated with aerobic EMP. This is the most familiar structure for eukaryotic metabolism: in aerobic, mesophilic conditions NAD(P)H is a versatile electron carrier and the difference in reduction potential between NAD(P)H and O₂ is generous^{3,5}. However, EMP is a conservative mechanism with origins predating aerobic metabolism, from an era of temperature, osmotic, and pH extremes^{1,3,20,22}.

Two modern EMP systems likely share mechanisms with ancient EMP complexes^{22,23}: the Membrane Bound Hydrogenase (MBH) uses electron transfer to facilitate initial export of protons that are exchanged for Na⁺ via a H⁺/Na⁺ antiporter; terminal passage of electrons to H⁺ generates H₂ gas. The Membrane Bound Sulfur reductase (MBS) uses electron transfer to generate a similar ion gradient and terminally passes electrons to elemental sulfur (S⁰) to produce hydrogen sulfide (H₂S) gas. Both MBH and MBS complexes are functionally and structurally considered progenitors to the Eukaryotic Complex I^{24,25}. Furthermore, these complexes are conserved throughout organisms today and the variety in anaerobic EMP-facilitating respiratory complexes is endless^{12,16,18,19} (**Fig. 7**).

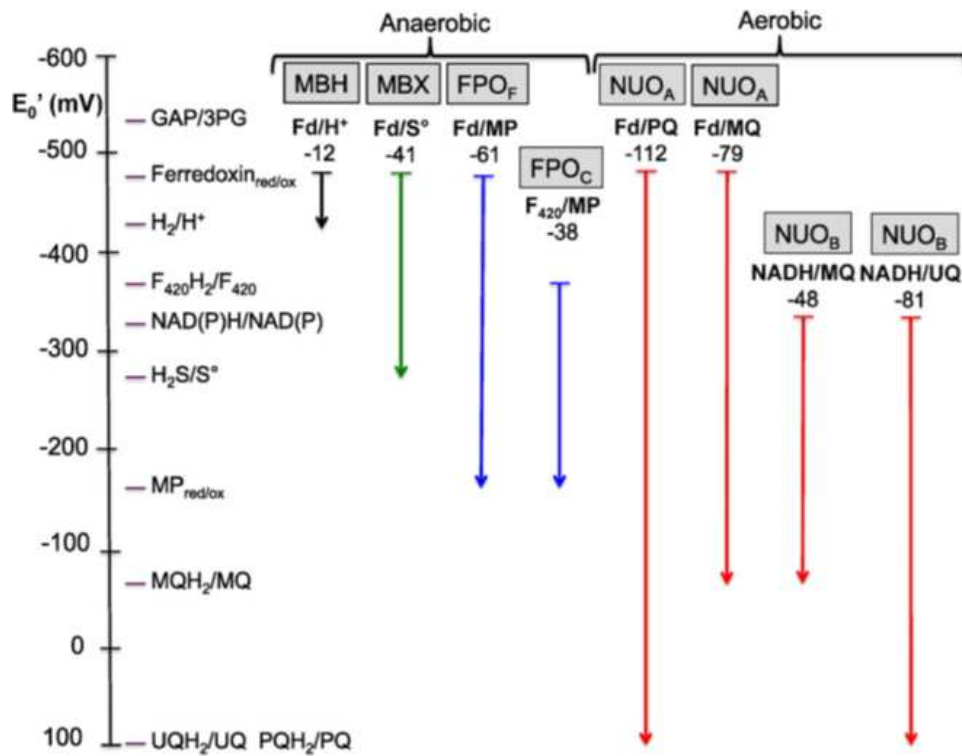


Figure 6

Adapted from Schut et al, 2016³

The energy garnered from metabolism differs based on the reduction potential of the starting substrate and terminal electron acceptor. *T. kodakarensis* is restricted to lower-energy transfer, using H^+ or S° as terminal electron acceptors, compared to aerobes (diagram shows transfer to intermediate quinones; not pictured is reduction potential of O_2).

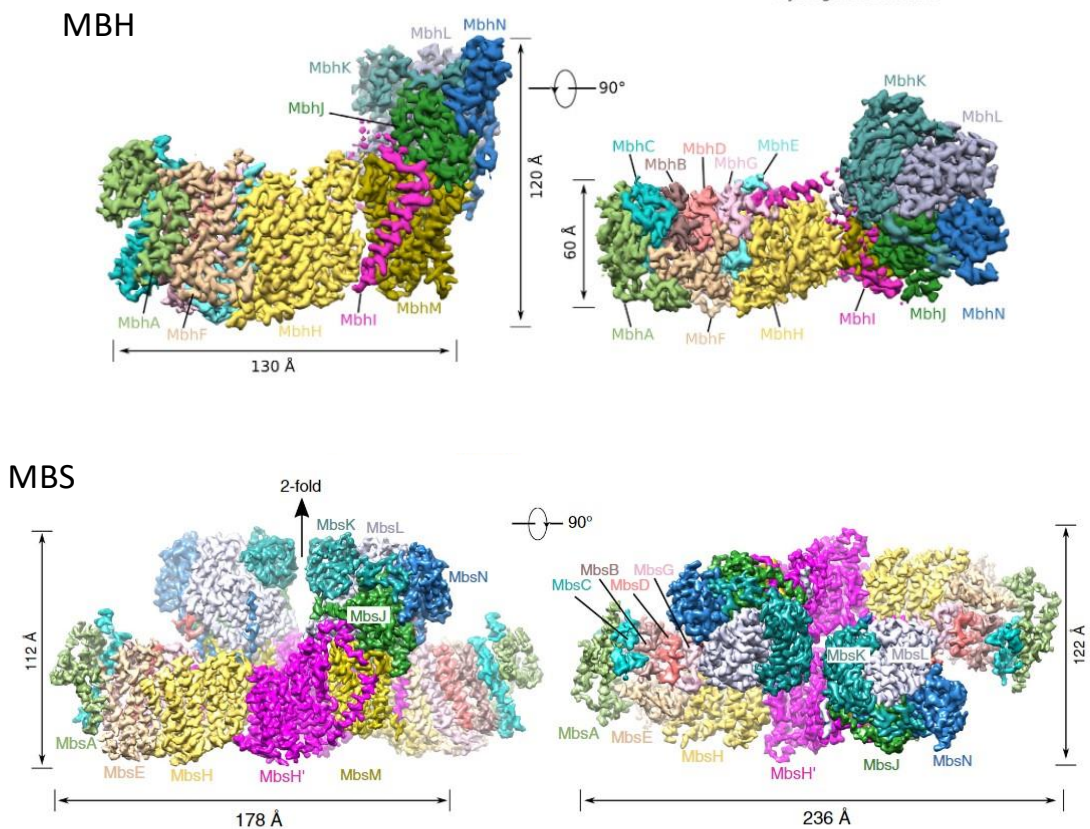


Figure 7

Adapted from Yu et al., 2018²² (MBH) and Yu et al., 2020²³ (MBS)

*MBH and MBS from *P. furiosus*. MBH is a monomeric, 14-subunit membrane-bound complex that uses H^+ as a terminal electron acceptor. MBS is a dimeric, 9-subunit membrane-bound complex that uses S^0 as a terminal electron acceptor. Both complexes are modern examples of ancient EMP complexes.*

EMP is an essential mechanism to efficient energy yield in all thermodynamic conditions, it is the cellular embodiment of “baby-stepping” energy gains. Many extremophiles and anaerobes proliferate under conventionally challenging conditions, notwithstanding the redox deficit caused by the inability to use O₂ as a terminal electron acceptor^{12,24}. Glucose is a model high-energy substrate but cannot be accessed or directly absorbed by many organisms^{10,26–28}. Starting with low-energy substrates and ending with low-energy terminal electron acceptors demands maximal efficiency in energy yield from each electron transfer—necessitating EMP.

Ferredoxins as electron carriers

In terms of reduction potentials, H⁺ and S[°] are less ideal terminal electron acceptors than O₂^{3,5}, and would be minimally effective or completely useless if paired only with NAD(P)H. In this case, maximal energy yield lies in the pairing of less-than-ideal terminal electron acceptors with strongly reducing electron carriers, usually in the form of proteinaceous electron carriers⁵. Thus far in this discussion, “energy” is an abstract force associated with cleavage of substrates. The energy of metabolism comes from the relative energies of electron transfer. Most transfer is facilitated by small molecules such as NAD(P)H or FADH₂, which are indiscriminate in their shuttling activity and have fixed reduction potentials (**Fig. 8**). However, electron transfer can also be mediated by proteinaceous electron carriers^{1,29,30}. Proteinaceous electron carriers are not fixed in their reduction potentials⁵, and can be physiologically distinct in their shuttling activities³¹. Ferredoxins (Fds), a dominant clade amongst proteinaceous electron carriers, are encoded by all domains of life and are characterized by coordinated iron-sulfur (Fe-S) centers used in electron transfer (**Fig. 9**).

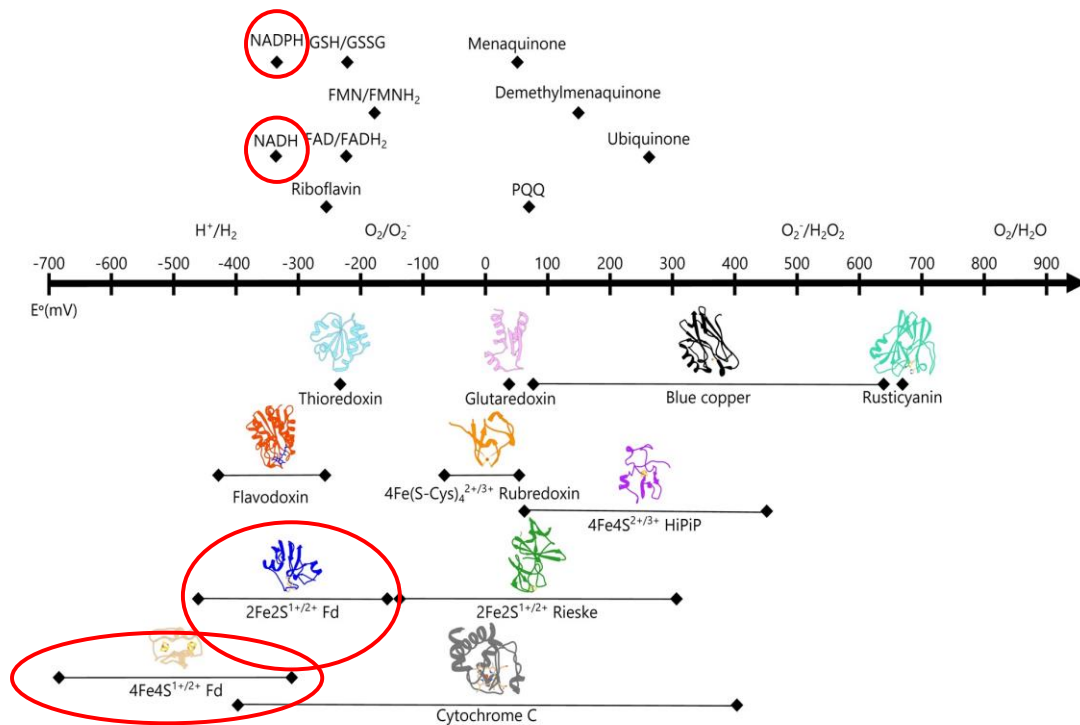


Figure 8

Adapted from Atkinson et al., 2016⁵

Small-molecule electron carriers (NAD(P)H highlighted in red) are limited by fixed midpoint reduction potentials and overall chemical stability. Proteinaceous electron carriers benefit from a range of midpoint reduction potentials, conferred by a variety of protein structures and coordinated redox centers. Ferredoxins (highlighted in red, lower panel) are the dominant clade among proteinaceous electron carriers.

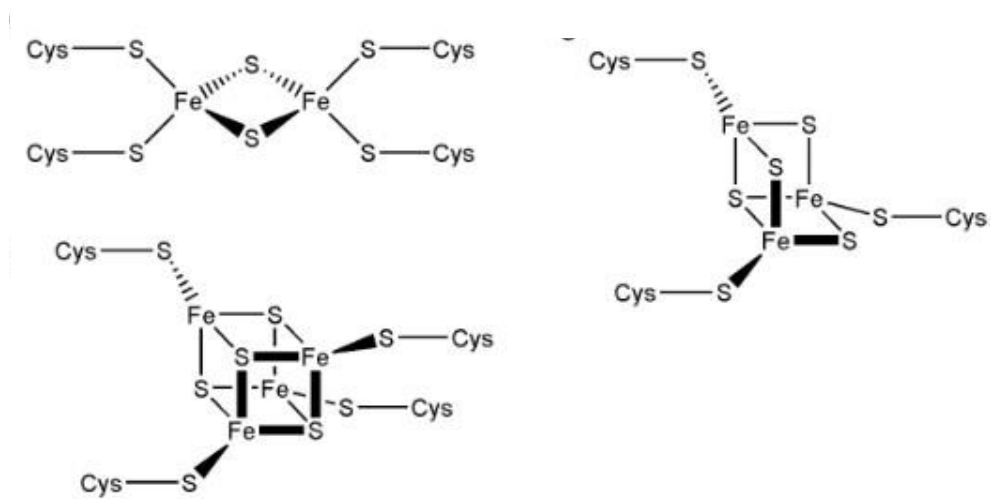


Figure 9

Adapted from Hwang and Han, 2015³¹

Fds are characterized by their coordination of Fe/S clusters: 2Fe-2S, 4Fe-4S, 3Fe-4S, typically coordinated via a conserved (CxxC)₂ motif. Fds are found in all domains of life, and can coordinate multiple, different Fe/S centers.

Fds support myriad functions in all domains of life, spanning from electron transfer to oxygen-sensitive redox switching^{33,34}. Fds were first characterized in *Clostridium*^{35,36} as Fe- and S-containing proteins that acted as redox factors for central metabolism. The 4Fe-4S center geometry was the first to be described³⁷, upending contemporary theories about the arrangement of inorganic redox centers³⁸. The chemistry of Fe-S centers indicates ancient origins for Fds^{39,40}, whose involvement in primitive metabolism has been long-theorized⁴¹. Overwhelmingly, Fds participate in pathways with ties to ancient respiration and metabolism^{1,42}.

The primary body of work describing Fds is in plants, where Fds play an active role in facilitating electron transport during photosynthesis^{43,44} along with a variety of other redox-based functions⁴⁵⁻⁴⁷. Plant-type Fds and microbial Fds are semi-distinct from one another, with plant-type Fds primarily coordinating 2Fe-2S centers⁴⁸ while microbial Fds can coordinate all observed geometries of Fe-S centers³⁴. In both cases, these proteins are soluble, redox-capable enzymes. However, little work exists describing individual Fd isoforms beyond their Fe-S center geometry and reduction potential. Greater investigation of the role of Fds in cellular metabolism was yet unexplored until recent work in *T. kodakarensis*.

Ferredoxins in T. kodakarensis:

The metabolic landscape of *Thermococcus kodakarensis* can be described in terms of the presence or absence of elemental sulfur (S°). When S° is available in the environment ($+S^{\circ}$), *T. kodakarensis* will use S° as a terminal electron acceptor via MBS, reducing S° to H_2S . In the absence of S° ($-S^{\circ}$), *T. kodakarensis* will use protons (H^+) as the terminal electron acceptor via MBH, reducing H^+ to H_2 gas⁴⁹. The extremophilic, anaerobic archaeon *T. kodakarensis* encodes three ferredoxin isoforms. Ferredoxin 1 (Fd1) is an essential protein and shuttles electrons from

catabolism to two, cytosolic Fd:NAD(P)H oxido-reductases; Ferredoxin 2 (Fd2) is essential and shuttles electrons to a membrane-associated geranyl-geranyl transferase (GGR) used in the maturation of membrane isoprenoids; Ferredoxin 3 (Fd3) is essential only in S^o-dependent conditions, and shuttles electrons to the Membrane Bound Hydrogenase (MBH) to facilitate the generation of a chemiosmotic gradient via electron transfer³² (**Fig. 10**). Each Fd is different in size and predicted to have distinct structures and surface charges (**Fig. 11**). These characteristics lead to the distinct protein-protein interactions and activities *in-vivo*. Current understanding of *in-vivo* interactions and predictive structures of the Fds allows for predictions of their midpoint reduction potentials, which will be distinct and specific to each Fd.

Hydrogen biosynthesis is a well-characterized pathway in *T. kodakarensis*, comprised of two main interacting partners: Fd3 and MBH. MBH is a 14-subunit membrane-bound protein complex, similar to Complex I of the mitochondrial electron transport chain^{22,30}. MBH is the site of terminal electron transfer, reducing soluble protons to H₂ gas. Fd3, as described above, is a small proteinaceous electron carrier. While the roles of these two proteins in biosynthesis is clear, it is unknown which partner limits the production of H₂ gas in this reaction. MBH and Fd3 are expressed at different levels in the cell, though both are dependent on S^o-dependent conditions for high levels of expression³². Previous studies revealed that overexpression of MBH led to a proportionate increase in H₂ production per unit substrate⁵⁰, the same experiment has not been completed for Fd3.

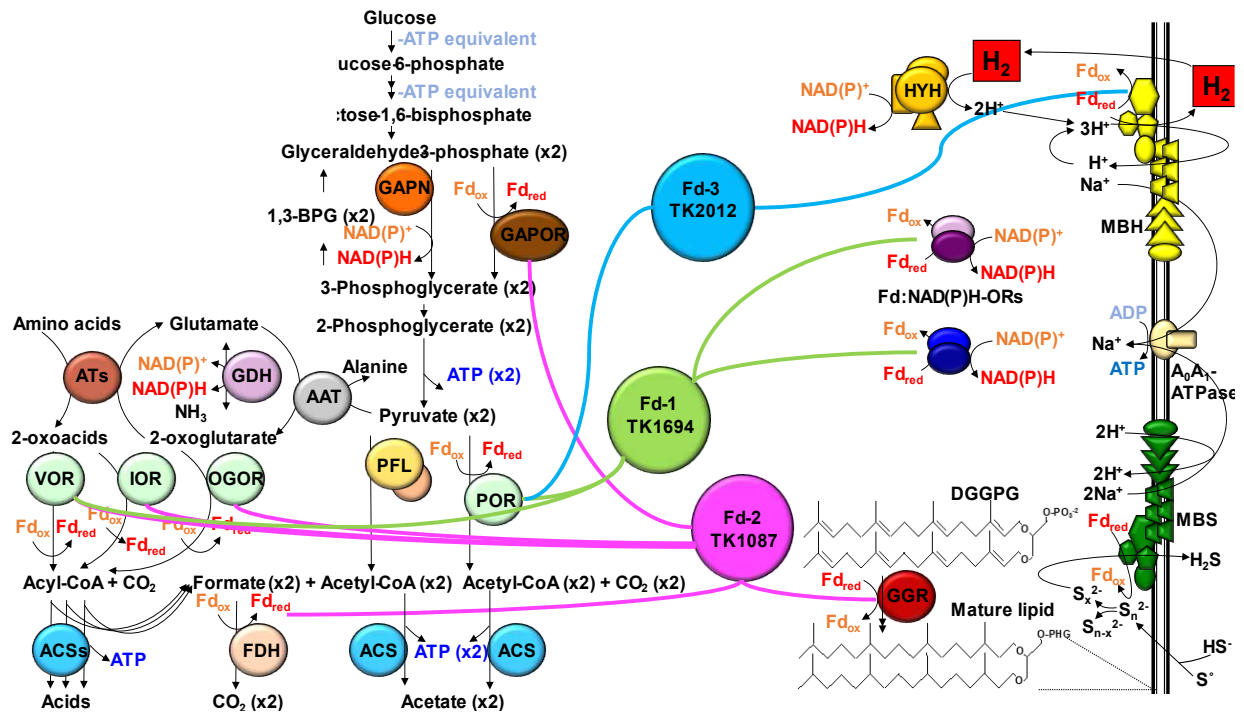


Figure 10

Adapted from Burkhart et. al, 2019³²

T. kodakarensis encodes for three, physiologically distinct Fds. The left side of this figure depicts catabolism, the right side depicts anabolism. In the center are the three *T. kodakarensis* Fds: Fd1 (green) shuttles electrons to two Fd:NAD(P)H oxidoreductases; Fd2 (pink) shuttles electrons to a geranyl-geranyl transferase (GGR); Fd3 (blue) transfers electrons to MBH.

A

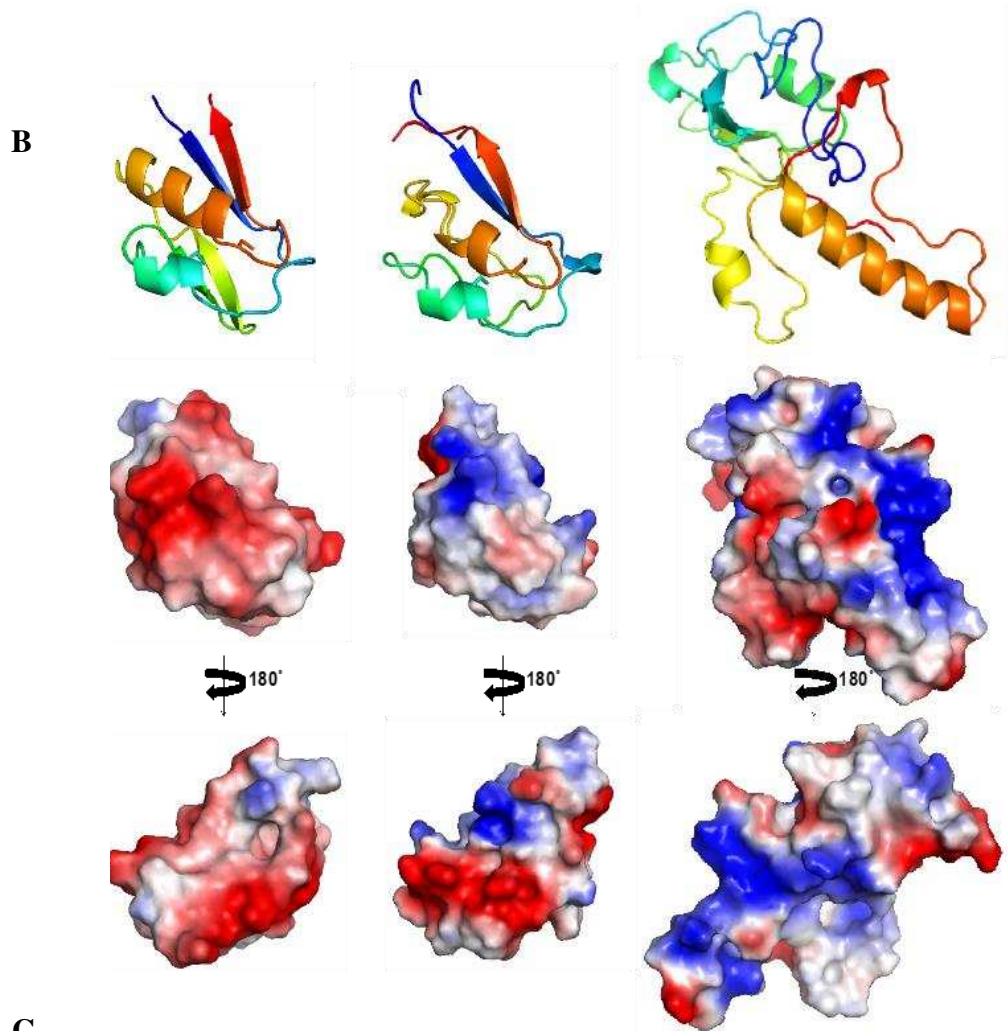
```

Fd-1 TK1694 -----MANKVSVVDVTCIGDAICASLCPD-VF 26
Fd-2 TK1087 -----MPEKIKVVVNEEDRCYLCGGCAGVCP--TL 27
Fd-3 TK2012 MADVKAPVIGRDALGREVKDLSVIPWWGVDRKEIEWYPKINYSVCARCGLCFITCGRRVF 60
                :: . * . * * . :

Fd-1 TK1694 EMGDDGKAHPVVETTD---LDCAQEAAEACVPGAITLEEA----- 63
Fd-2 TK1087 AIEVHSTGWFLQDKC---ISCR-ICINACVPGALSAPLEVSE----- 67
Fd-3 TK2012 DWDTE-EGKPVVARPYNCMVGCN-TCAILCPCNAIEFPPKEYVKKLVIEHGIIIRKAFEIT 118
                . . . : :.* . ** .*:

Fd-1 TK1694 -----
Fd-2 TK1087 -----
Fd-3 TK2012 KPLTKKKEESTNGAESVFN 138

```



C

Gene	Protein	Mass (da)	Essential	pl	Genome organization
TK1694	Fd-1	6528	Yes	3.7	Monocistronic
TK1087	Fd-2	7199	Yes	5.1	Co-transcribed with SurR (TK1086) and GGR (TK1088)
TK2012	Fd-3	15611	No	8.4	Monocistronic

Figure 11

Adapted from Burkhart et. al, 2019³²

The T. kodakarensis Fds are unique in their sequences (A), sizes and predicted structures (B). Fd1 and Fd2 are essential in all metabolic conditions, Fd3 is essential only in S-independent metabolism (C).

My thesis investigates the role of Fd3 in hydrogen metabolism in *T. kodakarensis*. Fd3 (TK2012) is essential in S⁰-independent conditions and the presumed exclusive shuttling of electrons to MBH³² therefore participating in the sole H₂ biosynthesis pathway in *T. kodakarensis*²⁷. The S⁰-independent phenotype of a Δ TK2012 *T. kodakarensis* strain as well as the limited interactome of Fd3 makes it an ideal candidate for investigation of hydrogen metabolism in *T. kodakarensis*.

My thesis addresses the following specific aims:

- What is the atomic structure and midpoint reduction potential of Fd3?
- Can Fd3 be sequestered to its apparent exclusive electron acceptor, MBH, and restore growth in S⁰-independent conditions?
- Are there additional effects to hydrogen metabolism by tethering Fd3 to MBH?

My work seeks to establish the atomic structure and midpoint reduction potential of Fd3 and describe the effects of Fd3 tethering to MBH in terms of cell viability and hydrogen metabolism. Through my study of Fd3, I also worked to characterize the structures and midpoint reduction potentials of Fd1 and Fd2. I was able to prepare high-quality Fd samples in large quantities for biophysical analyses, generate two Fd3:MBH tethers, and investigate the effects of tethering on hydrogen metabolism. My efforts in protein purification elucidated the structure of Fd1 to 1.1 Angstroms and determined the midpoint reduction potentials of Fd1 and Fd3. Understanding the underlying thermodynamic processes behind high-temperature metabolism generates avenues for application as energetically-conservative alternatives to existing biosynthetic processes as well as novel applications in other products^{51,52}.

REFERENCES

1. Martin, W. F. & Thauer, R. K. Energy in Ancient Metabolism. *Cell* **168**, 953–955 (2017).
2. Schäfer, G., Engelhard, M. & Müller, V. Bioenergetics of the Archaea. *Microbiology and Molecular Biology Reviews* **63**, 570–620 (1999).
3. Schut, G. J. *et al.* The role of geochemistry and energetics in the evolution of modern respiratory complexes from a proton-reducing ancestor. *Biochimica et Biophysica Acta - Bioenergetics* **1857**, 958–970 (2016).
4. Khawaja, Y. & Karaman, R. A Novel Mathematical Equation For Calculating The Number Of ATP Molecules Generated From Sugars In Cells. *World Journal of Pharmaceutical Research* **4**, 303–312 (2015).
5. Atkinson, J. T., Campbell, I., Bennett, G. N. & Silberg, J. J. Cellular Assays for Ferredoxins: A Strategy for Understanding Electron Flow through Protein Carriers That Link Metabolic Pathways. *Biochemistry* **55**, 7047–7064 (2016).
6. de Vos, W. M., Kengen, S. W. M., Voorhorst, W. G. B. & van der Oost, J. Sugar utilization and its control in hyperthermophiles. *Extremophiles* **2**, 201–205 (1998).
7. Kelly, D. P. & Wood, A. P. The chemolithotrophic prokaryotes in *The Prokaryotes: Prokaryotic Communities and Ecophysiology* **4**, 275–287 (Springer-Verlag Berlin Heidelberg, 2013).
8. Ghosh, W. & Dam, B. Biochemistry and molecular biology of lithotrophic sulfur oxidation by taxonomically and ecologically diverse bacteria and archaea. *FEMS Microbiology Reviews* **33**, 999–1043 (2009).
9. Thauer, R. K. A Fifth Pathway of Carbon Fixation. *Science* vol. 318 1731–1732 (2007).

10. Russell, J. B. & Cook, G. M. *Energetics of Bacterial Growth: Balance of Anabolic and Catabolic Reactions. Microbiol Rev* **59**, 48-62 (1995).
11. Müller, V., Chowdhury, N. P. & Basen, M. Electron Bifurcation: A Long-Hidden Energy-Coupling Mechanism. *Annual Review of Microbiology* **72**, 331–353 (2018).
12. Sapro, R., Bagramyan, K. & Adams, M. W. W. A simple energy-conserving system: Proton reduction coupled to proton translocation. *Proc Natl Acad Sci USA* **100**, 7545–7550 (2003).
13. Müller, V. & Hess, V. The minimum biological energy quantum. *Frontiers in Microbiology* **8**, 1-7 (2017).
14. Mayer, F. & Müller, V. Adaptations of anaerobic archaea to life under extreme energy limitation. *FEMS Microbiol Rev* **38**, 449–72 (2014).
15. Spaans, S. K., Weusthuis, R. A., van der Oost, J. & Kengen, S. W. M. NADPH-generating systems in bacteria and archaea. *Frontiers in Microbiology* **6**, 1-27 (2015).
16. Lubner, C. E. *et al.* Mechanistic insights into energy conservation by flavin-based electron bifurcation. *Nature Chemical Biology* **13**, 655–659 (2017).
17. Martin, W. F. Hydrogen, metals, bifurcating electrons, and proton gradients: The early evolution of biological energy conservation. *FEBS Letters* **586**, 485–493 (2012).
18. Feng, X., Schut, G. J., Haja, D. K., Adams, M. W. W. & Li, H. *Structure and electron transfer pathways of an electron-bifurcating NiFe-hydrogenase. Sci. Adv* **8**, 1-13 (2022).
19. Schoelmerich, C. M., Katsyv, A., Hackmann, T. J., designed research, V. & performed research, T. Energy conservation involving 2 respiratory circuits. *PNAS* **117**, 1167–1173 (2020).

20. Jormakka, M. *et al.* Molecular mechanism of energy conservation in polysulfide respiration. *Nature Structural and Molecular Biology* **15**, 730–737 (2008).
21. Slater, E. C. *The mechanism of the conservation of energy of biological oxidations.* *Eur. J. Biochem* **166**, 489-504 (1987).
22. Yu, H. *et al.* Structure of an Ancient Respiratory System. *Cell* **173**, 1636-1649 (2018).
23. Yu, H. *et al.* Structure of the respiratory MBS complex reveals iron-sulfur cluster catalyzed sulfane sulfur reduction in ancient life. *Nature Communications* **11**, 1-13 (2020).
24. Yu, H., Schut, G. J., Haja, D. K., Adams, M. W. W. & Li, H. Evolution of complex I-like respiratory complexes. *Journal of Biological Chemistry* **296**, 1-10 (2021).
25. Schut, G. J., Boyd, E. S., Peters, J. W. & Adams, M. W. W. The modular respiratory complexes involved in hydrogen and sulfur metabolism by heterotrophic hyperthermophilic archaea and their evolutionary implications. *FEMS Microbiology Reviews* **37**, 182–203 (2013).
26. Kanai, T. *et al.* Continuous hydrogen production by the hyperthermophilic archaeon, *Thermococcus kodakaraensis* KOD1. *J Biotechnol* **116**, 271–82 (2005).
27. Santangelo, T. J., Čuboňová, L. & Reeve, J. N. Deletion of alternative pathways for reductant recycling in *Thermococcus kodakaraensis* increases hydrogen production. *Molecular Microbiology* **81**, 897–911 (2011).
28. Drake, H. L. & Daniel, S. L. Erratum: Physiology of the thermophilic acetogen *Moorella thermoacetica* (Research in Microbiology (2004) 155 (422-436) DOI: 10.1016/j.resmic.2004.03.003). *Research in Microbiology* 155, 868 (2004).

29. Bräsen, C., Esser, D., Rauch, B. & Siebers, B. Carbohydrate metabolism in archaea: Current insights into unusual enzymes and pathways and their regulation. *MMBR Amer. Soc. Microbiology* **78**, 89-175 (2014).
30. Ren, X. *et al.* Identification of an Intermediate Form of Ferredoxin That Binds Only Iron Suggests That Conversion to Holo-Ferredoxin Is Independent of the ISC System in *Escherichia coli*. *Applied and Environmental Microbiology* **87**, 1–16 (2021).
31. Hwang, J., Han, J. Fe/Mossbauer analysis of biological and synthetic Fe/S clusters. *Research & knowledge* **1**, 53-61 (2015).
32. Burkhart, B. W., Febvre, H. P. & Santangelo, T. J. Distinct physiological roles of the three ferredoxins encoded in the hyperthermophilic archaeon *Thermococcus kodakarensis*. *mBio* **10**, 1-17 (2019).
33. Yan, R. *et al.* Cluster and fold stability of *E. coli* ISC-type ferredoxin. *PLoS ONE* **8**, 1-8 (2013).
34. Sticht, H. & Roè, P. The structure of iron-sulfur proteins. *Prod in Biophys. And Molec. Bio* **70**, 95-136 (1998).
35. Mortenson, L. E., Valentine, R. C. & Carnahan, J. E. An electron transport factor from *Clostridium pasteurianum*. *Biochemical And Biophysical Research Communications* **7**, 448-452 (1962).
36. Lovenberg, W., Buchanan, B. B. & Rabinowitz, J. C. Studies on the Chemical Nature of Clostridial Ferredoxin. *J Biol Chem* **238**, 3899–3913 (1963).
37. Sieker, L. C., Adman, E. & Jensen, L. H. Structure of the Fe-S Complex in a Bacterial Ferredoxin. *Nature* **235**, 40-42 (1972).

38. Sieker, L. C. & Jensen, L. H. An X-ray investigation of the structure of a bacterial ferredoxin. *Biochemical And Biophysical Research Communications* **20**, 33-35 (1965).
39. Huber, C. ; & Wachtershauser, G. Peptides by activation of amino acids with CO on (Ni,Fe)S surfaces: Implications for the origin of Life. *Science* **281**, 670-672 (1998).
40. Meyer, J. Iron–sulfur protein folds, iron–sulfur chemistry, and evolution. *JBIC Journal of Biological Inorganic Chemistry* **13**, 157–170 (2008).
41. Eck, R. v & Dayhoff, M. O. Evolution of the Structure of Ferredoxin Based on Living Relics of Primitive Amino Acid Sequences. *Science* **152**, 363-366 (1966).
42. Adams, M. W. W. Enzymes and proteins from organisms that grow near and above 100°C. *Annu. Rev. Microbiol.* **47**, 627-658(1993).
43. Tagawa, D. K., Daniel, P. & Arnon, I. Ferredoxins as electron carriers in photosynthesis and in the biological production and consumption of hydrogen gas. *Nature* **195**, 537-543 (1962).
44. Buchanan, B. B. & Arnon, D. I. A reverse KREBS cycle in photosynthesis: consensus at last. *Photosynthesis Research* **24**, 47-53 (1990).
45. Okada, K., Fujiwara, S. & Tsuzuki, M. Energy conservation in photosynthetic microorganisms. *Journal of General and Applied Microbiology* **66**, 59–65 (2020).
46. Ho, T. T. H. *et al.* Photosystem I light-harvesting proteins regulate photosynthetic electron transfer and hydrogen production. *Plant Physiology* **00**, 1-15 (2022).
47. Li, Q., Liu, R., Li, Z., Fan, H. & Song, J. Positive effects of NaCl on the photoreaction and carbon assimilation efficiency in Suaeda salsa. *Plant Physiology and Biochemistry* **177**, 32–37 (2022).

48. Hanke, G. & Mulo, P. Plant type ferredoxins and ferredoxin-dependent metabolism. *Plant, Cell and Environment* **36**, 1071–1084 (2013).
49. Schut, G. J., Boyd, E. S., Peters, J. W. & Adams, M. W. W. The modular respiratory complexes involved in hydrogen and sulfur metabolism by heterotrophic hyperthermophilic archaea and their evolutionary implications. *FEMS Microbiology Reviews* **37**, 182–203 (2013).
50. Kanai, T. *et al.* Overproduction of the membrane-bound [NiFe]-hydrogenase in *Thermococcus kodakarensis* and its effect on hydrogen production. *Frontiers in Microbiology* **6**, 1–11 (2015).
51. Straub, C. T. *et al.* Biotechnology of extremely thermophilic archaea. *FEMS Microbiology Reviews* **42**, 543–578 (2018).
52. Atkinson, J. T. *et al.* Metalloprotein switches that display chemical-dependent electron transfer in cells. *Nature Chemical Biology* **15**, 189–195 (2019).

CHAPTER 1: CLONING, EXPRESSION AND PURIFICATION OF THE THREE FERREDOXIN ISOFORMS IN *T. KODAKARENSIS*

Prior to this thesis, ferredoxins in *T. kodakarensis* were yet uncharacterized regarding their atomic structures and redox chemistry. Biophysical analyses of these proteins require large quantities of high-purity samples, necessitating generation and optimization of recombinant expression vectors for each ferredoxin isoform in *T. kodakarensis*. While genetically accessible and easily cultivated in large volumes, *T. kodakarensis* is not an ideal expression system for native proteins destined for biophysical analysis as it lacks an inducible expression mechanism, preventing controlled overexpression of the protein of interest. Additionally, separation of native proteins from cells can be difficult and low-yield in comparison to recombinant expression. Previous work in *Thermococcus profundus*¹ demonstrated aerobic cultivation of exogenously-expressed ferredoxins in *E. coli* did not disrupt the overall protein fold and the Fe/S cluster character could be restored using iron supplementation in anaerobic conditions.

Overexpression of Fe/S-centered proteins poses unique challenges compared to proteins coordinating organic prosthetic groups: iron and sulfur are essential components of many key biological prosthetic groups but their individual chemistry pose direct threats to cell viability². Expression of Fe/S cluster-containing proteins and Fe/S cluster coordination are tightly regulated in prokaryotes by *SUF* and *IscR* systems³. Overexpression of Fe/S-centered proteins can be bottlenecked in bacterial systems lacking *suf* and containing *iscR*, leading to either under expression of proteins or expression of proteins lacking the coordinated Fe/S cluster.

BL-21, a strain commonly used for overexpression of recombinant Fe/S-centered proteins, was shown to have a non-functional *suf* operon, which had to be synthetically restored⁴. Prior to this discovery, a BL-21 line lacking the *iscR* operon was engineered: $\Delta iscR$ ⁵. The

existing *ΔiscR* strain has restored SUF and lacks IscR as functional Fe/S-cluster regulation mechanisms, making these cells exceptionally suited for overexpression of Fe/S-centered proteins.

The work in this study was performed using first standard BL-21 cells, and later a *ΔiscR* strain shared by collaborators at Boston University. Both cell lines proved capable of transformation and expression of pQE-80L vectors encoding a recombinant, C-terminally tagged 6xHis-Ferredoxin protein. Each protein was initially purified using affinity chromatography, and later fully purified via size-exclusion chromatography. The fully-purified proteins were assayed for protein concentration, iron saturation and purity, then sent for biophysical characterization.

RESULTS

Cloning of the *T. kodakarensis* ferredoxins:

The *T. kodakarensis* Fds were cloned into pQE-80L using InFusion cloning techniques and sequence-confirmed via Sanger sequencing

Expression of the *T. kodakarensis* ferredoxins:

Figure 12 shows expression of the *T. kodakarensis* Fds before and after induction with 0.5 mM IPTG in BL-21 DE3 *E. coli* cells transformed with the pQE-80L-Fd vectors. There is a significant increase in protein expression from pre-induction to post-induction for pQE-80L-Fd2 and pQE-80L-Fd3 vectors. Expression of recombinant Fd1 from pQE-80L-Fd1 is weak, demonstrated by minimal band intensity increases but has minimal losses in overall protein yields from large-volume purifications.

Figure 13 shows expression of the *T. kodakarensis* Fds before and after induction with 0.5 mM IPTG in BL-21 DE3 Δ *iscR* *E. coli* cells transformed with the pQE-80L-Fd vectors. This cell line is optimized for expression of recombinant Fe/S-centered proteins. Expression in this cell line is nearly identical to that of the BL-21 DE3 line, validating the compatibility of BL-21 DE3 Δ *iscR* cells as a viable replacement expression system for BL-21 DE3 cells.

Purification of the *T. kodakarensis* ferredoxins:

Expression trials (**Fig. 13**) of Fd1 did not portray strong expression of Fd1 from pQE-80L-Fd1. Despite only low detectable levels of expression for Fd1, initial purification of Fd1 from biomass harvested from 30 ml of culture induced with IPTG, lysed, clarified, and passed through a 5 mL chelating column gave significant protein yields, regardless of expression strength. Further

purification using size-exclusion chromatography revealed minimal losses in protein yield (**Fig. 14**).

Expression trials (**Fig. 13**) of Fd2 showed strong expression of Fd2 from pQE-80L-Fd2. Initial purification of Fd2 from a 5 ml chelating column indicated slightly lower yields compared to Fd1, later confirmed via Bradford Assay (not depicted) after size-exclusion chromatography (**Fig. 14**).

Expression trials (**Fig. 13**) of Fd3 showed strong expression of Fd3 from pQE-80L-Fd3. Initial purification of Fd3 on a 5 ml chelating column was high-yield, and most purified protein content was retained through size-exclusion chromatography (**Fig. 14**).

Quantitation of iron content of purified Fds:

After purification, each Fd sample was quantitated for iron content using a colorimetric ferrozine-based assay. **Figures 15 & 16** show total iron content of purified Fd samples originating from standard BL-21 DE3 cells with and without iron and sulfur supplementation and BL-21 *ΔiscR* cells with and without iron and sulfur supplementation. BL-21 *ΔiscR* cells were able to produce Fds with higher iron saturation compared to BL-21 DE3 cells.

Total purification trials are summarized in **Figure 17**. Based on the results of purification and iron quantitation, BL-21 *ΔiscR* cells were selected as a superior expression line for the *T. kodakarensis* Fds due to increased iron saturation and protein yields.

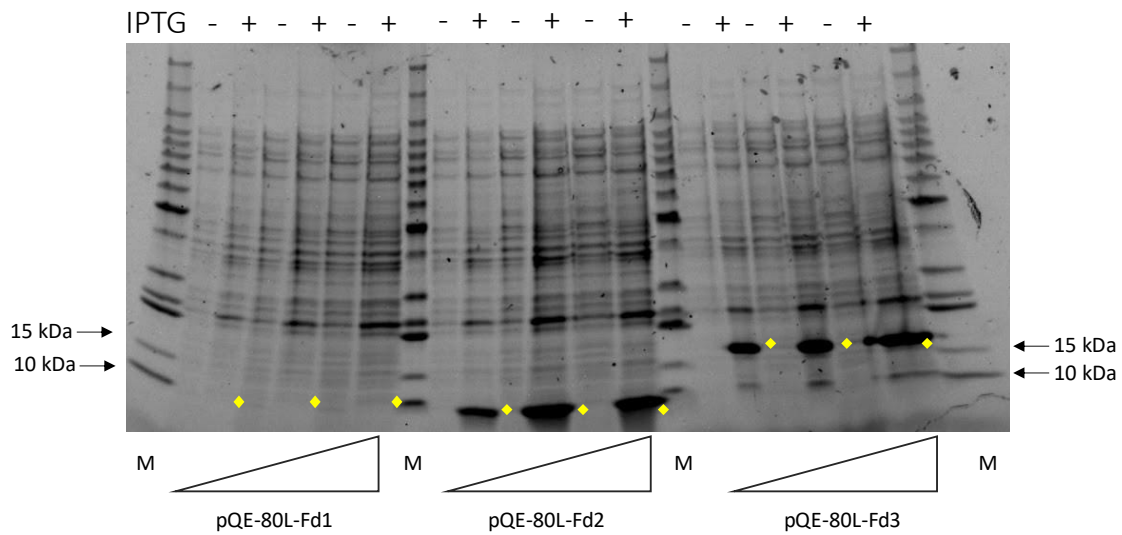


Figure 12

*SDS-PAGE of increasing volumes whole cell lysates from BL-21 DE3 cultures transformed with the pQE-80L-Fd vectors, expressing each Recombinant Fd. Each lane depicts total protein expression immediately pre-induction with IPTG (-), or 3 hours post-induction (+). Highlighted in yellow are bands matching the expected sizes of the recombinant *T. kodakarensis* Fds: 7 kDa (Fd1), 8 kDa (Fd2), 15 kDa (Fd3). Fd2 and Fd3 are strongly expressed, shown by the distinct difference in band intensity between pre- and post-induction lanes. Fd1 is not strongly expressed but when grown in large volumes, substantial yields are still possible.*

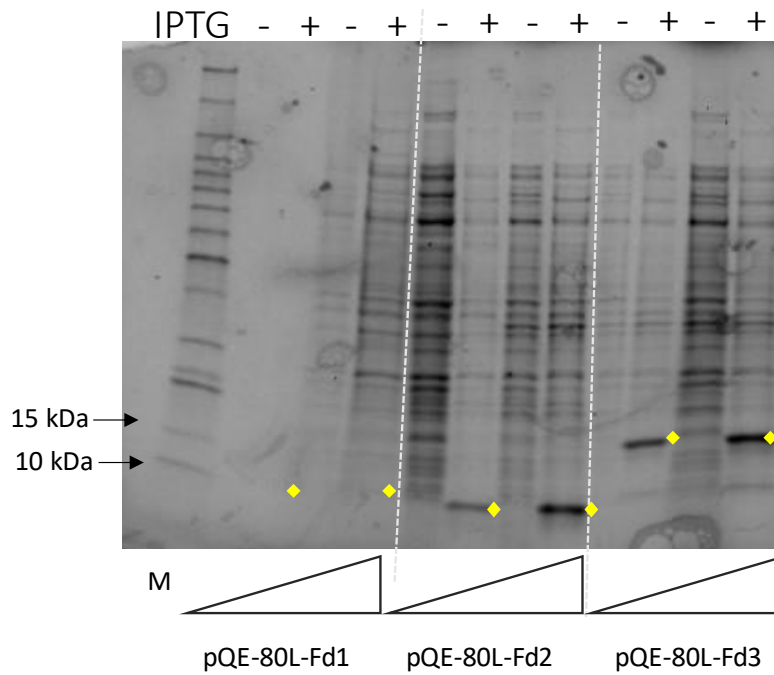


Figure 13

*SDS-PAGE of increasing volumes of whole cell lysates from BL-21 DE3 Δ iscR cultures transformed with the pQE-80L-Fd vectors, expressing each recombinant Fd. Each lane depicts total protein expression immediately pre-induction with IPTG (-), or 3 hours post-induction (+). Highlighted in yellow are bands matching the expected sizes of the recombinant *T. kodakarensis* Fds: 7 kDa (Fd1), 8 kDa (Fd2), 15 kDa (Fd3). Fd2 and Fd3 are strongly expressed, shown by the distinct difference in band intensity between pre- and post-induction lanes. Fd1 is not strongly expressed but when grown in large volumes, substantial yields are still possible.*

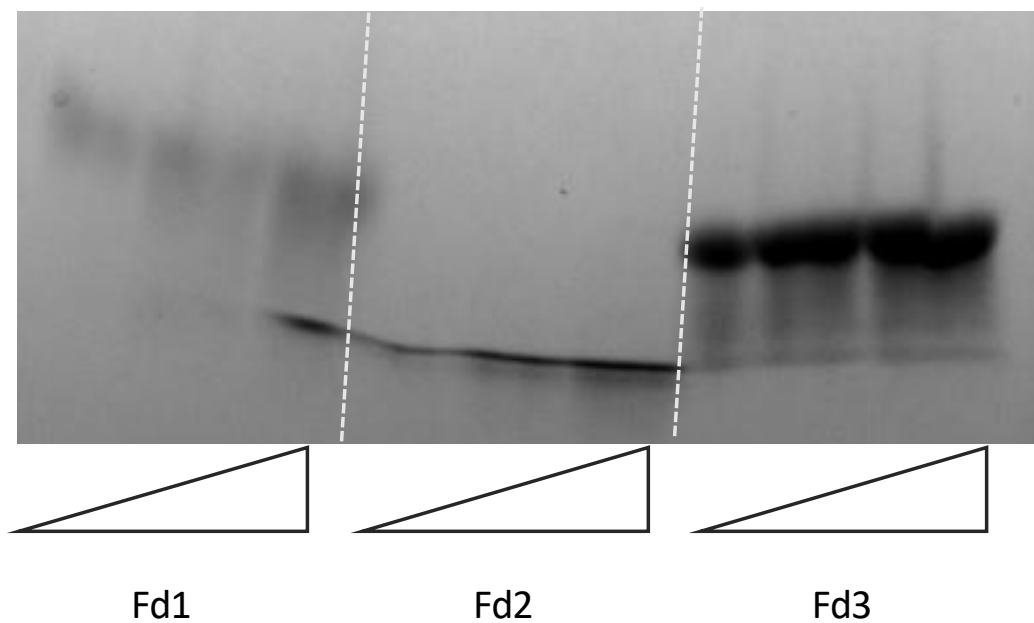


Figure 14

*SDS-PAGE of SEC-purified recombinant *T. kodakarensis* Fds. Iron/sulfur-centered proteins notoriously do not resolve at their predicted sizes during SDS-PAGE due to how tightly the Fe/S center is coordinated in the protein structure. The smearing and size distortion seen in this image for Fd1 and Fd3 is indicative of protein samples saturated with Fe/S clusters.*

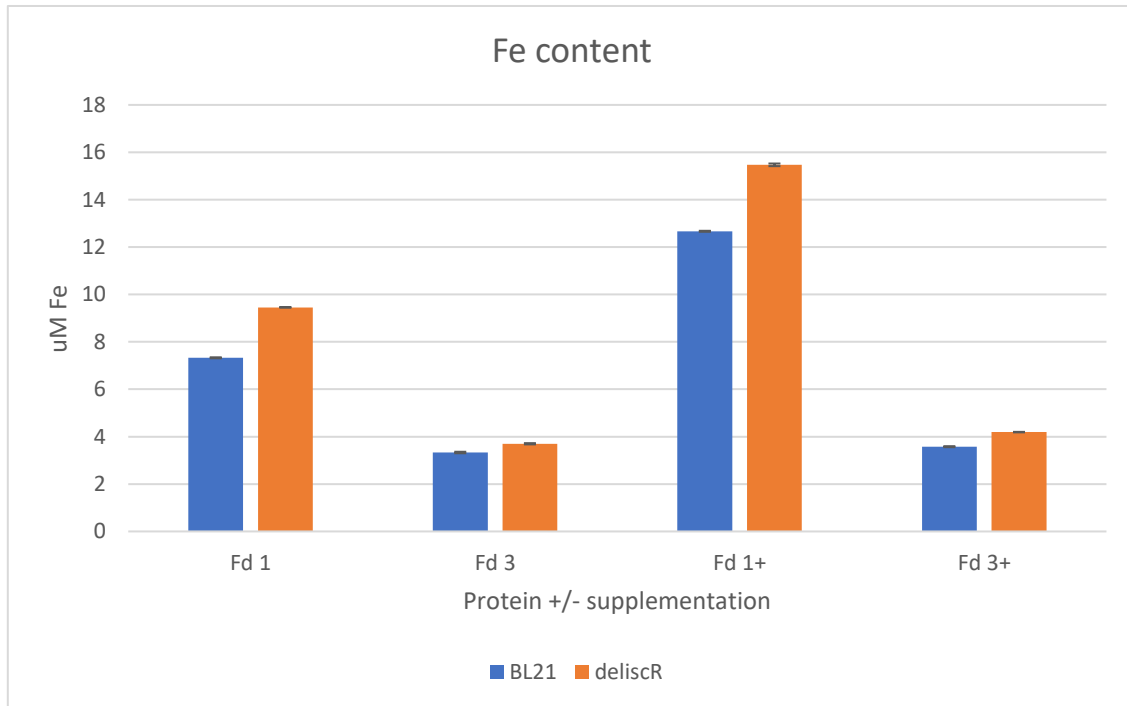


Figure 15

*Total iron content from affinity-purified recombinant *T. kodakarensis* Fds expressed in +/- Fe/S supplementation in both BL-21 DE3 and BL-21 DE3 Δ iscR *E. coli* strains. Content was determined using a colorimetric ferrozine-based assay. Expression from BL-21 DE3 Δ iscR strains with Fe/S supplementation showed the greatest Fe saturation per unit protein.*

Protein	Strain	Supplemented	Absolute uM Fe at 0.01 mg/ml protein	% Fe-S bound protein, 1 4Fe-4S center	% Fe-S bound protein, 2 4Fe-4S centers
Fd 1 (7.3 kDa, 1.4 uM) (5.6 uM total 4Fe-4S saturation)	BL-21	-	7.33	130%	65%
		+	12.67	225%	113%
	Δ IscR	-	9.46	170%	85%
		+	15.47	275%	138%
Fd 3 (15.6 kDa, 0.64 uM) (2.7 uM total 4Fe-4S saturation)	BL-21	-	3.33	125%	63%
		+	3.57	135%	68%
	Δ IscR	-	3.70	145%	73%
		+	4.19	165%	83%

Figure 16

*Summary of prosthetic group optimization in Fd1 and Fd3 in standard BL-21 and BL-21 Δ IscR cell lines, with and without Fe and S supplementation in media. The greatest gains in total Fe content came from BL-21 Δ IscR cells in supplemented media. Calculations were completed under the assumption the *T.kodakarensis* Fds coordinated 4Fe-4S centers, based on Phyre models of structures from Burkhart et. al, 2019.*

Protein	E. coli strain	Media	Supplementation	mM IPTG	Concentration	Buffer Exchange
Fd1	Rosetta II Yes, low BL-21 Yes, moderate BL-21 Δ iscR Yes, high	LB Yes	Fe/S Yes, high	0.25	3 kDa MWCO filter Yes, high	3.5 kDa Dialysis overnight 4°C Yes, high
				0.5		
		TB Yes	4% Sorbitol Yes, low	0.75	1 mL Ni ²⁺ chelating Yes, moderate	3 kDa MWCO filter No, moderate
				1		
Fd2	Rosetta II Yes, low BL-21 Yes, moderate BL-21 Δ iscR Yes, high	LB Yes	Fe/S Yes, high	0.25	3 kDa MWCO filter Yes, high	3.5 kDa Dialysis overnight 4°C Yes, high
				0.5		
		TB Yes	4% Sorbitol Yes, low	0.75	1 mL Ni ²⁺ chelating Yes, moderate	3 kDa MWCO filter No, high
				1		
Fd3	Rosetta II Yes, low BL-21 Yes, moderate BL-21 Δ iscR Yes, high	LB Yes	Fe/S Yes, high	0.25	3 kDa MWCO filter No	3.5 kDa Dialysis overnight 4°C No
				0.5		
		TB Yes	4% Sorbitol Yes, low	0.75	1 mL Ni ²⁺ chelating Yes, moderate	3 kDa MWCO filter Yes, high
				1		

Figure 17

Summary of Fd purification trials. In black are categories relevant to purification. In red is compatibility (Yes/No), and resultant yield/quality (High/Moderate/Low).

DISCUSSION

The cloning, expression and purification of the recombinant Fd isoforms underlines the importance of optimizing sample preparation for biophysical assays. The original approach taken to generating the *T. kodakarensis* Fds: expression in BL-21s, without media supplementation, purification relying only on molecular weight cutoff filters for buffer exchange and concentration—did have acceptable yields of total protein, but were completely lacking in protein quality. That is, the Fds produced using the original protocol were unsaturated in Fe/S centers. For proteins whose structures and enzymatic activity is innately tied to coordinating their prosthetic groups in the appropriate geometry, it is not an option to do biophysics on samples of proteins lacking their redox centers.

Preliminary work on generating the Fds proved that the *T. kodakarensis* Fds could be expressed under standard conditions and remain soluble with minimal formation of inclusion bodies with the host BL-21 proteins. In large part, this is due to the substantial difference in thermal tolerance between native BL-21 proteins and the *T. kodakarensis* Fds. Being able to heat treat cell lysate at 85°C reduces effectively separates mesophilic proteins from thermophilic proteins, allowing for substantially fewer confounding interactions between host and recombinant proteins, promoting recombinant protein solubility. Shown in **(Fig. 11)**, the recombinant Fds are expressed at $\geq 50\%$ total protein even in non-supplemented BL-21 cells. This initial result was promising for the *T. kodakarensis* Fds being candidates for large-scale purification for biophysics.

Moving into large-scale protein purification for the Fds expressed in BL-21s revealed an obstacle for down-stream protein processing: Fd1 and Fd2 were intolerant of simultaneous buffer

exchange and protein concentration using centrifuge molecular weight cutoff filters, and Fd3 was intolerant of slow buffer exchange using dialysis at 4°C (**Figure 17**). This emphasized the need for individual tailoring of purification and handling protocols for each isoform, and led to the development of the protocol depicted in **Figure 18**. After initial purification on the 5 mL affinity column, each Fd spent the minimum amount of time possible in a compatible buffer exchange method (dialysis for Fd1 and Fd2; exchange over a centrifuge filter for Fd3). After buffer exchange, the bulk of protein concentration was done on a 1 mL affinity column. Reducing the column volume reduces the volume of buffer needed to wash and elute the bound material. Overall, this leads to a decrease in sample dilution coming off the column. The samples then had to be quickly buffer exchanged again in their respective methods as well as have the final concentration steps done quickly on a centrifuge filter. This material was then purified using size exclusion chromatography and concentrated quickly over centrifuge filters. However, when purified in large quantities, the Fd samples coming from non-supplemented BL-21 cells were pale. Even in aerobic conditions, Fe/S-centered proteins are a dark, cherry-cola color in high concentrations. The protein samples garnered from unoptimized expression conditions were pale, low-yield, and low-volume. Further discussion with collaborators at Boston University indicated that samples of this quality were unlikely to yield fruitful electrochemical results.

Trials with supplementation of biologically accessible Fe and S as well as use of an optimized cell line (BL-21 *ΔiscR*) led to drastic improvements in Fe/S cluster coordination in the purified proteins. Supplementing Fe and S in media is a difficult task. When oxidized to its 3+ state, Fe is insoluble in aqueous solutions. At high enough concentrations, Fe and S are toxic to cells. Due to the speed at which Fe is oxidized in aerobically-made media, Fe cannot be

supplemented into the media slowly to prevent toxicity. Using the same purification structure as before, total Fe content was increased 200% in supplemented BL-21 $\Delta iscR$ cells compared to non-supplemented BL-21 cells. Visibly, the samples were much darker and cherry-cola colored. The combined iron saturation data and visual results clearly indicated a higher quality protein. Ultimately, supplemented growth in BL-21 $\Delta iscR$ cells under the same purification conditions was chosen as the final method for large volume preparation of the *T. kodakarensis* Fds.

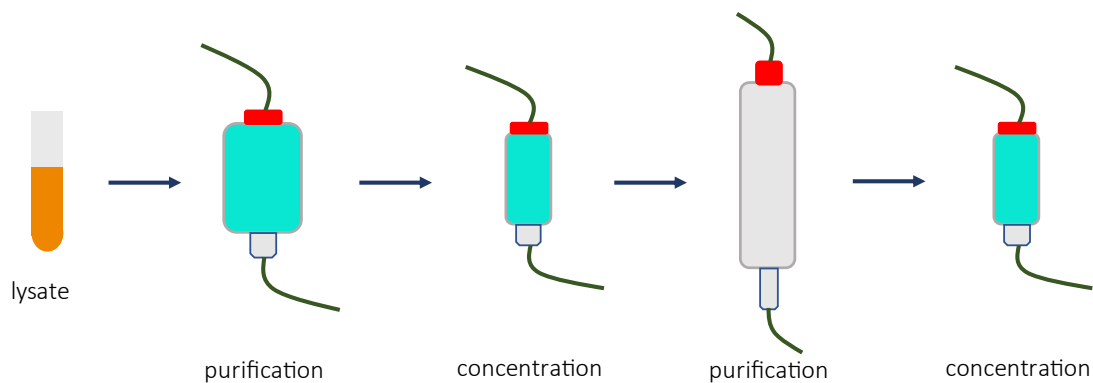


Figure 18

*Summary of purification protocol used for the recombinant Fds. Aggregative interactions with filter media in molecular weight cutoff filters made concentration of the *T. kodakarensis* Fds difficult. The above protocol used 1 mL nickel chelating columns as a preliminary concentration device to reduce losses from concentration in molecular weight cutoff filters. Additionally, Fd3 is intolerant of buffer exchange using dialysis, and must undergo fast buffer exchange over a centrifuge filter, necessitating the use of centrifuge filters during the purification protocol.*

MATERIALS AND METHODS

Luria-Bertani (LB) Media (x1 L)

Per 1 L: 10.0 g Tryptone, 5.0 g Bacteriological Yeast Extract, 5.0 g NaCl, 1 L double-distilled water. Add dry ingredients to 900 mL of ddH₂O, mix until fully dissolved. Add ddH₂O to final 1 L volume. Autoclave liquid cycle 20 minutes.

LB Solid Media

Per 1 L: 10.0 g Tryptone, 5.0 g Bacteriological Yeast Extract, 5.0 g NaCl, 5.0 g Agar, 1 L ddH₂O. Add dry ingredients to 900 mL ddH₂O, mix until fully dissolved. Add ddH₂O to final 1 L volume. Autoclave in 2 L Erlenmeyer flask, liquid cycle 20 minutes. After autoclaving, cool media to 45°C while stirring, add selective agents. Aliquot media into sterile plastic petri plates (approx. 25 mL/plate) under flame. Allow media to cool and solidify, invert plates and store at 4°C.

Construction of pQE-80L-Fd expression vectors

Each pQE-80L-Fd expression vector was constructed using a synthetic oligonucleotide encoding for the Fd gene (TK1694/Fd1, TK1087/Fd2, or TK2012/Fd3) and a C-terminal 6xHis tag with complementary ends to the EcoRI/SalI-digested linear pQE-80L vector. The insert amplicon and linearized vector were combined in a 2:1 μ M ratio according to the TakaraBio Infusion Cloning protocol. Recircularized vectors were transformed into Stellar cells and transformants were selected on solid LB/Amp media at 37°C for 12-16 hrs. Colonies grown from the selective plate were picked to ddH₂O and spotted in 1:10 dilutions in ddH₂O onto solid LB/Amp (100 μ g/mL) media and grown at 37°C for 12 hrs.

Transformation of *E. coli* cells

100 μ L of BL-21 competent *E. coli* cells were thawed on ice for 20 minutes, and 2 μ L of ~100 μ g/mL pQE-80L-Fd1/Fd2/Fd3 plasmid was added to the cells. The cells incubated on ice for 30 min, heat shocked at 42°C for 45 seconds, and then rested on ice for 5 min. Using a P1000, cells dispensed via pipetting and then spread onto LB/amp (100 μ g /mL) plates and incubated overnight at 37°C.

Colony PCR

Confirmation of pQE-80L-Fd constructs was performed via colony PCR. Using a p10 pipette tip, part of the spotted colonies was picked and resuspended vigorously in 10 μ l ddH₂O. The following master mix was added to the lysed cell suspension: For a total reaction volume of 50 μ L per sample: 1U of Phusion DNAP, 200 μ M of dNTPS, 1X HF buffer (NEB), 0.5 μ M forward and reverse primers, and ~250 ng of gDNA and amplified using the PCR protocol of 98°C for min, and the 35 cycles of 98°C for 10 s, 60°C for 30 s, 72°C for 30 s/kb. The samples were then run on a 1% agarose gel using gel electrophoresis at 120V for 35 min in 1X TBE (89 mM Tris, 89 mM boric acid, 2 mM EDTA), stained for 10 min in 0.5 μ g/mL ethidium bromide and imaged.

Expression of pQE-80L vectors in *E. coli*

One colony from previously prepared transformation plate was picked to 5mL liquid LB media and 5 μ L 100 μ g/mL ampicillin was added. Liquid culture was grown at 37°C with 200 RPM agitation until the culture reached $OD_{600} \geq 0.5$, where 0.5 mM isopropyl β -D-1-thiogalactopyranoside (IPTG) was added to induce protein expression. Cultures were then grown at 37°C with agitation for another 3 hrs. Cells were harvested at 20,000 xg for 5 min, supernatant

removed by pipetting, resuspended in 20mM Tris HCl pH 8.0, 1.5M NaCl, 10% glycerol (3 mL/g pellet), and mixed vigorously by pipetting. For SDS PAGE, 10 μ L of cell suspension/lysate was added to 3 μ L of 6XSDS loading dye and heat treated at 95°C for 10 min, and the total sample volume was resolved on a 4 – 20 % precast stain free SDS-PAGE gel at 170V for 35 min. Precast stain-free gels were immediately imaged.

Protein purification of Fd1

Ferredoxin proteins from *T. kodakarensis* were recombinantly expressed and purified from BL-21 (DE3) *ΔiscR E. coli* cells transformed with the pQE-80L-Fd1 plasmid. Cells were grown in LB medium at 37°C with agitation and aeration in a 65L bioreactor, with 50 μ g/mL kanamycin and 100 μ g/ml ampicillin to an OD₆₀₀ of 0.5 before expression was induced with 0.5 mM isopropyl β -D-1-thiogalactopyranoside (IPTG). Cultures were grown for an additional 3 hrs at 37°C with agitation and aeration before biomass was harvested via centrifugation at 16,000 xg for 10 min at 4°C, resuspended and mechanically lysed (3ml/g biomass) in 20mM Tris HCl pH 8.0, 1.0M NaCl, 10% glycerol (Buffer A), heated to 85°C for 20 min to denature host proteins, and clarified by centrifugation (~20,000 xg, 15 min, 4°C). Heat-treated clarified cell lysates were resolved through a 5ml HiTrap Chelating column (Cytiva) charged with 1 M NiSO₄, at 1 mL/min flowrate. The flow through was collected in a 200 mL glass beaker covered with aluminum foil. The bound material on the column was washed with 5 column volumes of Buffer A or until the UV₂₈₀ signature on the chromatogram reached baseline levels. Bound material was eluted with a linear gradient from 0 - 250 mM imidazole dissolved in 20 mM Tris HCl pH 8.0, 100 mM NaCl, 10% glycerol (Buffer B). Eluent was collected in 1 mL fractions. Fractions containing pure Fd were identified by SDS-PAGE, pooled, and underwent buffer exchange into Buffer A using 3.5 kDa MWCO dialysis tubing first for 4 hrs at 4°C in 4 L Buffer A, then for 8 hrs at 4°C in 2 L

Buffer A. The buffer-exchanged material was then passed over a 1 mL HiTrap Chelating column (Cytiva) charged with 1 M NiSO₄, using the same flowthrough and washing scheme as the 5 mL column. Bound material was eluted using an isocratic elution at 100% Buffer B. Fractions containing pure Fd were pooled and exchanged into 5 mM Tris HCl pH 8.0, 0.1 M NaCl (crystal storage buffer) using a 3 kDa MWCO centrifuge filter and reduced to a volume of ≤ 2 mL. This material was passed over an S-100 sephacryl size exclusion column (Cytiva) at 0.25 mL/min flowrate, with all flowthrough collected as 1 mL fractions. Fractions containing pure Fd were identified via SDS-PAGE and colorimetric identification (Fd-containing fractions are dark brown in color), pooled, quantitated via Bradford Assay and stored at 4°C.

Protein purification of Fd2

Ferredoxin proteins from *T. kodakarensis* were purified from BL-21 (DE3) *ΔiscR E. coli* cells transformed with the pQE-80L-Fd2 plasmid. Cells were grown in LB medium at 37°C with agitation and aeration in a 65L bioreactor, with 50 µg/mL kanamycin and 100 µg/ml ampicillin to an OD₆₀₀ of 0.5 before expression was induced with 0.5 mM isopropyl β-D-1-thiogalactopyranoside (IPTG). Cultures were grown for an additional 3 h at 37°C with agitation and aeration before biomass was harvested via centrifugation at 16,000 xg for 10 minutes at 4°C, resuspended and mechanically lysed (3ml/g biomass) in 20mM Tris HCl pH 8.0, 1.0M NaCl, 10% glycerol (Buffer A), heated to 85°C for 20 min to denature host proteins, and clarified by centrifugation (~20,000 xg, 15 min, 4°C). Heat-treated clarified cell lysates were resolved through a 5ml HiTrap Chelating column (Cytiva) charged with 1 M NiSO₄, at 1 mL/min flowrate. The flow through was collected in a 200 mL glass beaker covered with aluminum foil. The bound material on the column was washed with 5 column volumes of Buffer A or until the UV₂₈₀ signature on the chromatogram reached baseline levels again. Bound material was eluted

with a linear gradient from 0 - 250 mM imidazole dissolved in 20 mM Tris HCl pH 8.0, 100 mM NaCl, 10% glycerol (Buffer B). Eluent was collected in 1 mL fractions. Fractions containing pure Fd were identified by SDS-PAGE, pooled, and underwent buffer exchange into Buffer A using 3.5 kDa MWCO dialysis tubing first for 4 hrs at 4°C in 4 L Buffer A, then for 8 hrs at 4°C in 2 L Buffer A. The buffer-exchanged material was then passed over a 1 mL HiTrap Chelating column (Cytiva) charged with 1 M NiSO₄, using the same flowthrough and washing scheme as the 5 mL column. Bound material was eluted using an isocratic elution at 100% Buffer B. Fractions containing pure Fd were pooled and exchanged into 5 mM Tris HCl pH 8.0, 0.1 M NaCl (crystal storage buffer) using a 3 kDa MWCO centrifuge filter and reduced to a volume of ≤ 2 mL. This material was passed over an S-100 sephacryl size exclusion column (Cytiva) at 0.25 mL/min flowrate, with all flowthrough collected as 1 mL fractions. Fractions containing pure Fd were identified via SDS-PAGE and colorimetric identification (Fd-containing fractions are dark brown in color), pooled, quantitated via Bradford Assay and stored at 4°C.

Protein purification of Fd3

Ferredoxin proteins from *T. kodakarensis* were purified from BL-21 (DE3) *ΔiscR E. coli* cells transformed with the pQE-80L-Fd3 plasmid. Cells were grown in LB medium at 37°C with agitation and aeration in a 65L bioreactor, with 50 μg/ml kanamycin and 100 μg/ml ampicillin to an OD₆₀₀ of 0.5 before expression was induced with 0.5 mM isopropyl β-D-1-thiogalactopyranoside (IPTG). Cultures were grown for an additional 3 h at 37°C with agitation and aeration before biomass was harvested via centrifugation at 16,000 xg for 10 minutes at 4°C, resuspended and mechanically lysed (3ml/g biomass) in 20mM Tris HCl pH 8.0, 1.0M NaCl, 10% glycerol (Buffer A), heated to 85°C for 20 min to denature host proteins, and clarified by centrifugation (~20,000 xg, 15 min, 4°C). Heat-treated clarified cell lysates were

resolved through a 5ml HiTrap Chelating column (Cytiva) charged with 1 M NiSO₄, at 1 mL/min flowrate. The flow through was collected in a 200 mL glass beaker covered with aluminum foil. The bound material on the column was washed with 5 column volumes of Buffer A or until the UV₂₈₀ signature on the chromatogram reached baseline levels again. Bound material was eluted with a linear gradient from 0 - 250 mM imidazole dissolved in 20 mM Tris HCl pH 8.0, 100 mM NaCl, 10% glycerol (Buffer B). Eluent was collected in 1 mL fractions. Fractions containing pure Fd were identified by SDS-PAGE, pooled, and underwent buffer exchange into Buffer A using 3 kDa MWCO centrifuge filter at 4,000 xg using a 1:2 dilution until the total imidazole content was <1%. The buffer-exchanged material was then passed over a 1 mL HiTrap Chelating column (Cytiva) charged with 1 M NiSO₄, using the same flowthrough and washing scheme as the 5 mL column. Bound material was eluted using an isocratic elution at 100% Buffer B. Fractions containing pure Fd were pooled and exchanged into 5 mM Tris HCl pH 8.0, 0.1 M NaCl (crystal storage buffer) using a 3 kDa MWCO centrifuge filter and reduced to a volume of ≤2 mL. This material was passed over an S-100 sephacryl size exclusion column (Cytiva) at 0.25 mL/min flowrate, with all flowthrough collected as 1 mL fractions. Fractions containing pure Fd were identified via SDS-PAGE and colorimetric identification (Fd-containing fractions are dark brown in color), pooled, quantitated via Bradford Assay and stored at 4°C.

Isolation of plasmid DNA from *E. coli* cells (All buffers from Zymogen Plasmid Miniprep kit)

10 mL of liquid *E. coli* transformant culture was spun down in 1.7 mL increments in 2, 1.7 mL Eppendorf tubes at 20,000 xg for 5 minutes. Supernatant was snapped out of tubes. The remaining pellet was resuspended in 200 µL P1 buffer and vortexed 30 seconds. 200 µL of P2 buffer was added, the tubes vortexed for 5 seconds, shaken vigorously, then incubated at room

temperature for 1-2 min. 400 μ L of P3 buffer was added and mixed via pipette until the solution was opaque and yellow. The tubes were spun at 20,000 xg for 7 min. The supernatant was transferred to a plasmid prep column in a collection tube. The columns were spun at 20,000 xg for 30 seconds. 400 μ L of Plasmid Wash Buffer was added to the columns, which were then spun at 20,000 xg for 1 min. The flowthrough was discarded, then the columns were dried by spinning at 20,000 xg for 1 min. The columns were then transferred to 1.7 mL Eppendorf tubes. 16 μ L of 10 mM Tris HCl pH 8.0 was added to the column and incubated for 5 min at room temperature before being spun at 20,000 xg for 1 min.. The previous step was repeated for a final flowthrough volume of 32 μ L. The isolated plasmid was then quantitated via fluorometry.

Table 1: Primers used for pQE-80L-Fd colony PCR

Name	Sequence (all 5' to 3')	Description
UniF	GGATAACAATTATAATAGATTCAATTGTGAGC	Universal forward primer used to amplify pQE-80L multiple cloning site insertion
UniR	CATCTGGATTTGTTTCAGAACGCTCGGTTGCCG	Universal reverse primer used to amplify pQE-80L multiple cloning site insertion
0071694	CCTGCATTGGAGATGCCATCTGTGC	Primer encoding internal sequence for Fd1/TK1694
0071087	CGGCGGTTGTGCCGGTGTCTGCCCCG	Primer encoding internal sequence for Fd2/TK1087
0022009	GCTGTAGTTTATCTTTGGATACCAC	Primer encoding internal sequence for Fd3/TK2012

Table 2: pQE-80L Expression Vectors

Vector	Description
pQE-80L-Tk1694	<i>E. coli</i> expression vector encoding a C-terminally tagged 6xHis/Fd1
pQE-80L-Tk1087	<i>E. coli</i> expression vector encoding a C-terminally tagged 6xHis/ Fd2
pQE-80L-Tk2012	<i>E. coli</i> expression vector encoding a C-terminally tagged 6xHis/Fd3

Table 3: List of *E. coli* Strains

Name	Description
BL-21	Expression line of <i>E. coli</i>
BL-21 Δ<i>iscR</i>	Expression line of <i>E. coli</i> encoding for functional <i>suf</i> operon and deletion of <i>iscR</i> operon
Stellar	Line of <i>E. coli</i> used for large-volume plasmid replication

REFERENCES

1. Imai, T. *et al.* Characterization and cloning of an extremely thermostable, *Pyrococcus furiosus*-type 4Fe ferredoxin from *Thermococcus profundus*. *J. Biochem.* **130**, 649–655 (2001).
2. Baussier, C. *et al.* Making iron-sulfur cluster: structure, regulation and evolution of the bacterial ISC system. *Advances in Microbial Physiology* **76**, 1-39 (Elsevier Ltd, 2020).
3. Braymer, J. J., Freibert, S. A., Rakwalska-Bange, M. & Lill, R. Mechanistic concepts of iron-sulfur protein biogenesis in Biology. *Biochim. Biophys. Acta - Mol. Cell Res.* **1868**, 1-28 (2021).
4. Corless, E. I., Mettert, E. L., Kiley, P. J. & Antony, E. Elevated Expression of a Functional Suf Pathway in *Escherichia Sulfur Cluster-Containing Protein*. *J. Bacteriol.* **202**, 1–11 (2020).
5. Akhtar, M. K. & Jones, P. R. Deletion of *iscR* stimulates recombinant clostridial Fe-Fe hydrogenase activity and H₂-accumulation in *Escherichia coli* BL21(DE3). *Appl. Microbiol. Biotechnol.* **78**, 853–862 (2008).

CHAPTER 2: BIOPHYSICAL ANALYSIS OF THE *T. KODAKARENSIS* FERREDOXINS

Biophysical characterization is an essential part of protein characterization.

Understanding protein structure provides valuable insights into the steric of reaction mechanisms. The interactome presented in Burkhart et. al 2019 was constructed using LC-MS/MS analysis of products co-purified with each Fd. Characterizing the structures and redox potentials of the *T. kodakarensis* Fds substantiates these interactions. Understanding how Fd3 and MBH physically interaction offers insights into optimizing electron transfer to increase hydrogen yield. Furthermore, redox characterization of the *T. kodakarensis* Fds establishes their overall utility as proteinaceous electron carriers. Discussed in Ewen¹, there is significant interest in using thermophilic Fds in biotechnology and pharmaceutical development as biological catalysts. Additional interest lies in thermophilic Fds, as their increased stability at high temperatures increases their range of applications.

Among the earliest of biocatalysts^{2,3}, iron-sulfur (Fe-S) clusters are found in all domains of life in nearly all environmental conditions⁴. As a prosthetic group, Fe-S clusters are varied in their function, coordinated by enzymes ranging from DNA polymerases to redox-restricted proteinaceous electron carriers (including Fds)⁴. Iron-sulfur chemistry is a powerful tool for cellular redox, but this power has risks: in its 3+ state Fe is insoluble and produces reactive oxygen species, while in high concentrations S is potentially toxic³. As such, expression of Fe-S clusters is tightly regulated by a suite of well-conserved mechanisms encoded by *suf* and *iscR*^{3,5}. Isolation of Fe-S centered proteins must first then consider the bottlenecking effects of Fe-S cluster regulation in expression systems.

Ferredoxins exist as apo- and holoenzymes, coordinating their Fe-S centers depending on the availability of Fe and S in the cell^{6,7}. Cells commonly maintain physiological levels of Fe and S regardless of an increased demand for those elements via an overexpressed Fd or through element starvation⁸. Accurate assays of Fe-S cluster activity in Fds requires optimization of the coordinated holoenzyme, making any Fe-S cluster bottlenecking from the host cell unacceptable. Use of specialized expression systems lacking *iscR* overcomes the issue of bottlenecking and maximizes total purified holoenzyme content.

Iron-sulfur clusters benefit from the versatile chemical properties of their constitutive elements—Fe and S are stable in multiple geometries with one another and enjoy a variety of redox states⁹⁻¹¹. As a class of proteins, the redox potentials of Fds range from -711 mV to -150 mV¹⁰, making them flexible electron carriers and ideal for use in extremophilic energy-restricted conditions^{9,12,13}.

Ferredoxins in *T. kodakarensis* were yet uncharacterized for their electrochemical properties, leaving a gap in our understanding of overall metabolic energetics. Given the known starting substrates and terminal electron acceptors, several key assumptions could be made: each Fd in *T. kodakarensis* must be capable of receiving electrons from a variety of catabolic donors; Fd1 must be less reductive than NAD(P)H, Fd2 less reductive than acceptor isoprenoids, and Fd3 less reductive than H⁺¹⁰. These benchmarks are useful in the context of understanding the basics of energetics in *T. kodakarensis* but are wholly useless for external applications. Characterizing the Fds in *T. kodakarensis* offers insights into the metabolic interactome presented in Burkhart et. al (2019) and places their utility as thermophilic electron carriers in biosynthetic applications.

RESULTS

Cloning of pETSUMO crystallography vectors

pETSUMO-Fd vectors were generated using InFusion cloning techniques identical to the construction of the pQE-80L-Fd vectors. The generated plasmid was checked using colony PCR (**Fig. 19**) then confirmed using Sanger sequencing.

Expression of pETSUMO vectors

BL-21 DE3 cells were able to express the SUMO-tagged Fds, shown in **Figure 20**. Given the size of the SUMO tag in comparison to the Fds, there is a substantial shift in expected size of the tagged construct.

Biophysical analyses of the purified *T. kodakarensis* fds:

X-ray crystallographic analysis of the purified recombinant Fd1 revealed a near-identical structure to *P. furiosus* Fd, coordinating a 3Fe/4S center (**Fig. 21**).

AlphaFold2 modeling of Fd2 and Fd3 revealed structures similar to those previously predicted using Phire (**Fig.22**). The Fd2 and Fd3 models show cysteines arranged in an ideal geometry for Fe/S cluster coordination. The model for Fd3 suggests a long N-terminal projection. Each Fd model predicts a strongly-conserved Fd fold domain internal to the protein, consistent with Fe/S cluster coordination (not pictured).

The redox capabilities of the purified recombinant Fd1 and Fd3 were assayed using protein-film voltammetry. Fd1 has a midpoint reduction potential of -407 mV, and Fd3 has two midpoint reduction potentials: -363 mV and -409 mV (**Fig. 23**).

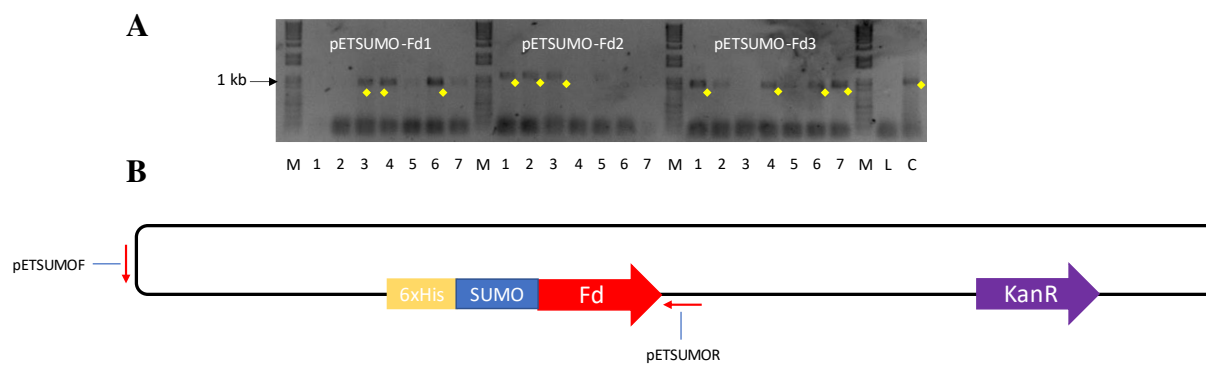


Figure 19

Colony PCR results from the construction of the pETSUMO-Fd vectors. (A) Highlighted in yellow are bands that match the expected size for each product. These bands were excised from the gel, purified, and confirmed using sanger sequencing. (B) Diagram depicting the primer locations used for colony PCR.

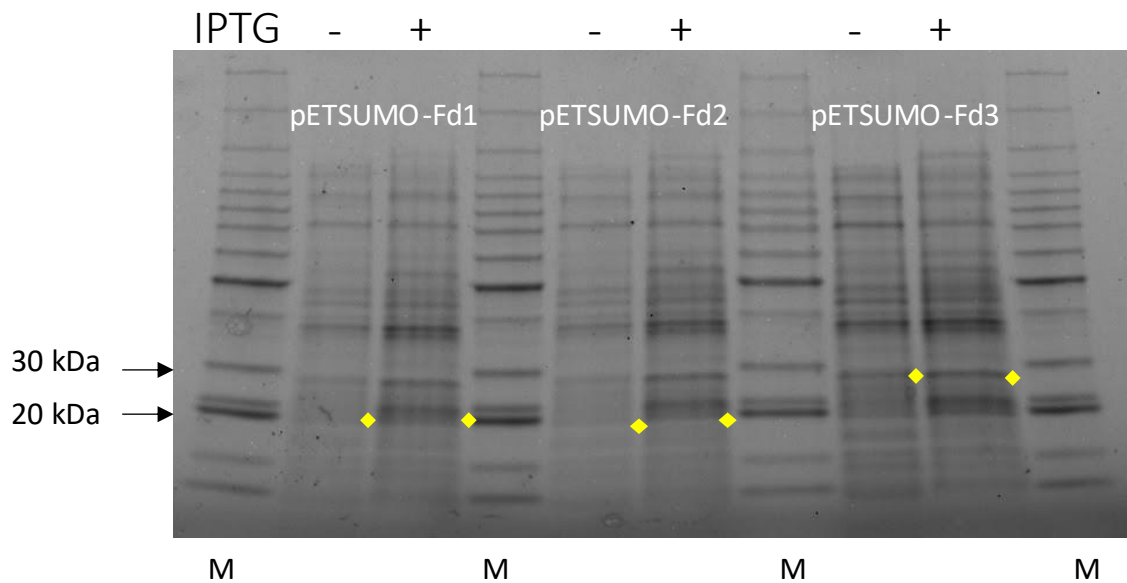


Figure 20

SDS-PAGE of whole cell lysates from BL-21 DE3 cultures transformed with the pETSUMO-Fd vectors. Each lane depicts total protein expression immediately pre-induction with IPTG (-), or 3 hours post-induction (+). Highlighted in yellow are bands matching the expected sizes of the SUMOylated. Fds: 20kDa (Fd1), 20 kDa (Fd2), 27 kDa (Fd3). Expression of these proteins is acceptable, and the confirmed vectors were sent to collaborators for purification.

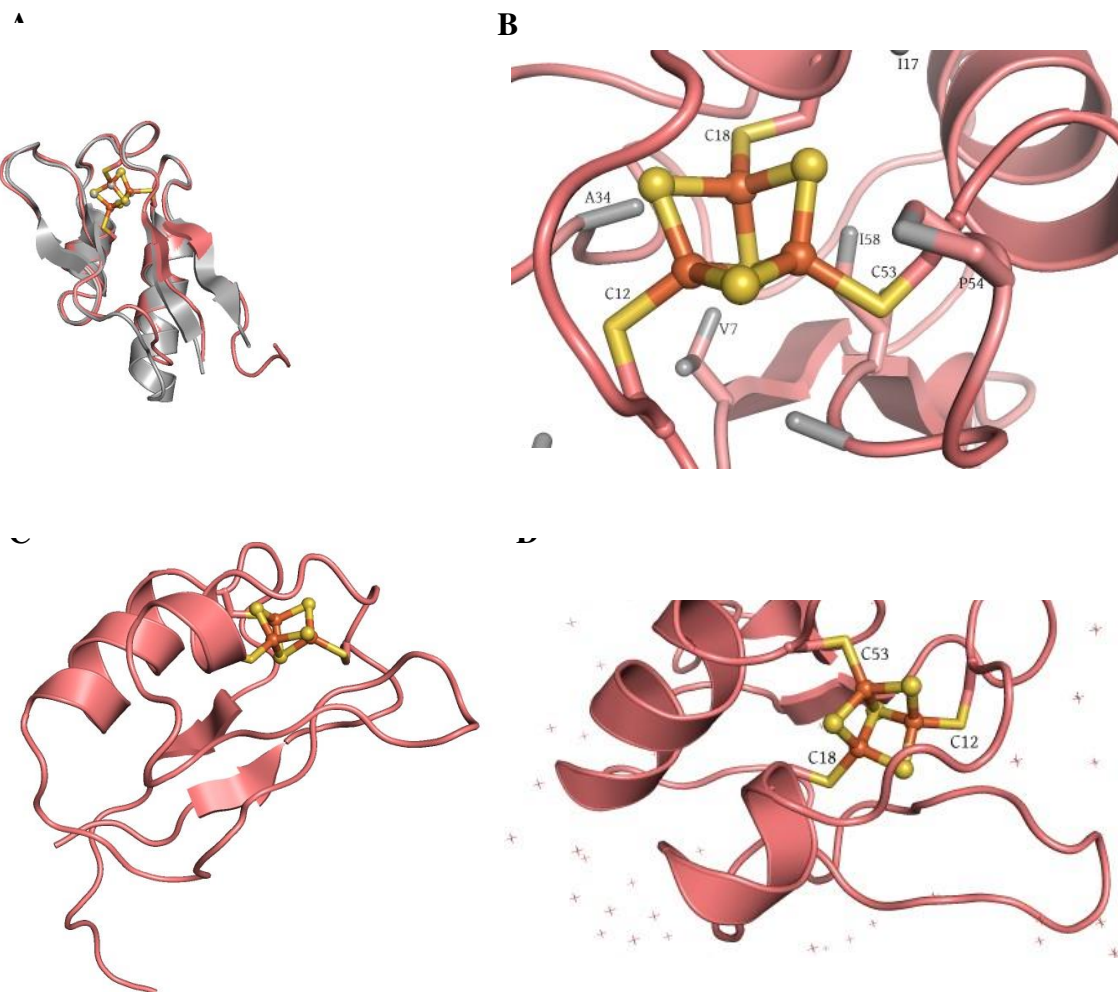


Figure 21

Crystal structure of *T. kodakarensis* Fd1 to 1.1 Å. (A) Overlay of *T. kodakarensis* Fd1 (salmon) and *P. furiosus* (grey) (PDB code: 1SIZ). (B) Close perspective of the 3Fe/4S center in *T. kodakarensis* Fd1. Fe in orange, S in yellow. (C) Full depiction of Fd1 (D) Coordinated waters surrounding Fd1.

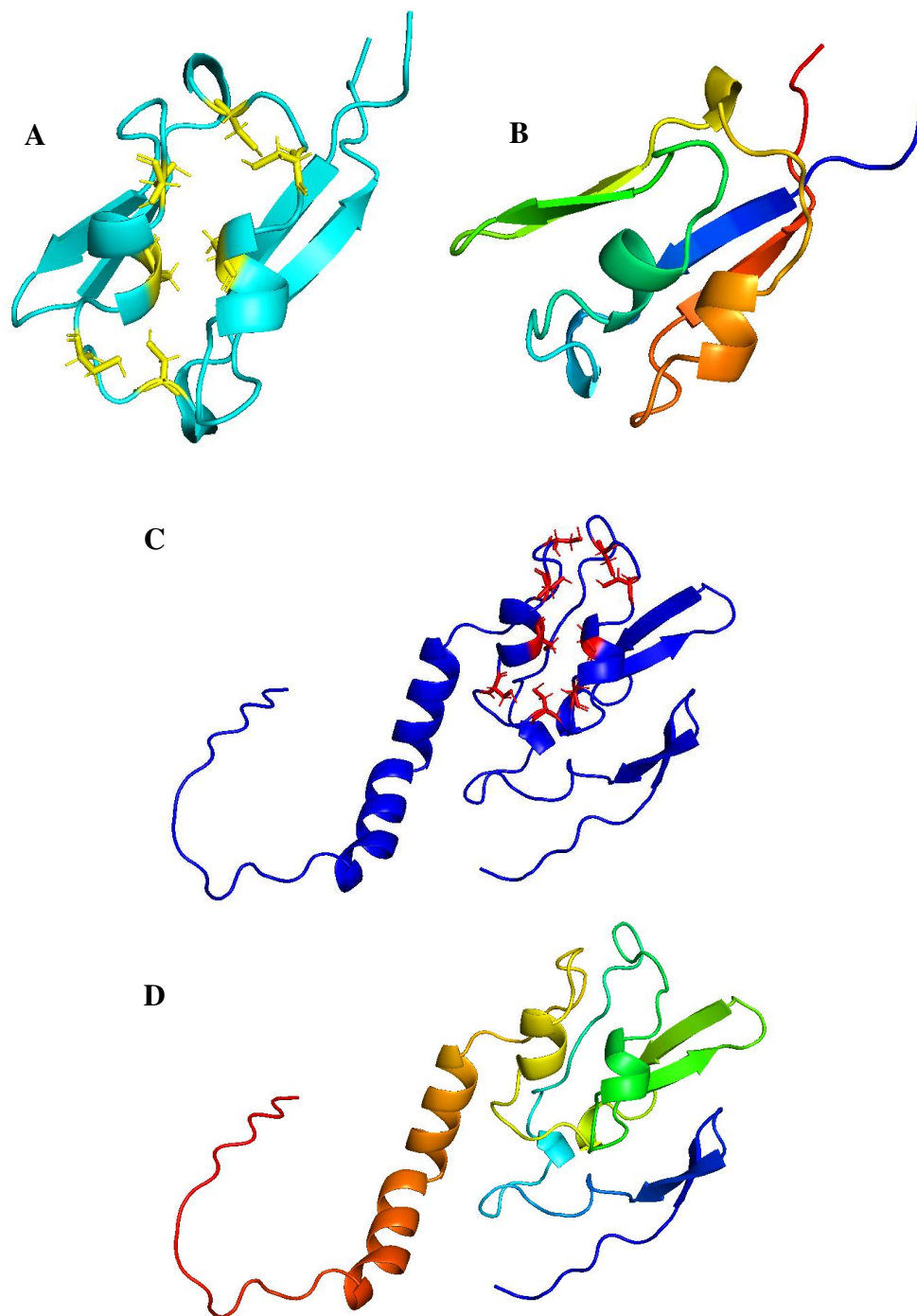


Figure 22

AlphaFold2 models of *T. kodakarensis* Fd1 and *T. kodakarensis* Fd3. (A) Structure of Fd2 with cysteine residues highlighted in yellow. (B) Cartoon depiction of *T. kodakarensis* Fd2. (C) Structure of Fd3 with cysteine residues highlighted in red. (D) Cartoon depiction of *T. kodakarensis* Fd3.

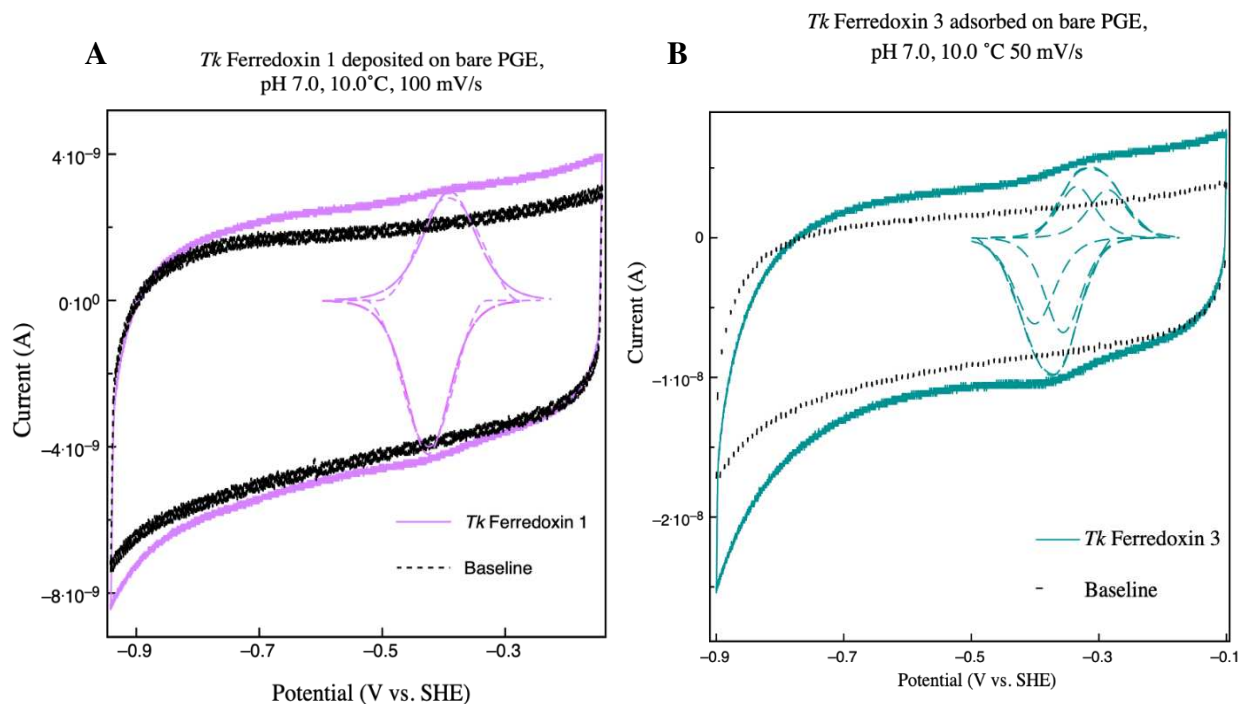


Figure 23

Voltammograms of Fd1 and Fd3. (A) Voltammetry of Tk ferredoxin 1 measured at pH 7 and 10°C. Cyclic voltammogram measured with a scan rate of 100mV/s for ferredoxin 1 (solid purple line) and fitting for one, one electron transfer (dashed lines). The E_m potential was determined to be -407 mV. The PGE baseline is shown as a dashed black line. (B) Electrochemical characterization of Tk ferredoxin 3. Cyclic voltammogram measured with a scan rate of 100 mV/s for ferredoxin 3 (solid teal line) and fitting for two, one electron transfers (dashed line). The E_m potentials of the two independent fittings were determined to be -409 mV, and -363 mV, respectively. The PGE baseline is shown as a dotted black line.

DISCUSSION

Biophysical characterization of the *T. kodakarensis* Fds is an essential component to understanding central metabolism in Archaea. Thus far, protein modeling indicates each Fd having distinct structures and surface charges—suggesting that the exclusive interactions described by earlier studies does represent the landscape of electron flux in *T. kodakarensis*. Characterizing the midpoint reduction potential of each Fd validates the likelihood of each electron flux pathway, and crystal structures provide a framework for the sterics of electron transfer between donor, Fd, and acceptor. In particular, the biophysical characterization of Fd3 provides information necessary to model electron flux through H₂ metabolism. Without an accurate model of H₂ metabolism, there is no effective means of targeting this pathway for optimization and application as a potential biofuel source.

At the behest of my collaborator at the University of Nebraska, I generated SUMOylated, 6xHis tagged Fds for recombinant expression. SUMO (Small Ubiquitin-like Modifier) protein is often used to increase solubility of recombinantly expressed protein but also provides a platform to remove tags used in purification. SUMOylating proteins allows for quick purification via affinity chromatography using the external 6xHis tag and then removal of that tag using a SUMO-compatible protease, Ulp-1 peptidase. The removed SUMO-tag peptide and the target protein can then be separated using size exclusion or ion exchange chromatography.

Ultimately, while the *T. kodakarensis* Fds could be SUMOylated and affinity purified, their overall expression and purification were substantially lower yield compared to the pQE-80L-Fd vectors. The primary difference between these two vectors is their promoter regions: pETSUMO encodes a T7 promoter, while pQE-80L encodes a T5 promoter. This promoter

change could be responsible for the substantial difference in protein expression¹⁴. Alternately, this difference in expression level could be due to the relatively large size of the SUMO protein in comparison to the *T. kodakarensis* Fds (12 kDa for SUMO, 7-15 kDa for the Fds). Fusing the SUMO protein to the smaller Fd may be hindering the overall integrity of these proteins—the structure of Fds is reliant on appropriate coordination of Fe/S centers which may be prohibited by fusion to the SUMO protein. The limited yields from the pETSUMO vector ultimately ruled out the use of the pETSUMO-Fds in large-scale protein preparation for biophysics.

In crystallization condition trials, both Fd1 and Fd3 were able to form organized structures and Fd1 was able to crystalize. This crystal diffracted to a resolution of 1.1 Å. The structure of Fd1 from this crystal was found to be nearly identical to the Fd encoded in *P. furiosus*, supporting earlier work describing the close sequence and functional homology of these two proteins. This is promising for future work in using x-ray crystallography to determine the structure of the remaining two *T. kodakarensis* Fds.

The midpoint reduction potentials of the *T. kodakarensis* Fds is determined using protein-film voltammetry. This method involves coating the cathode with the purified protein of interest, then applying varying potentials (voltages) to the anode. At the potential matching the midpoint reduction potential of the protein of interest, electrons will be conducted by the adsorbed protein and measured as a spike in current at the cathode (**Fig. 24**). Current work by collaborators at Boston University provided preliminary data regarding the midpoint reduction potentials of Fd1 and Fd3.

Data for Fd3 suggests, agreeing with predictions, that Fd3 coordinates two Fe/S centers, demonstrated by the two distinct peaks at -363 mV and -409 mV. These reduction potentials, however, are incongruent with past predictions regarding its midpoint reduction potential—

which assumed Fd3 must be more reductive than H^+ (-414 mV) to facilitate electron transfer between Fd3 and MBH. Fd3 being less reductive than H^+ signals several potential scenarios, the most like regarding Fe/S cluster coordination and quality. Discussed in Chapter 1, each *T. kodakarensis* Fd was generated aerobically in supplemented media. Iron content quantitation showed incomplete saturation of Fe/S centers in Fd3, even in supplemented media. Furthermore, aerobic purification of Fe/S centered proteins can often result in the coordination of redox centers with incomplete Fe/S geometry¹⁵ potentially skewing the measured midpoint reduction potential of the purified protein. Future work on Fd3 must include anaerobic reconstitution of the protein² and repeated midpoint reduction potential assays with the reconstituted protein.

Data for Fd1 is promising as an electron donor to the Fd:NAD(P)H-ORs encoded in *T. kodakarensis* and identified as possible electron acceptors¹⁶. The reduction potential of NAD^+ is +300 mV, making the transfer of Fd1 to the Fd:NAD(P)H-ORs very favorable (-407 mV to +300 mV)¹⁷. Additionally, *T. kodakarensis* Fd1 is more reductive than *P.f.* Fd (-365 mV)¹⁸, possibly due to the difference in Fe/S centers (3Fe/4S vs 4Fe/4S), though Fe/S cluster geometry is not the sole contributor to midpoint reduction potential in proteins¹⁹. Altogether, these data suggest that the *T. kodakarensis* Fds are able to perform the roles suggested for them, substantiating their import in *T. kodakarensis* metabolism and as extremophilic electron carriers.

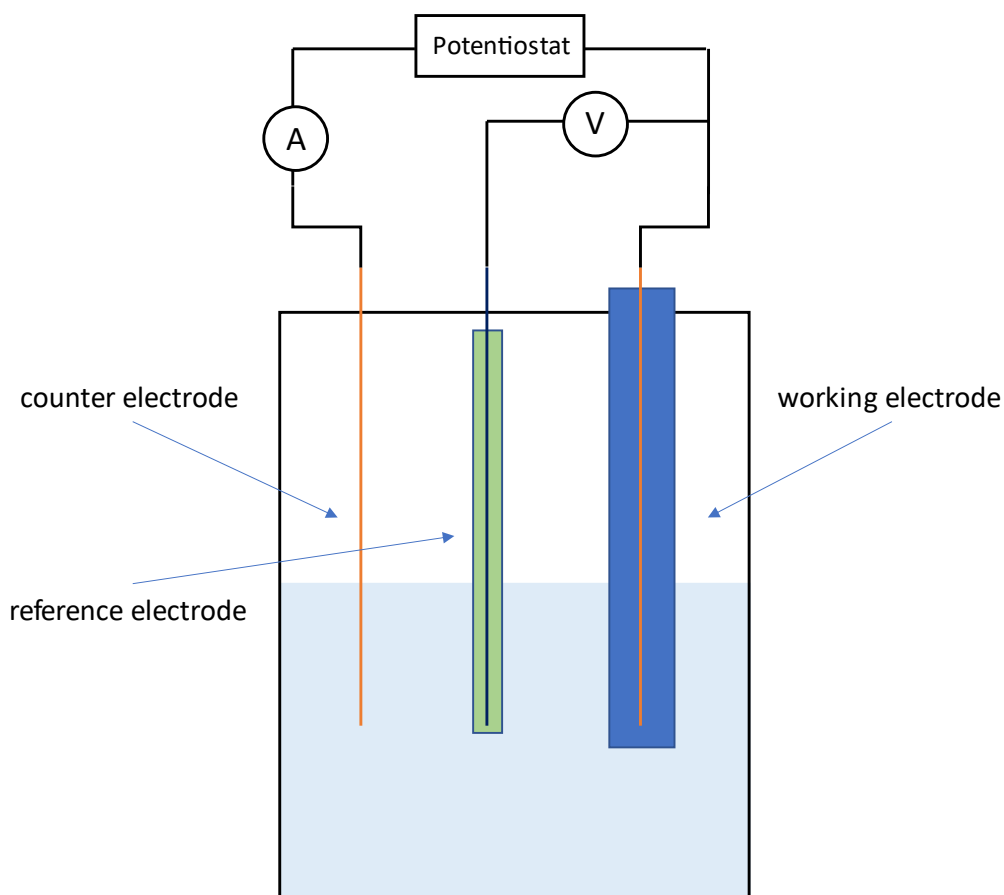


Figure 24

Diagram depicting protein-film voltammetry apparatus. The apparatus is comprised of an application electrode and a sample electrode submerged in a voltaic cell. Electrical potential (voltage) is applied at the working and reference electrodes in either cycles or pulses (pulses pictured). Current (amperage) is measured at the counter electrode. At the applied voltage matching the midpoint reduction potential of the sample, electrons will flow from the working electrode through the counter electrode, resulting in current.

MATERIALS AND METHODS

Luria-Bertani (LB) Media (x1 L)

Per 1 L: 10.0 g Tryptone, 5.0 g Bacteriological Yeast Extract, 5.0 g NaCl, 1 L double-distilled water. Add dry ingredients to 900 mL of ddH₂O, mix until fully dissolved. Add ddH₂O to final 1 L volume. Autoclave liquid cycle 20 minutes.

LB Solid Media

Per 1 L: 10.0 g Tryptone, 5.0 g Bacteriological Yeast Extract, 5.0 g NaCl, 5.0 g Agar, 1 L ddH₂O. Add dry ingredients to 900 mL ddH₂O, mix until fully dissolved. Add ddH₂O to final 1 L volume. Autoclave in 2 L Erlenmeyer flask, liquid cycle 20 minutes. After autoclaving, cool media to 45°C while stirring, add selective agents. Aliquot media into sterile plastic petri plates (approx. 25 mL/plate) under flame. Allow media to cool and solidify, invert plates and store at 4°C.

Construction of pETSUMO expression vectors

The pETSUMO expression vectors were constructed using synthesized oligonucleotides encoding for the partial upstream sequence (20 bp) from the insertion site of the pETSUMO vector Fd gene (Tk1694/Fd1, Tk1087/Fd2, or Tk2012/Fd3) a C-terminal HA/6xHis tag and a partial downstream sequence (20 bp) from the insertion site of the pETSUMO vector. These oligonucleotides were amplified using primers complementary to 35 bp of their 5'- and 3'- ends, then gel purified. The purified amplicons were used in Infusion cloning reactions with a BamHI/XhoI-digested linear pETSUMO vector, according to TakaraBio Infusion Cloning protocol. The generated plasmid was transformed into Stellar cells which were then plated on LB/Amp/Kan (100 µg/mL Amp, 50 µg/mL Kan) solid media and grown at 37°C for 12 hrs.

Colonies from this plate were resuspended in ddH₂O and then diluted 1:10 in ddH₂O and spotted onto solid LB+Amp+Kan media and grown at 37°C for 12 hrs.

Colony PCR

Colonies from the spot plates were picked and vigorously resuspended in 10 μ L ddH₂O. The following master mix was added to the cell lysate: For a total reaction volume of 50 μ L per sample: 1U of Phusion DNAP, 200 μ M of dNTPS, 1X HF buffer (NEB), 0.5 μ M forward and reverse primers, and ~250 ng of gDNA and amplified using the PCR protocol of 98°C for min, and the 35 cycles of 98°C for 10 s, 60°C for 30 s, 72°C for 30 s/kb. The samples were then run on a 1% agarose gel using gel electrophoresis at 120V for 35 mins in 1X TBE (89 mM Tris, 89 mM boric acid, 2 mM EDTA), stained for 10 minutes in 0.5 μ g/mL ethidium bromide and imaged.

Transformation of *E. coli* cells

100 μ L of BL-21 competent *E.coli* cells were thawed on ice for 20 min, and 2 μ L of ~100 μ g/mL pQE-80L-1694/1087/2012 plasmid was added to the cells. The cells incubated on ice for 30 minutes, heat shocked at 42°C for 45 s, and then rested on ice for 5 min. Using a P1000, cells were dispensed via pipetting and then spread onto LB/amp (100 μ g /mL) plates and incubated overnight at 37°C.

Expression of pQE-80L vectors in *E.coli*

One colony from previously prepared transformation plate was picked to 5 mL liquid LB media and 5 μ L of 100mg/mL ampicillin was added. Liquid culture was grown at 37°C with 200 RPM agitation until the culture reached OD₆₀₀ \geq 0.5, where 0.5 mM isopropyl β -D-1-thiogalactopyranoside (IPTG) was added to induce protein expression. Cultures were then grown at 37°C with agitation for another 3 hrs. Cells were then harvested at 20,000 xg for 5 min,

supernatant removed by pipetting, resuspended in 20mM Tris HCl pH 8.0, 1.5M NaCl, 10% glycerol (3 mL/g pellet), and mixed vigorously by pipetting. For SDS PAGE, 10 μ L of cell suspension/lysate was added to 3 μ L of 6XSDS loading dye and heat treated at 95°C for 10 min, and the total sample volume was resolved on a 4 – 20 % precast stain free SDS-PAGE gel at 170V for 35 min. Precast stain-free gels were immediately imaged.

Protein purification of Fd1

Ferredoxin proteins from *T. kodakarensis* were purified from BL-21 (DE3) *ΔiscR E. coli* cells transformed with the pQE-80L-Fd1 plasmid. Cells were grown in LB medium at 37°C with agitation and aeration in a 65L bioreactor, with 50 μ g/ml kanamycin and 100 μ g/ml ampicillin to an OD₆₀₀ of 0.5 before expression was induced with 0.5 mM isopropyl β -D-1-thiogalactopyranoside (IPTG). Cultures were grown for an additional 3 hrs at 37°C with agitation and aeration before biomass was harvested via centrifugation at 16,000 xg for 10 minutes at 4°C, resuspended and mechanically lysed (3ml/g biomass) in 20mM Tris HCl pH 8.0, 1.0M NaCl, 10% glycerol (Buffer A), heated to 85°C for 20 min to denature host proteins, and clarified by centrifugation (~20,000 xg, 15 min, 4°C). Heat-treated clarified cell lysates were resolved through a 5ml HiTrap Chelating column (Cytiva) charged with 1 M NiSO₄, at 1 mL/min flowrate. The flow through was collected in a 200 mL glass beaker covered with aluminum foil. The bound material on the column was washed with 5 column volumes of Buffer A or until the UV₂₈₀ signature on the chromatogram reached baseline levels again. Bound material was eluted with a linear gradient from 0 - 250 mM imidazole dissolved in 20 mM Tris HCl pH 8.0, 100 mM NaCl, 10% glycerol (Buffer B). Eluent was collected in 1 mL fractions. Fractions containing pure Fd were identified by SDS-PAGE, pooled, and underwent buffer exchange into Buffer A using 3.5 kDa MWCO dialysis tubing first for 4 hrs at 4°C in 4 L Buffer A, then for 8 hrs at 4°C

in 2 L Buffer A. The buffer-exchanged material was then passed over a 1 mL HiTrap Chelating column (Cytiva) charged with 1 M NiSO₄, using the same flowthrough and washing scheme as the 5 mL column. Bound material was eluted using an isocratic elution at 100% Buffer B.

Fractions containing pure Fd were pooled and exchanged into 5 mM Tris HCl pH 8.0, 0.1 M NaCl (crystal storage buffer) using a 3 kDa MWCO centrifuge filter and reduced to a volume of ≤2 mL. This material was passed over an S-100 sephacryl size exclusion column (Cytiva) at 0.25 mL/min flowrate, with all flowthrough collected as 1 mL fractions. Fractions containing pure Fd were identified via SDS-PAGE and colorimetric identification (Fd-containing fractions are dark brown in color), pooled, quantitated via Bradford Assay and stored at 4°C.

Protein purification of Fd2

Ferredoxin proteins from *T. kodakarensis* were purified from BL-21 (DE3) *ΔiscR E. coli* cells transformed with the pQE-80L-Fd2 plasmid. Cells were grown in LB medium at 37°C with agitation and aeration in a 65L bioreactor, with 50ug/ml kanamycin and 100 μg/ml ampicillin to an OD₆₀₀ of 0.5 before expression was induced with 0.5 mM isopropyl β-D-1-thiogalactopyranoside (IPTG). Cultures were grown for an additional 3 hrs at 37°C with agitation and aeration before biomass was harvested via centrifugation at 16,000 xg for 10 minutes at 4°C, resuspended and mechanically lysed (3ml/g biomass) in 20mM Tris HCl pH 8.0, 1.0M NaCl, 10% glycerol (Buffer A), heated to 85°C for 20 min to denature host proteins, and clarified by centrifugation (~20,000 xg, 15 min, 4°C). Heat-treated clarified cell lysates were resolved through a 5ml HiTrap Chelating column (Cytiva) charged with 1 M NiSO₄, at 1 mL/min flowrate. The flow through was collected in a 200 mL glass beaker covered with aluminum foil. The bound material on the column was washed with 5 column volumes of Buffer A or until the UV₂₈₀ signature on the chromatogram reached baseline levels again. Bound material was eluted

with a linear gradient from 0 - 250 mM imidazole dissolved in 20 mM Tris HCl pH 8.0, 100 mM NaCl, 10% glycerol (Buffer B). Eluent was collected in 1 mL fractions. Fractions containing pure Fd were identified by SDS-PAGE, pooled, and underwent buffer exchange into Buffer A using 3.5 kDa MWCO dialysis tubing first for 4 hrs at 4°C in 4 L Buffer A, then for 8 hrs at 4°C in 2 L Buffer A. The buffer-exchanged material was then passed over a 1 mL HiTrap Chelating column (Cytiva) charged with 1 M NiSO₄, using the same flowthrough and washing scheme as the 5 mL column. Bound material was eluted using an isocratic elution at 100% Buffer B. Fractions containing pure Fd were pooled and exchanged into 5 mM Tris HCl pH 8.0, 0.1 M NaCl (crystal storage buffer) using a 3 kDa MWCO centrifuge filter and reduced to a volume of ≤ 2 mL. This material was passed over an S-100 sephacryl size exclusion column (Cytiva) at 0.25 mL/min flowrate, with all flowthrough collected as 1 mL fractions. Fractions containing pure Fd were identified via SDS-PAGE and colorimetric identification (Fd-containing fractions are dark brown in color), pooled, quantitated via Bradford Assay and stored at 4°C.

Protein purification of Fd3

Ferredoxin proteins from *T. kodakarensis* were purified from BL-21 (DE3) *ΔiscR E. coli* cells transformed with the pQE-80L-Fd3 plasmid. Cells were grown in LB medium at 37°C with agitation and aeration in a 65L bioreactor, with 50ug/ml kanamycin and 100 μg/ml ampicillin to an OD₆₀₀ of 0.5 before expression was induced with 0.5 mM isopropyl β-D-1-thiogalactopyranoside (IPTG). Cultures were grown for an additional 3 hrs at 37°C with agitation and aeration before biomass was harvested via centrifugation at 16,000 xg for 10 minutes at 4°C, resuspended and mechanically lysed (3ml/g biomass) in 20mM Tris HCl pH 8.0, 1.0M NaCl, 10% glycerol (Buffer A), heated to 85°C for 20 min to denature host proteins, and clarified by centrifugation (~20,000 xg, 15 min, 4°C). Heat-treated clarified cell lysates were

resolved through a 5ml HiTrap Chelating column (Cytiva) charged with 1 M NiSO₄, at 1 mL/min flowrate. The flow through was collected in a 200 mL glass beaker covered with aluminum foil. The bound material on the column was washed with 5 column volumes of Buffer A or until the UV₂₈₀ signature on the chromatogram reached baseline levels again. Bound material was eluted with a linear gradient from 0 - 250 mM imidazole dissolved in 20 mM Tris HCl pH 8.0, 100 mM NaCl, 10% glycerol (Buffer B). Eluent was collected in 1 mL fractions. Fractions containing pure Fd were identified by SDS-PAGE, pooled, and underwent buffer exchange into Buffer A using 3 kDa MWCO centrifuge filter at 4,000 xg at a 1:2 dilution until total imidazole content was <1%. The buffer-exchanged material was then passed over a 1 mL HiTrap Chelating column (Cytiva) charged with 1 M NiSO₄, using the same flowthrough and washing scheme as the 5 mL column. Bound material was eluted using an isocratic elution at 100% Buffer B. Fractions containing pure Fd were pooled and exchanged into 5 mM Tris HCl pH 8.0, 0.1 M NaCl (crystal storage buffer) using a 3 kDa MWCO centrifuge filter and reduced to a volume of ≤2 mL. This material was passed over an S-100 sephacryl size exclusion column (Cytiva) at 0.25 mL/min flowrate, with all flowthrough collected as 1 mL fractions. Fractions containing pure Fd were identified via SDS-PAGE and colorimetric identification (Fd-containing fractions are dark brown in color), pooled, quantitated via Bradford Assay and stored at 4°C.

Iron quantitation assay

The following iron quantitation protocol was adapted from Reimer et al., 2004: FeCl₃ standards were made in 10 mM HCl (0 μM, 1.5 μM, 3 μM, 7.5 μM, 15 μM, 22.5 μM, 30 μM, 45 μM) to a total volume of 1 mL. In a 1.7 mL Eppendorf tube, 300 μL of standard was mixed with 300 μL Buffer B (25 mM Tris HCl pH 8.8, 0.1 M NaCl, 250 mM Imidazole, 10% glycerol) and 300 μL Releasing agent (1.4 M HCl, 4.5% KMnO₄). The reaction was incubated at 60°C in a dry bath in

a chemical vent hood for 2 hrs. The reactions were then removed from the dry bath and allowed to cool to room temperature. 90 μL of Detection agent (6.5 mM ferrozine, 6.5 mM Neocuproine, 2.5 M $(\text{NH}_4)_2\text{SO}_4$, 1 M ascorbic acid in H_2O) was added to the reactions and incubated at room temperature for 30 min. Absorbance at 550 nm was measured for each standard. To quantitate iron in the purified protein samples: 300 μL of purified protein was mixed with 300 μL of releasing agent, incubated at 60°C in a dry bath in a chemical vent hood for 2 hrs then allowed to cool to room temperature. 90 μL of detection agent was added to the reaction and incubated at room temperature for 30 min. Absorbance at 550 nm was recorded for each sample.

Isolation of plasmid DNA from *E. coli* cells (All buffers from Zymogen Plasmid Miniprep kit)

10 mL of liquid culture was spun down in 1.7 mL increments in 2, 1.7 mL Eppendorf tubes at 20,000 xg for 5 min. Supernatant was snapped out of tubes. The remaining pellet was resuspended in 200 μL P1 buffer and vortexed 30 s. 200 μL of P2 buffer was added, the tubes vortexed for 5 s, shaken vigorously, then incubated at room temperature for 1-2 minutes. 400 μL of P3 buffer was added and mixed via pipette until the solution was opaque and yellow. The tubes were spun at 20,000 xg for 7 min. The supernatant was transferred to a plasmid prep column in a collection tube. The columns were spun at 20,000 xg for 30 s. 400 μL of Plasmid Wash Buffer was added to the columns, which were then spun at 20,000 xg for 1 min. The flowthrough was discarded, then the columns were dried by spinning at 20,000 xg for 1 min. The columns were then transferred to 1.7 mL Eppendorf tubes. 16 μL of 10 mM Tris HCl pH 8.0 was added to the column and incubated for 5 min at room temperature before being spun at 20,000 xg for 1 min. The previous step was repeated for a final flowthrough volume of 32 μL . The isolated plasmid was then quantitated via fluorometry.

Generation of competent BL-21 $\Delta iscR$ cells

A plate of BL-21 $\Delta iscR$ cells was sent to the author by collaborators. A colony was picked from the plate to 5 mL liquid LB media and incubated at 37°C with shaking for 1 hr. 5 μ L of 50 mg/mL kanamycin was added to the 5 mL culture, which was then grown to an $OD_{600} = 0.5$. The entire 5 mL culture was then transferred under flame to sterile 1 L liquid LB in a 2 L flask and grown at 37°C with shaking to an $OD_{600} = 0.3-0.4$. The culture was then rapidly cooled by submerging the flask in an ice-water bath for 5-10 min, then divided into 4, 250 mL aliquots in pre-chilled 500 mL centrifuge bottles. The bottles were spun at 12,500 xg for 8 min at 4°C. The supernatant was carefully decanted. On ice, the pellets were resuspended in 100 mM $CaCl_2$ to a combined final volume of 200 mL. The cell suspension was transferred to a clean, pre-chilled 500 mL centrifuge bottle and spun at 12,500 xg for 8 min at 4°C. The supernatant was carefully decanted. The remaining cell pellet was carefully resuspended in 100 mM $CaCl_2$, 15% glycerol to a final volume of 100 mL. The suspension was redistributed to 4, 50 mL pre-chilled centrifuge tubes and incubated on ice for 4-6 hrs. The tubes were spun at 18,500 xg for 8 min at 4°C. The supernatant was carefully decanted, and the remaining cell pellet gently resuspended in 3 mL of pre-chilled 100 mM $CaCl_2$, 15% glycerol. The suspension was divided into 50 μ L aliquots in 1.7 mL Eppendorf tubes and snap-frozen in liquid nitrogen. The frozen aliquots were then stored at -80°C.

Protein-film voltammetry

Electrochemical studies of *Tk* ferredoxin 1 and 3 were achieved using an Ecochemie PGSTAT30 potentiostat under a predominantly N_2 atmosphere of the MBraun Labmaster glovebox to create an anoxic environment favorable for FeS cluster handling. A three- electrode setup was used consisting of a standard calomel electrode as the reference and a platinum wire as a counter

electrode. The temperature (10°C) at which experiments were carried out was maintained by a water jacket. The electrochemical data was reported relative to the standard hydrogen electrode. Baseline scans were collected using pyrolytic graphite edge (PGE) electrode that was prepared via mechanical polishing with sandpaper, followed by 1.0 μM alumina. Electrodes were placed in an electrochemical cell filled with a multicomponent buffer solution (10 mM HEPES, MOPS, CHES, CAPS, TAPS (pH 7.0)), supplemented with 200 mM NaCl. An aliquot (8 μL) of the protein was loaded onto an electrode along with 2 μL of 2.5 mg/mL polymyxin sulfate and allowed to incubate for 3 mins, prior to immersing the electrode in the electrochemical cell to measure cyclic voltammograms (CV). The CV scans were recorded at 10°C with scan rates of either 50 or 100 mV/s. Signals obtained were analyzed by correction of the non-Faradaic component of the current from raw data, using the QSoaS package.

Crystallography

Initial crystallization screening was done at room temperature by sitting-drop vapor diffusion, followed by optimization of the crystal hits. The crystal used for diffraction data collection was obtained by mixing 0.7ul of Fd1 at [concentration] mg/ml in [buffer] with an equal volume of reservoir solution containing 2.6M ammonium sulfate, 0.3 M NaCl, and 0.1M sodium cacodylate pH 6.8. The crystal was soaked in the reservoir solution with 20% glycerol for cryoprotectant before flash-freezing in liquid nitrogen. X-ray diffraction data were collected at Beamline 12-2 of the Stanford Synchrotron Radiation Lightsource at Se K-edge (12,658 eV) from a single crystal maintained at 100 K using a 6M Pixel Array Detector. The diffraction data were indexed, integrated and scaled using the XDS software package. Model building and structure refinement were performed in COOT and CCP4.

Table 4: pETSUMO Expression Vectors

Vector	Description
pETSUMO-Tk1694	<i>E. coli</i> expression vector encoding a C-terminally tagged 6xHis/SUMO Fd1
pETSUMO-Tk1087	<i>E. coli</i> expression vector encoding a C-terminally tagged 6xHis/SUMO Fd2
pETSUMO-Tk2012	<i>E. coli</i> expression vector encoding a C-terminally tagged 6xHis/SUMO Fd3

Table 5: List of Primers used in pETSUMO Vector Construction

Name	Sequence (5'-3')	Description
pETSUMOF	CACGGGCCTGCCACCAT ACCCACGCCGAAACAAG C	Primer encoding for upstream region of pETSUMO multiple cloning site
pETSUMOR	CCAAGGGGTTATGCTAG TTATTGCTCAGCGGTGG CA	Primer encoding for downstream region of pETSUMO multiple cloning site
Infusion_SUMOFd1F	AGAGAACAGATTGGTGG ATCCATGGCTTGGAAAGG T	Primer with 35 bp homology to 5' end of SUMO-Fd1 oligonucleotide; used for insert amplification
Infusion_SUMOFd1R	TCTTTACCAGACTCGAGT CAGGCCTCTTCGAGGGT	Primer with 35 bp homology to 3' end of SUMO-Fd1 oligonucleotide; used for insert amplification
Infusion_SUMOFd2F	AGAGAACAGATTGGTGG ATCCATGCCGGAAGA T	Primer with 35 bp homology to 5' end of SUMO-Fd2 oligonucleotide; used for insert amplification
Infusion_SUMOFd2R	CTTTACCAGACTCGAGT CATTCGCTCACCTCCAG G	Primer with 35 bp homology to 3' end of SUMO-Fd2 oligonucleotide; used for insert amplification

Infusion_SUMOFd3F	AGAGAACAGATTGGTGG ATCCATGGCCGATGTTA A	Primer with 35 bp homology to 5' end of SUMO-Fd3 oligonucleotide; used for insert amplification
Infusion_SUMOFd3R	TCTTTACCAGACTCGAGT CAAGGATTGAACACGCT	Primer with 35 bp homology to 3' end of SUMO-Fd3 oligonucleotide; used for insert amplification
SUMO-Fd1	AGAGAACAGATTGGTGG ATCCATGGCTTGGAAGG TAAGTGTGATGTCGAC ACCTGCATTGGAGATGC CA6TCTGTGCTAGCCTCT GCCCGGACGTCTTTGAG ATGGGCGACGACGGCAA GGCCACCCGGTAGTTG AGACCACCGACCTTGAC TGCGCCCAGGAGGCCGC CGAGGCCTGCCCGGTCG GCGCTATAACCCTCGAA GAGGCCTGACTCGAGTC TGGTAAA	Synthesized oligonucleotide encoding C-terminally 6xHis tagged Fd1, used as insert for Infusion Cloning
SUMO-Fd2	GAGAACAGATTGGTGG TCCATGCCGAGAGAAGAT TAAAGTGGTCGTGAACG AAGATAGATGCTATCTC TGCGGCGGTTGTGCCGG TGTCTGCCCGACACTCG CGATAGAGGTGCACTCA ACAGGCTGGGAGTTCCT TCAAGACAAGTGCATAA GCTGCAGGATATGCATC AACGCCTGCCCCGTTGG AGCCCTGAGCGCTAAAC CCCTGGAGGTGAGCGAA TGA CTGAGTCTGGTAA AGAAACC	Synthesized oligonucleotide encoding C-terminally 6xHis tagged Fd2, used as insert for Infusion Cloning
SUMO-Fd3	AGAGAACAGATTGGTGG ATCCATGGCCGATGTTA AGGCTCCCGTCATCGGG AGGGACGCTCTCGGGAG AGAGGTTAAGGACCTAA GCGTTATTCCGTGGTGG GGGGTTGATAGAAAGGA GATAGAGTGGTATCCAA	Synthesized oligonucleotide encoding C-terminally 6xHis tagged Fd3, used as insert for Infusion Cloning

	AGATAAACTACAGCGTC TGCGCCCGCTGTGGCCTT TGCTTTATAACCTGTGGA CGGAGGGTCTTCGACTG GGACACCGAAGAGGGA AAGCCCGTTGTTGCGAG GCCCTACAACCTGCATGG TTGGTTGCAACACTTG TG CAATCCTCTGCCCATGTA ACGCCATAGAGTTCCCA CCAAAGGAGTACGTAA GAAGCTCGTCATAGAGC ACGGGATCATAAGAAAG GCCTTTGAGATAACAAA GCCCCTGACGAAAAAGA AGGAAGAAAGCACGAA CGGAGCTGAGAGCGTGT TCAATCCTTGACTCGAGT CTGGTAAA	
--	--	--

Table 6: pQE-80L Expression Vectors

Vector	Description
pQE-80L-Tk1694	<i>E. coli</i> expression vector encoding a C-terminally tagged 6xHis/HA Fd1
pQE-80L-Tk1087	<i>E. coli</i> expression vector encoding a C-terminally tagged 6xHis/HA Fd2
pQE-80L-Tk2012	<i>E. coli</i> expression vector encoding a C-terminally tagged 6xHis/HA Fd3

Table 7: List of *E. coli* strains

Name	Description
BL-21	Expression line of <i>E. coli</i>
BL-21 ΔiscR	Expression line of <i>E. coli</i> encoding for functional <i>suf</i> operon and deletion of <i>iscR</i> operon
Stellar	Line of <i>E. coli</i> used for large-volume plasmid replication

REFERENCES

1. Ewen, K. M., Ringle, M. & Bernhardt, R. Adrenodoxin-A versatile ferredoxin. *IUBMB Life* **64**, 506–512 (2012).
2. Tsaousis, A. D. On the Origin of Iron/Sulfur Cluster Biosynthesis in Eukaryotes. *Front. Microbiol.* **10**, (2019).
3. Baussier, C. *et al.* Making iron-sulfur cluster: structure, regulation and evolution of the bacterial ISC system. *Advances in Microbial Physiology* **76**, 1-39 (Elsevier Ltd, 2020).
4. Meyer, J. Iron–sulfur protein folds, iron–sulfur chemistry, and evolution. *JBIC J. Biol. Inorg. Chem.* **13**, 157–170 (2008).
5. Corless, E. I., Mettert, E. L., Kiley, P. J. & Antony, E. Elevated Expression of a Functional Suf Pathway in Escherichia Sulfur Cluster-Containing Protein. *J. Bacteriol.* **202**, 1–11 (2020).
6. Braymer, J. J., Freibert, S. A., Rakwalska-Bange, M. & Lill, R. Mechanistic concepts of iron-sulfur protein biogenesis in Biology. *Biochim. Biophys. Acta - Mol. Cell Res.* **1868**, 1-28 (2021).
7. Ren, X. *et al.* Identification of an Intermediate Form of Ferredoxin That Binds Only Iron Suggests That Conversion to Holo-Ferredoxin Is Independent of the ISC System in Escherichia coli. *Appl. Environ. Microbiol.* **87**, 1–16 (2021).
8. Vuorijoki, L., Tiwari, A., Kallio, P. & Aro, E. M. Inactivation of iron-sulfur cluster biogenesis regulator SufR in Synechocystis sp. PCC 6803 induces unique iron-dependent protein-level responses. *Biochim. Biophys. Acta - Gen. Subj.* **1861**, 1085–1098 (2017).
9. Martin, W. F. & Thauer, R. K. Energy in Ancient Metabolism. *Cell* **168**, 953–955 (2017).

10. Atkinson, J. T., Campbell, I., Bennett, G. N. & Silberg, J. J. Cellular Assays for Ferredoxins: A Strategy for Understanding Electron Flow through Protein Carriers That Link Metabolic Pathways. *Biochemistry* **55**, 7047–7064 (2016).
11. Hanke, G. & Mulo, P. Plant type ferredoxins and ferredoxin-dependent metabolism. *Plant, Cell Environ.* **36**, 1071–1084 (2013).
12. Schäfer, G., Engelhard, M. & Müller, V. Bioenergetics of the Archaea. *Microbiol. Mol. Biol. Rev.* **63**, 570–620 (1999).
13. Brereton, P. S., Verhagen, M. F. J. M., Zhou, Z. H. & Adams, M. W. W. Effect of iron-sulfur cluster environment in modulating the thermodynamic properties and biological function of ferredoxin from *Pyrococcus furiosus*. *Biochemistry* **37**, 7351–7362 (1998).
14. Thomson, N. M. & Pallen, M. J. Restoration of wild-type motility to flagellin-knockout *Escherichia coli* by varying promoter, copy number and induction strength in plasmid-based expression of flagellin. *Current Research in Biotechnology* **2**, 45–52 (2020).
15. Imai, T. *et al.* Characterization and cloning of an extremely thermostable, *Pyrococcus furiosus*-type 4Fe ferredoxin from *Thermococcus profundus*. *Journal of Biochemistry* **130**, 649–655 (2001).
16. Burkhart, B. W., Febvre, H. P. & Santangelo, T. J. Distinct physiological roles of the three ferredoxins encoded in the hyperthermophilic archaeon *Thermococcus kodakarensis*. *mBio* **10**, 1–17 (2019).
17. Farrington, J. A., Land, E. J. & Swallow, A. J. *BBA Report the one-electron reduction potentials of NAD*. *Biochimica et Biophysica Acta* **590**, 273–276 (1980).
18. Park, J. B., Fan, C., Hoffman, B. M. & Adams, M. W. W. Potentiometric and electron nuclear double resonance properties of the two spin forms of the [4Fe-4S]⁺ cluster in the

novel ferredoxin from the hyperthermophilic archaeobacterium *Pyrococcus furiosus*.

Journal of Biological Chemistry **266**, 19351–19356 (1991).

19. Atkinson, J. T., Campbell, I., Bennett, G. N. & Silberg, J. J. Cellular Assays for Ferredoxins: A Strategy for Understanding Electron Flow through Protein Carriers That Link Metabolic Pathways. *Biochemistry* **55**, 7047–7064 (2016).

CHAPTER 3: TETHERING OF FERREDOXIN 3 TO THE MEMBRANE BOUND HYDROGENASE IMPACTS HYDROGEN METABOLISM

Thermococcus kodakarensis produces hydrogen gas via electron flux to MBH. Optimization of hydrogen production is extensively discussed in the literature, focusing on differences in hydrogen yields from differing starting substrates^{1,2} as well as the role of MBH and the A₁A₀ATPase. Members of the *Thermococcales* utilize a modified Embden-Meyerhof Parnas pathway featuring GAPOR, a GAP:ferredoxin oxidoreductase³. This system channels electron flux towards ferredoxin-dependent reactions (including hydrogen production) rather than to the direct phosphorylation of ADP to ATP. Additional work demonstrated that upregulation of MBH or the A₁A₀ ATPase found in the membrane of *T. kodakarensis* increased hydrogen output proportional to an increase in provided starting substrates^{4,5}. Biological hydrogen production offers an alternative to current hydrogen generation methods that largely involve the oxidation of extended hydrocarbons⁶. Aslam¹ discussed the use of *T. kodakarensis* as a hydrogen-producing chitin biorefinery but did little demonstrate the efficiency of *T. kodakarensis* as a source of biological hydrogen beyond showing small H₂ gas output increase using chitin as a starting substrate compared to long-chain carbohydrates.

Investigation of the role of Fd3 in hydrogen biosynthesis was facilitated by the development of Fd3:MBH fusion proteins, wherein Fd3 was C-terminally linked to either MBH-N or N-terminally linked to MBH-J, cytosolic subunits of the MBH complex. MBH-N coordinates the Fe/S center responsible for electron transfer from Fd3 to MBH⁷. Two subunits of MBH were targeted for tethering because the steric interaction of electron transfer between MBH and Fd3 is yet unknown. These fusion proteins were introduced to a *T. kodakarensis* strain

lacking the locus for Fd3 (Δ TK2012), meaning the only expression of Fd3 is linked to expression of MBH as part of the tether constructs.

Earlier work describing the physiological roles of each Fd in *T. kodakarensis* relied on lasting interactions between a tagged Fd and its partners through the processes of affinity chromatography and Multidimensional Protein Identification Technology (MudPIT) for identification and mapping of the Fd interactome, leaving transient interactions unidentified. Data from that same work suggests potential alternative pathways for Fd3 in +S° conditions⁸. Tethering of Fd3 to MBH limits Fd3 electron donation only to MBH, effectively channeling all Fd3-mediated electron flux to hydrogen biosynthesis. It is essential to characterize the viability of Fd3:MH tethers in +S° and S°-independent conditions. Additionally, tethering of Fd3 to MBH increases the local concentration of Fd3 to MBH, potentially increasing electron flux through MBH and thus increasing H₂ gas output. Analysis of hydrogen biosynthesis was done using a joint growth curve/gas chromatography technique, wherein cultures were monitored for cell growth while the headspace of each culture was sampled for hydrogen. These two metrics were used to calculate Ω , the standard measure for hydrogen biosynthesis⁹.

Standard methods for hydrogen gas production rely largely on the oxidation of hydrocarbons for large yields⁶. The metabolic schema utilized by *T. kodakarensis* offers ample alternative substrates for hydrogen biosynthesis^{8,9,10}. Identifying novel systems for hydrogen biosynthesis that are independent of hydrocarbon oxidation are valuable as low-impact methods for the generation of biofuels and increase the viability of hydrogen as an alternative fuel source^{11,12}.

My thesis examines the role of Fd3 on hydrogen production via a Fd3:MBH tether in a Fd3 deletion background, thus restoring Fd3 to the *T. kodakarensis* genome in the same operon as its sole electron acceptor. By tethering Fd3 to MBH, all Fd3-mediated electron flux is exclusively channeled to MBH, potentially increasing the availability of reducing electrons to MBH for hydrogen gas evolution.

Figures 25 & 26 shows the desired final structure of each Fd3:MBH tether in *T. kodakarensis*. These *T. kodakarensis* strains were characterized using growth phenotype and hydrogen production assays via tandem OD₆₀₀ measurements and direct sampling of culture headspace using gas chromatography.

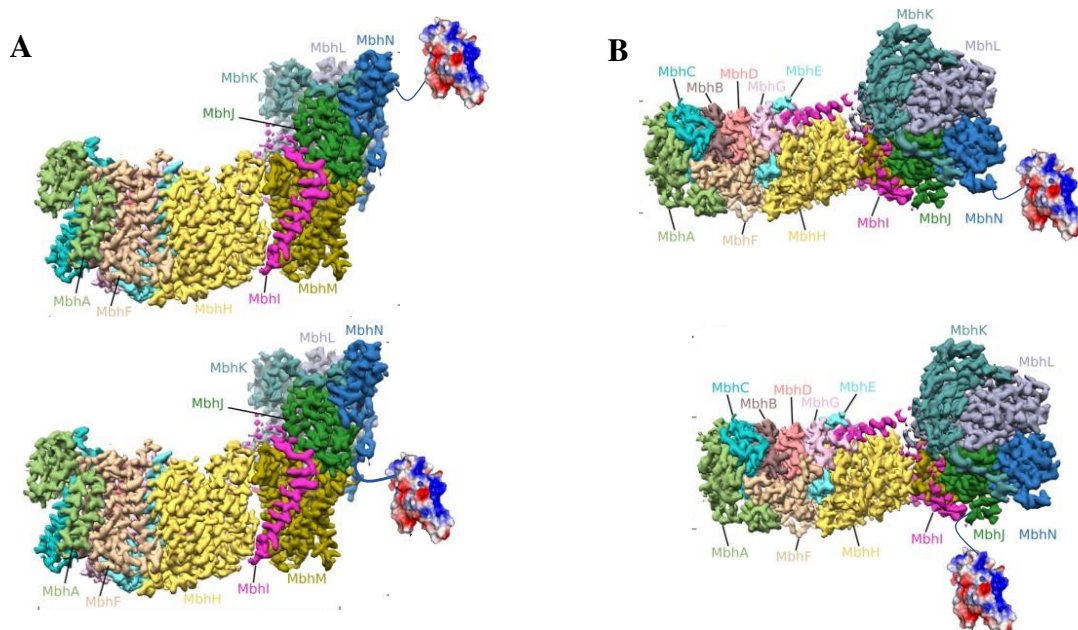


Figure 25

Adapted from Yu et al., 2018¹³ (MBH), Burkhart et al., 2019⁸ (Fd3)

Cartoon depiction of the structures of the MBH-N:Fd3 (B) and Fd3:MBH-J (A) tethers. Fd3 was tethered to a cytosolic subunit of MBH using a 5 glycine linker domain. Fd3 is tagged with a 6xHis-HA tag on the terminus opposite the linker domain for each tether protein.

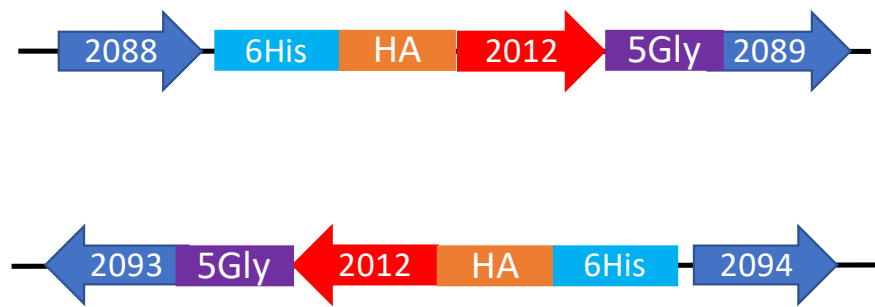


Figure 26

General structure of the synthetic oligonucleotide used in the construction of the Fd3:MBH tethers. Both oligonucleotides encode for a partial downstream sequence as well as a partial sequence of the tether locus of interested (TK2089 or TK2093). The 6xHis:HA-tagged Fd3 (TK2012) is in-frame with the target locus.

RESULTS

Cloning of the Fd:MBH tethers:

The oligonucleotides encoding for the Fd3:MBH tethers were successfully cloned into the non-replicative genome-editing plasmid pTS700 using Quikchange PCR (**Fig. 27**), identified via diagnostic colony PCR (**Fig. 28**) and confirmed using Sanger sequencing of the gel-isolated fragment.

Construction of Tether 1 *T. kodakarensis* strain:

The tether strain was made using two separate homologous recombination events between the parent *T. kodakarensis* genome (Δ 2012) and the respective plasmid (pTS700-2012:2089). The initial recombination event was confirmed using diagnostic PCR (**Fig. 29, 30**), the secondary recombination event was identified using diagnostic PCR (**Fig. 31**) and later confirmed using whole-genome sequencing (**Fig. 32**).

Construction of Tether 2 *T. kodakarensis* strain:

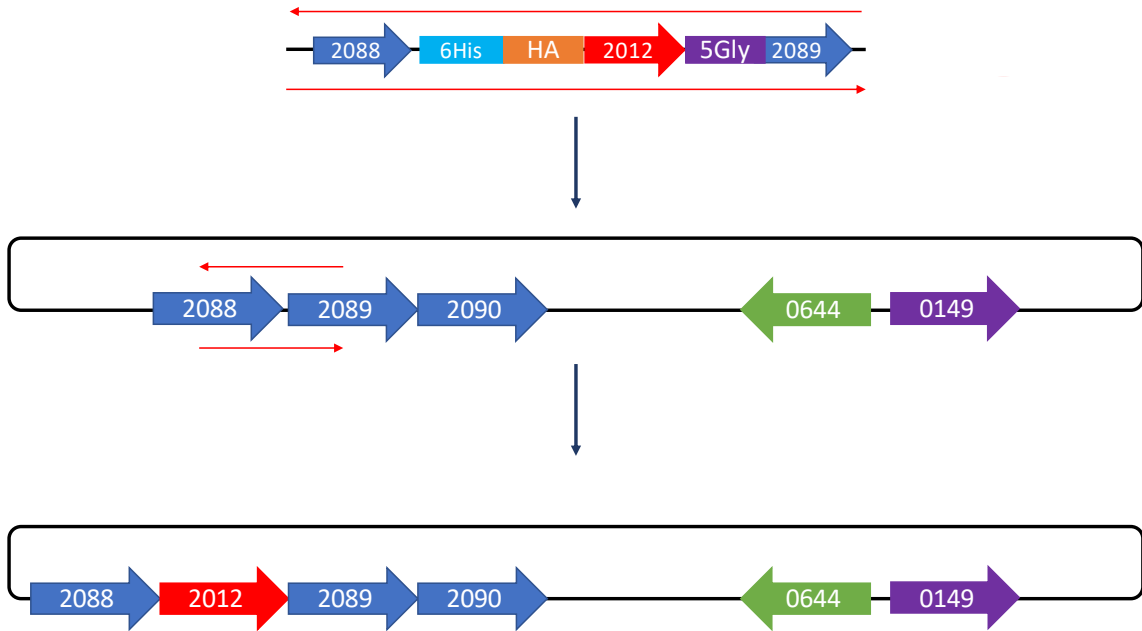
The tether strains were made using two separate homologous recombination events between the parent *T. kodakarensis* genome (Δ 2012) and the respective plasmid (pTS700-2093:2012). The initial recombination event was confirmed using diagnostic PCR (**Fig. 33, 34**), the secondary recombination event was identified using diagnostic PCR (**Fig. 35**) and later confirmed using whole-genome sequencing (**Fig. 36**).

The Fd3:MBH tethers are retained *in-vivo* in *T. kodakarensis*, shown in **Figure 37 & 38** via anti-HA western blot.

Characterization of the Fd3:MBH tether strains:

The sequence-confirmed, retained Fd3:MBH tether strains were characterized for growth phenotypes compared to the parent Δ TK2012 *T. kodakarensis* and TS559 strains. Tethering of Fd3 to either MBH-J or MBH-N restored sulfur-independent growth compared to Δ TK2012 (**Fig. 39**). Endpoint hydrogen measurements revealed tethering Fd3 to MBH-J decreased hydrogen production (**Fig. 40**). Tethering Fd3 to MBH-N decreased hydrogen production (**Fig 40**).

A



B

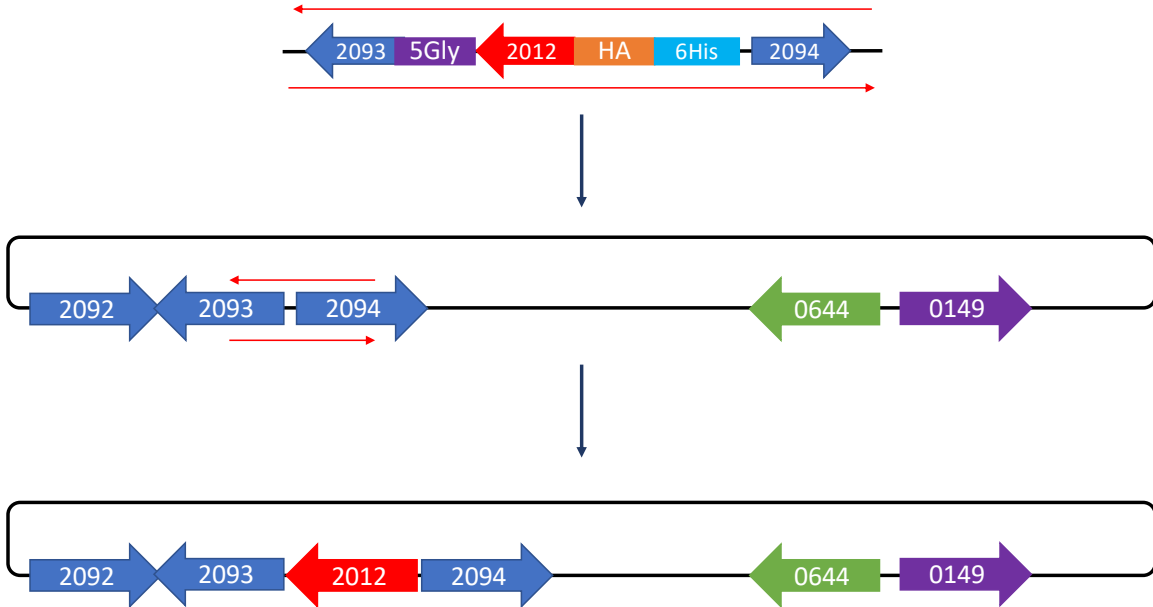


Figure 27

(A) *Diagram depicting the Quikchange PCR reaction used to generate the Fd3:MBH-J tether vector. The oligonucleotide described in Fig. 25 was used as long Quikchange PCR primers to anneal to the parent plasmid, and then the insert was introduced to the parent plasmid during extension.* (B) *Diagram depicting the Quikchange PCR reaction used to generate the Fd3:MBH-N tether vector. The oligonucleotide described in Fig. 25 was used as long Quikchange PCR primers to anneal to the parent plasmid, and then the insert was introduced to the parent plasmid during extension.*

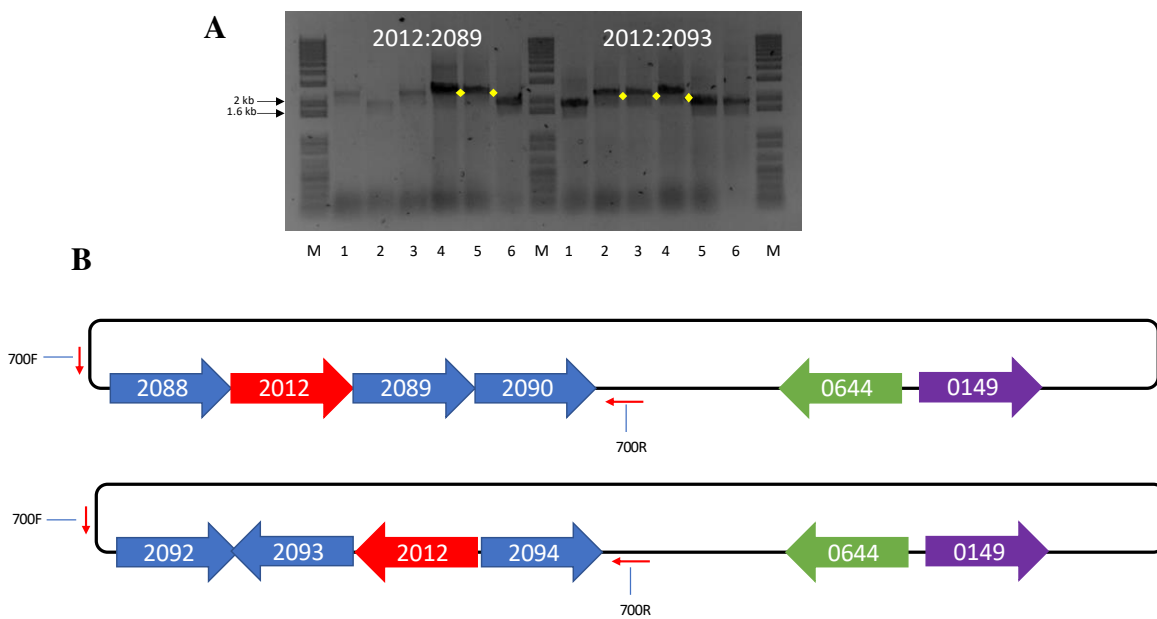


Figure 28

(A) Colony PCR results for the Fd3:MBH tether vectors. Highlighted in yellow are bands whose sizes match the expected size for the generated amplicon. (B) Diagram depicting the primer positions for each amplicon from the Fd3:MBH tethers.

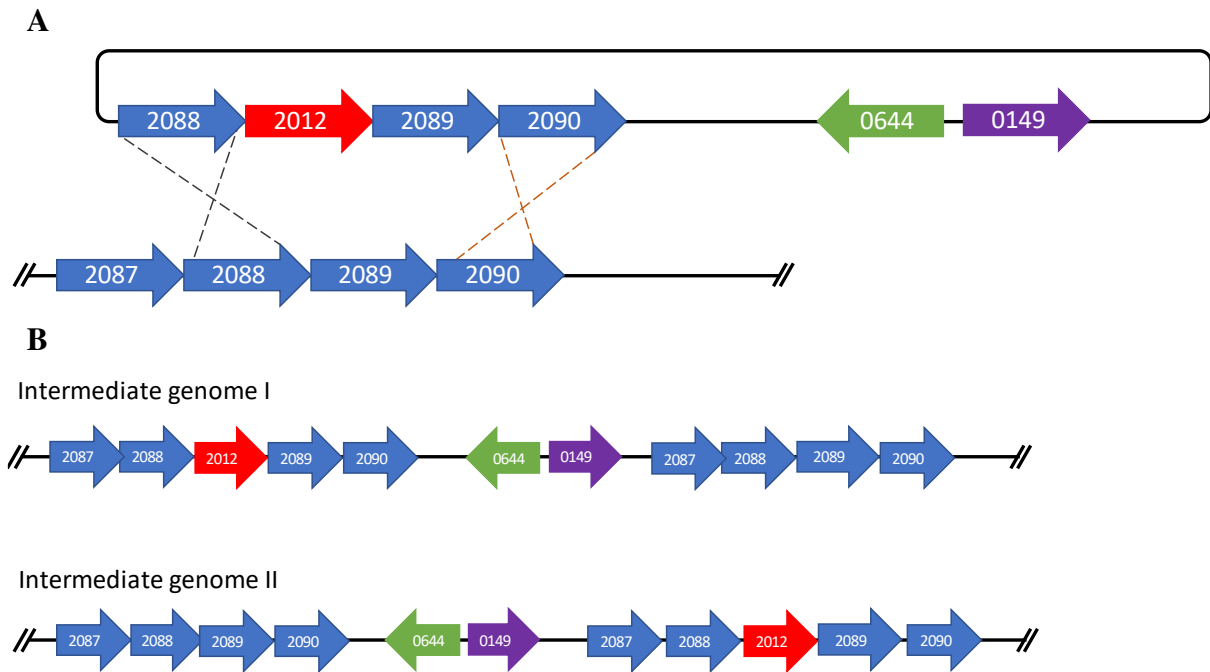


Figure 29

(A) Diagram depicting the two possible recombination events between the *Fd3:MBH-J* vector and the Δ TK2012 *T. kodakarensis* parent genome. (B) The resulting genotypes from the two recombination events.

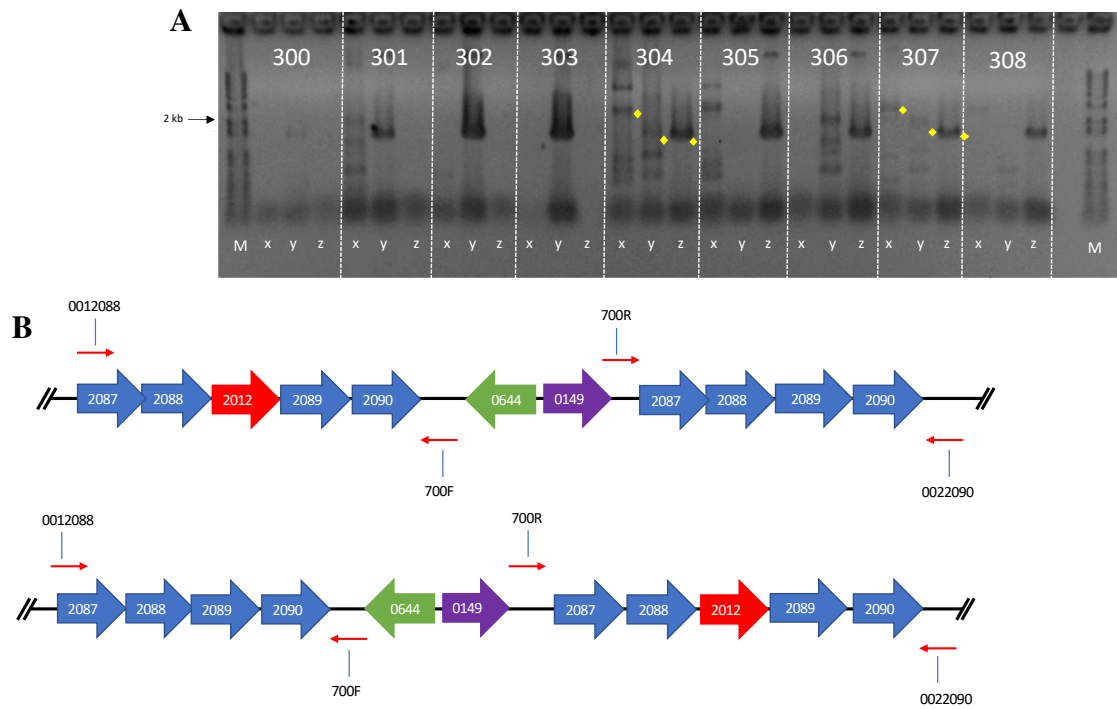


Figure 30

(A) Diagnostic PCR results from Δ TK2012 *T. kodakarensis* transformants. Highlighted in yellow are bands matching the expected sizes for the amplicons. (B) Diagram of the primer positions on each possible genotype to result in the shown amplicons.

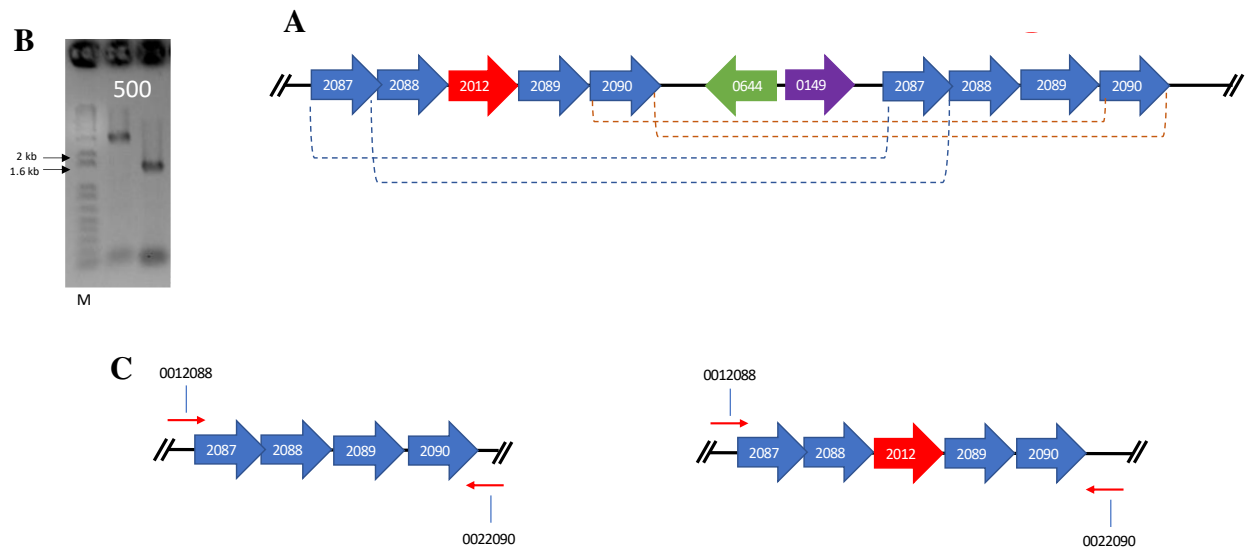


Figure 31

(A) Diagram depicting the two possible plasmid excision events within the Δ TK2012 *T. kodakarensis* transformant genome, resulting in either the restoration of the parent genotype, or the inclusion of the Tether genotype. (B) PCR results from Δ TK2012 *T. kodakarensis* transformant genome confirming the retention of the Tether genotype. (C) Diagram depicting the primer positions on the possible Δ TK2012 *T. kodakarensis* transformant genome used for PCR identification.

Figure 32

Whole genome sequencing results for the Fd3:MBH-J tether. (A) Integrative genome viewer display of gene locus for Fd3 (TK2012). The blue marking above the sequencing reads indicates a significant variance in the sample reads from the reference genome. The complete reduction in sample read coverage at this locus indicates a retention of the Fd3 deletion in the Fd3:MBH-J tether strain (Tether I). (B) Integrative genome viewer display of gene locus encoding for an Fd3:MBH-J tether. There is no indication of deviation from the sample reads to the reference genome, and read coverage is consistent in this area, indicating successful incorporation of Fd3 into the MBH locus at the desired position.

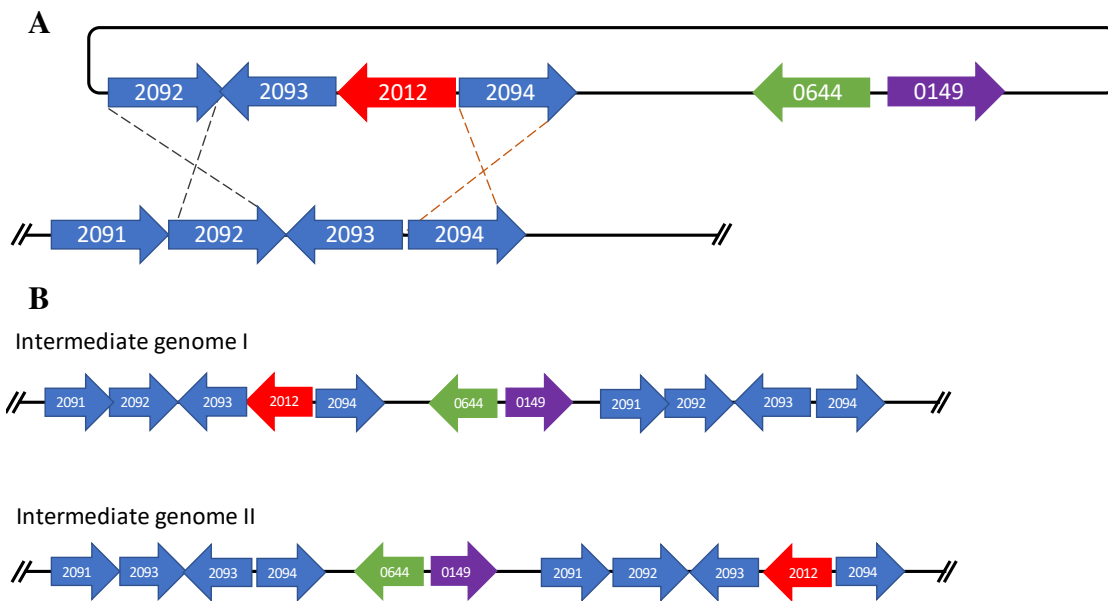


Figure 33

(A) Diagram depicting the two possible recombination events between the *Fd3:MBH-N* vector and the Δ TK2012 *T. kodakarensis* parent genome. (B) The resulting genotypes from the two recombination events.

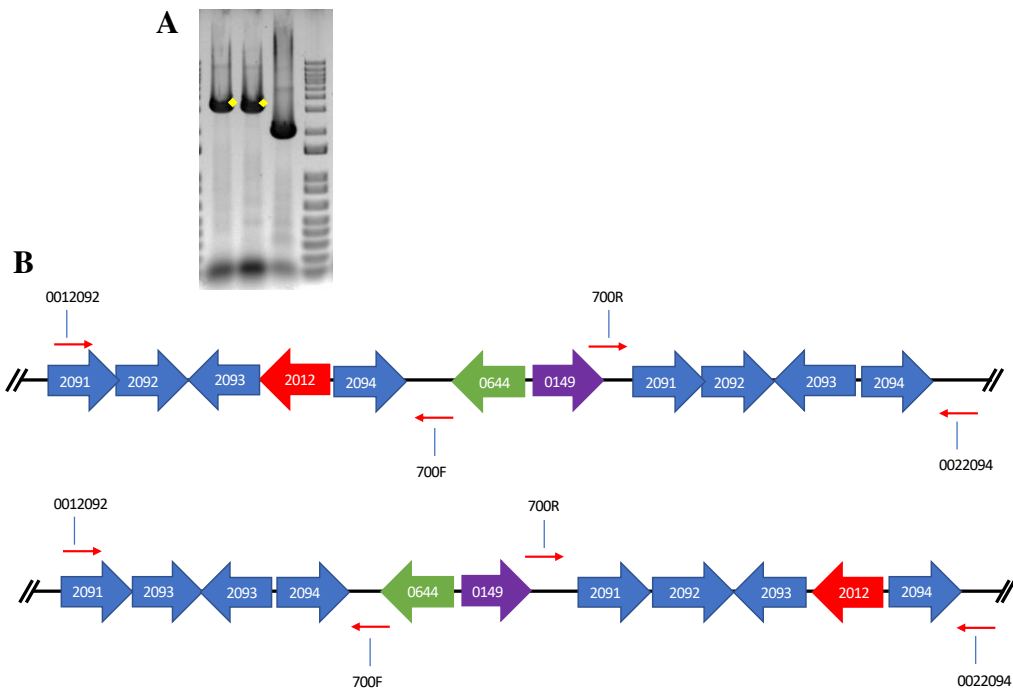


Figure 34

(A) Diagram depicting the two possible recombination events between the *Fd3:MBH-N* vector and the Δ TK2012 *T. kodakarensis* parent genome. (B) The resulting genotypes from the two recombination events.

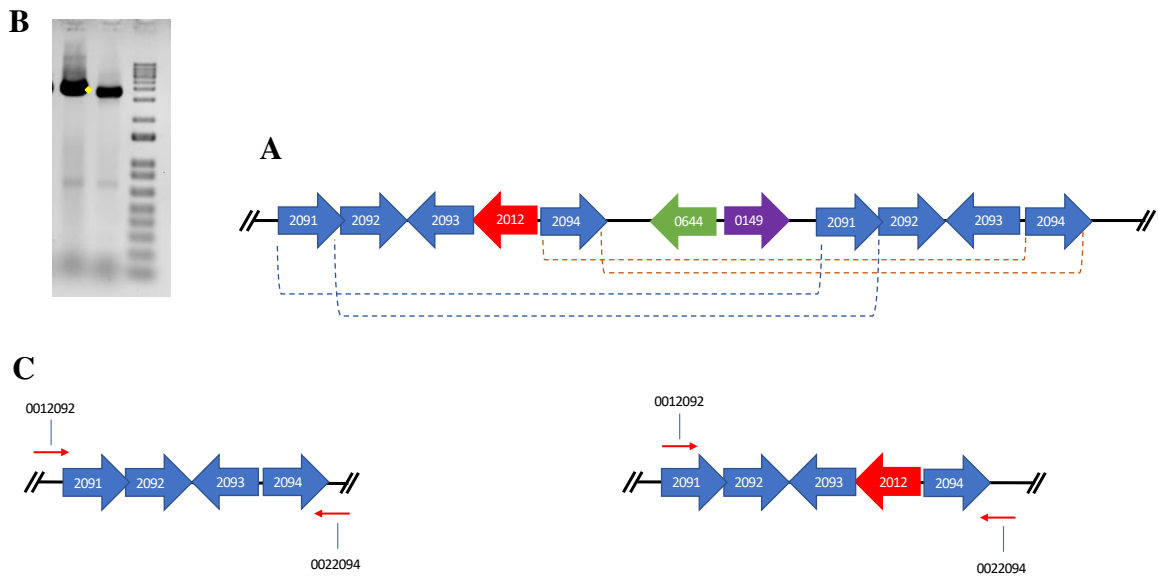


Figure 35

(A) Diagram depicting the two possible recombination events between the *Fd3:MBH-N* vector and the Δ TK2012 *T. kodakarensis* parent genome. (B) The resulting genotypes from the two recombination events.

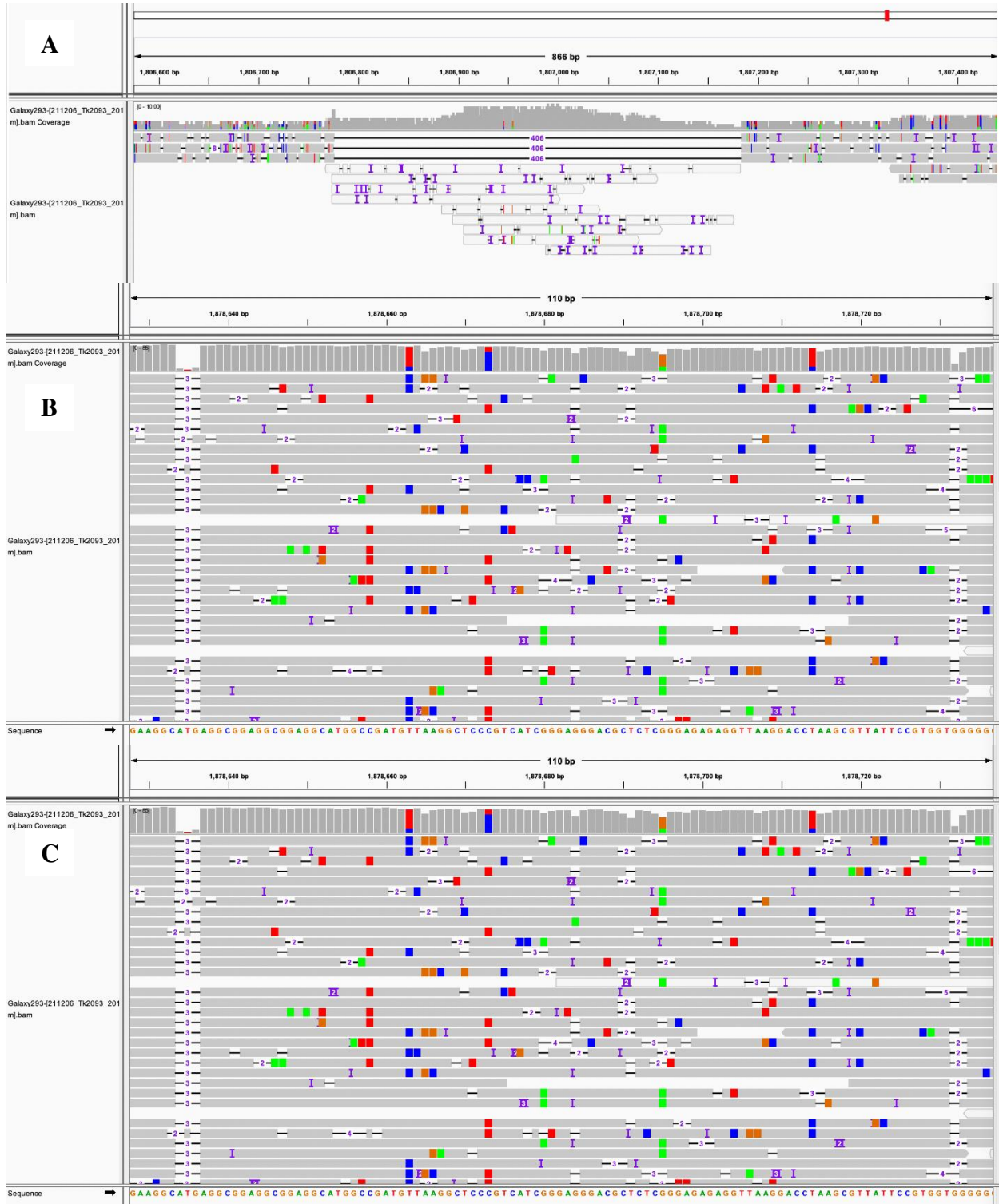


Figure 36

Whole genome sequencing of the Tether 2 strain. (A) Reads confirming retention of the deletion of Fd3 (TK2012) at its native locus. (B,C) Reads showing the inclusion of Fd3 at the desired locus, upstream of MBH-N (TK2093).

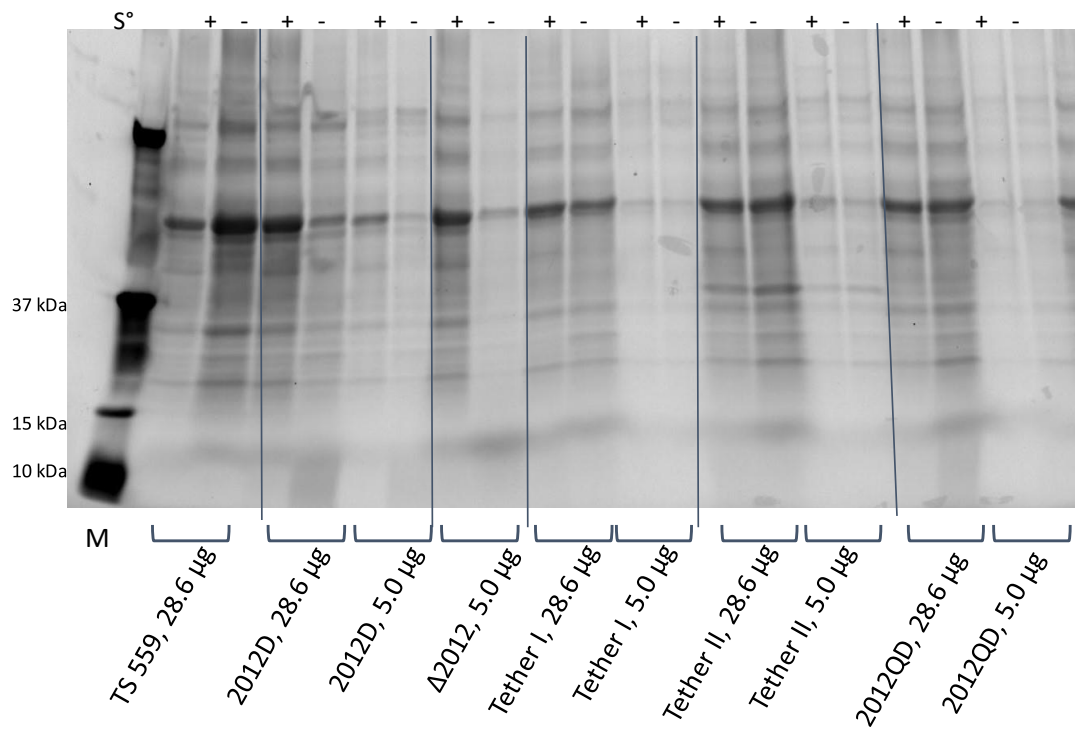


Figure 37
*SDS-PAGE of whole cell lysates for each *T. kodakarensis* strain used to characterize the Tether strains. The designated amount of protein was loaded into each lane.*

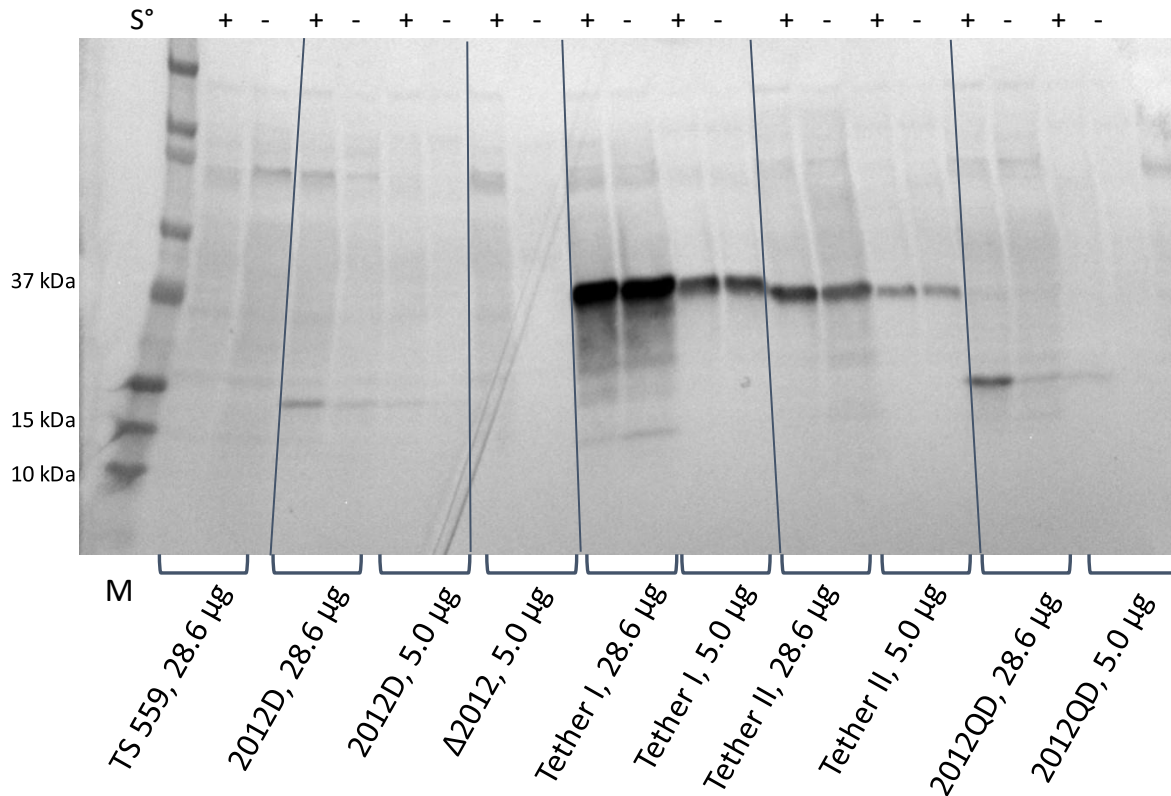


Figure 38

Western blot of the SDS-PAGE shown in **Figure 31**. TS559 does not encode an HA-tagged Fd3 and does not have a signal. The 2012D strain encodes for an N-terminal HA tagged Fd3 and has a signal at the predicted 15.6 kDa for Fd3. The Δ 2012 strain does not encode for a tagged Fd3 and has no signal. Tether I encodes for a tagged Fd3:MBH complex, and has a signal at the expected 37 kDa. Tether II encodes for a tagged Fd3:MBH complex and has a signal at the expected 35 kDa. The 2012QD strain encodes for a tagged Fd3 and has a signal at the expected 15.6 kDa. MBH is expressed at higher levels than Fd3 natively. The change in intensity of the bands relative to the 2012D strain reflects a change in expression levels of Fd3. The 2012QD strain encodes a constitutively pHmtb promoter for Fd3, increasing expression levels compared to the native Fd3 promoter.

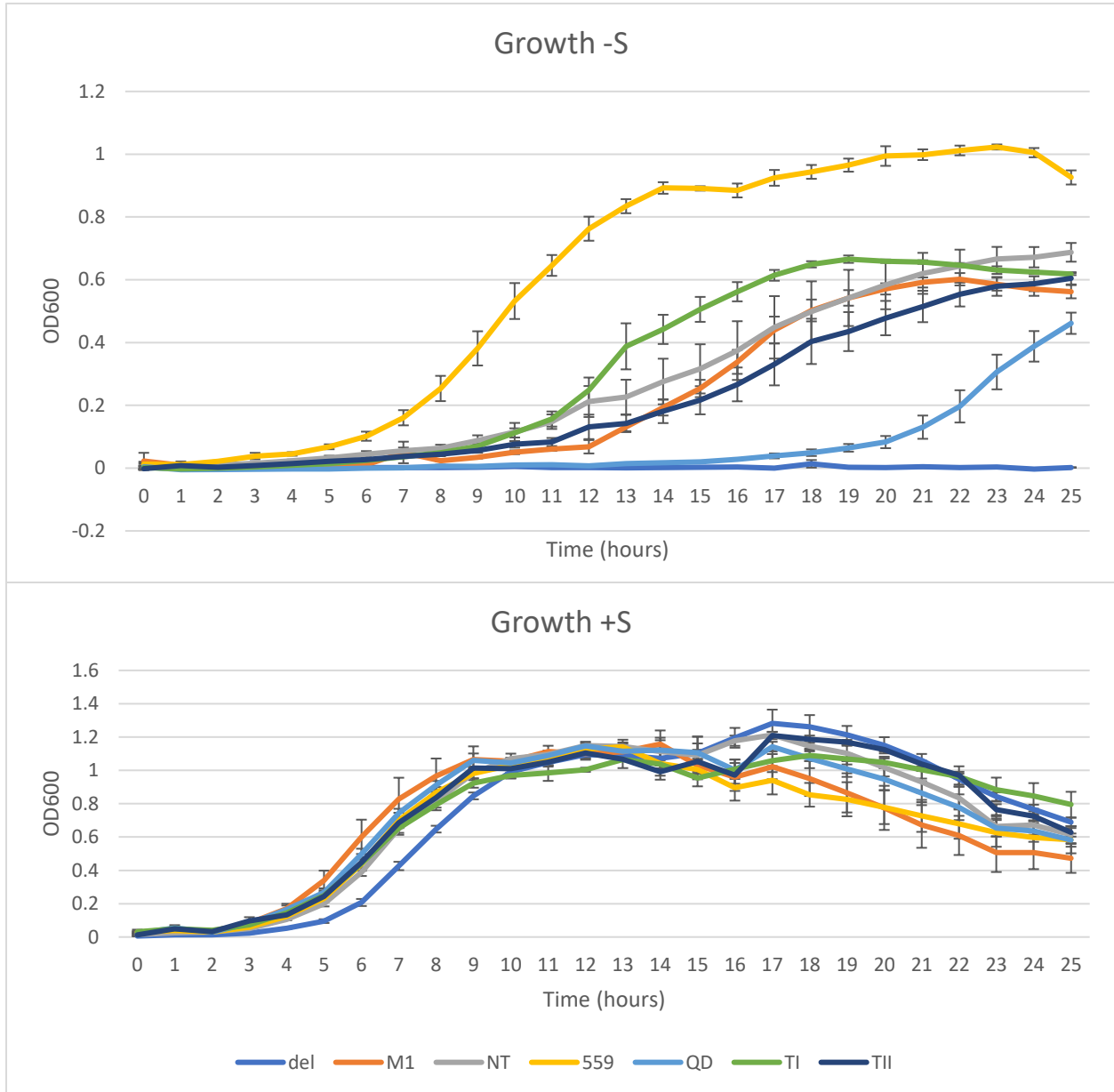


Figure 39

Growth curves for Tether I, Tether II, TS559 (Control), Δ 2012 (Control), 2012D (Control), MI (Fd3 mRNA knockdown), and 2012QD (Control). In S° -independent conditions, tethering Fd3 to MBH restores growth compared to Δ 2012, but does not achieve the same growth rate or terminal optical density compared to TS559.

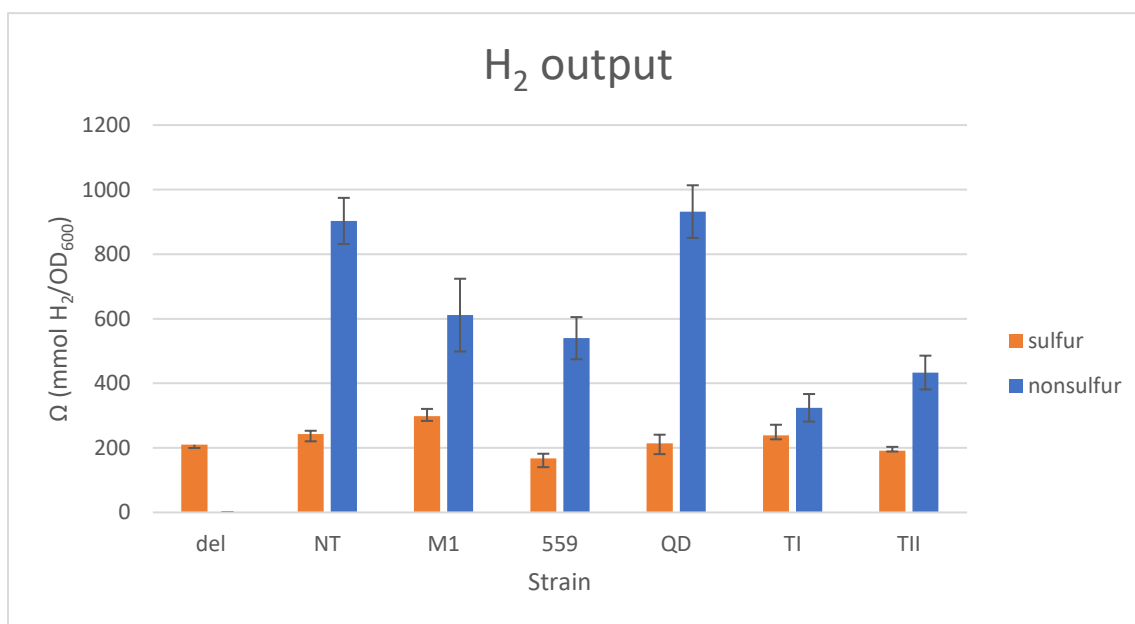


Figure 40

Measurements of hydrogen in culture headspace after 24 hours growth at 85 °C, normalized to OD₆₀₀ (Ω). Prior to incubation, culture headspace was purged using 100% nitrogen gas. In blue, cultures grown in the absence of sulfur. In orange, cultures grown in the presence of sulfur. All cultures grown in the absence of sulfur produced more hydrogen than cultures grown in the presence of sulfur. The tethering of Fd3 to MBH reduces total hydrogen output compared to TS559 and Δ2012 strains.

DISCUSSION

Fd3 plays a unique role in *T. kodakarensis*. It is nonessential in sulfur-dependent metabolism, the sole electron donor to MBH, and differs greatly from its counterparts in sequence, size, and predicted structure. Previous study showed that Fd3 (TK2012) can be deleted from the *T. kodakarensis* genome as long as the cell are maintained in a sulfur-dependent metabolic state. In my thesis, I was able to restore TK2012 to the genome, not at its original locus but in the operon of its sole electron acceptor MBH as a fusion protein and restore the sulfur-independent growth phenotype lost in the parent strain, Δ 2012.

While the structure of MBH is well known, the sterics of protein interaction between Fd3 and MBH for electron transfer remain unelucidated. Two subunits of MBH were targeted for tethering: MBH-J and MBH-N. MBH-N coordinates the Ni/Fe center used for initial electron transfer from Fd3. MBH-J is a nearby subunit that is orthogonal to MBH-N. Generating two fusion proteins allowed for a greater number of potential steric interactions, increasing the likelihood of electron transfer between Fd3 and MBH.

The tether constructs were generated using an adaptation of Quikchange PCR: rather than use a separate primer pair to amplify the insert into the vector, the insert was used as a set of large primers. This was enabled by each gblock encoding for two homologous regions on the vector, allowing for the strands of the gblock to anneal to the accompanying region on the vector and be amplified. Using this system of insertion compared to standard Quikchange requires fewer reagents and can increase efficiency by better matching the melting temperature of the vector to the oligonucleotide insertion. Ultimately, shown in **Figure 28**, the oligonucleotide was successfully included in the vector.

Strain construction in *T. kodakarensis* is based on two separate homologous recombination events, selected for using agmatine auxotrophy and 6-methylpurine (6MP) toxicity. The ultimate goal of markerless gene editing in *T. kodakarensis* is a strain that encodes for the desired modification, is an agmatine auxotroph and resistant to 6MP. The first recombination event is between the vector and the genome, leading to the inclusion of the vector into the genome at the locus of interest (**Fig. 29, 33**) based on positive selection for agmatine prototrophy (encoded by the vector). The second recombination event leads to the excision of the vector sequence and the retention of the gene modification (**Fig 31, 35**), caused by the counter selective pressure of 6MP toxicity (encoded by the vector).

This marker less gene editing technique allows for the “cleaning up” of intermediate strains when the genotype is mixed, as seen in **Figure 30**. Colonies with mixed, but potentially positive genotypes were plated as serial dilutions on minimal media containing agmatine and 6MP, motivating the second recombination event and a refinement of the genotype (**Fig. 10**). Utilization of selective and counter-selective pressures in strain constructions allows for this efficient genotype refinement without having to restart the strain construction workflow. This method was further validated by whole genome sequencing techniques used to confirm both Tether strains, showing their only substantial deviations from the parental strain being the insertion of TK2012 at the MBH locus (**Fig 32, 36**).

The genetically viable Tether strains in *T. kodakarensis* had a clear phenotype that deviated from their Δ TK2012 parent: The Tether strains were capable of growing independent of S^o in media. This suggests that sequestering Fd3 to MBH does not significantly impede the function of either of these proteins, potentially indicating that Fd3 facilitates electron tunneling between catabolic electron donor and anabolic electron acceptor. Increasing the local

concentration of Fd3 relative to MBH also opens the question: Does Fd3 play a significant role in H₂ biosynthesis?

Investigating hydrogen metabolism in *T. kodakarensis* is not revolutionary. Discussed earlier in this thesis, *T. kodakarensis* has two metabolic modes with distinct associated machinery: sulfur-dependent and sulfur-independent growth. In the presence of sulfur, *T. kodakarensis* secretes H₂S gas via MBS. In the absence of sulfur, *T. kodakarensis* secretes H₂ gas via MBH. This strict difference in metabolic by-products and machinery allows for the optimization of hydrogen gas production by the manipulation of genes associated with S⁰-independent metabolism. Previous investigations into hydrogen metabolism described the role of MBH and the A₁A₀ATPase on outgoing H₂ flux, but thus far there is no investigation on the effects of altering Fd3 levels on H₂ metabolism. Tethering Fd3 to MBH both artificially increases the local concentration of Fd3 relative to MBH and increases the overall expression of Fd3 compared to basal levels. The joint overexpression and high local concentration of Fd3 could have significant impacts on electron flux through the H₂ synthesis pathway, increasing total H₂ gas output from Tethered strains compared to the parent strain.

Hydrogen output measurements for the Tether strains indicated a decrease H₂ gas production from the tethers compared to the global parent, TS559, contradicting original predictions of the outcome of the tether strains. The constitutively overexpressed Fd3 strain (2012QD) produced more hydrogen than the parent strain, TS559, (**Fig. 40**) suggesting that overexpression of Fd3 does not cause catastrophic stress on hydrogen biosynthesis in *T. kodakarensis*. Instead, the decrease in output from the Tether strains must be associated with the physical tethering of Fd3 to MBH.

The steric interaction between Fd3 and MBH-N for electron transfer is uncharacterized; tethering Fd3 to MBH with a short, 5-glycine linker domain may impede effective contact and transfer. Additionally, data from Chapter 2 suggests that Fd3 is not reductive enough on its own to pass electrons to MBH to reduce H^+ , indicating there may be an additional factor that aids in electron transfer between MBH and Fd3. The short linker between Fd3 and MBH in the tether strains may interfere with the interaction between this potential additional factor and either Fd3 or MBH, reducing overall electron flux through MBH, reducing hydrogen output.

MATERIALS AND METHODS

Luria-Bertani (LB) Media (x1 L)

Per 1 L: 10.0 g Tryptone, 5.0 g Bacteriological Yeast Extract, 5.0 g NaCl, 1 L double-distilled water. Add dry ingredients to 900 mL of ddH₂O, mix until fully dissolved. Add ddH₂O to final 1 L volume. Autoclave liquid cycle 20 minutes.

LB Solid Media

Per 1 L: 10.0 g Tryptone, 5.0 g Bacteriological Yeast Extract, 5.0 g NaCl, 5.0 g Agar, 1 L ddH₂O. Add dry ingredients to 900 mL ddH₂O, mix until fully dissolved. Add ddH₂O to final 1 L volume. Autoclave in 2 L Erlenmeyer flask, liquid cycle 20 minutes. After autoclaving, cool media to 45°C while stirring, add selective agents. Aliquot media into sterile plastic petri plates (approx. 25 mL/plate) under flame. Allow media to cool and solidify, invert plates and store at 4°C.

2x Artificial Sea Water (2xASW)

Per 1 L: 40.0 g NaCl, 6.0 g MgCl₂·6H₂O, 12.0 g MgSO₄·7H₂O, 2.0 g NH₄SO₄, 0.4 g NaHCO₃, 0.6 g CaCl₂·2H₂O, 1.0 g KCl, 0.84 g KH₂PO₄, 100 mg NaBr, 40 mg SrCl₂·6H₂O, 20 mg Fe(NH₄)₂(SO₄)₃·6H₂O, 1 L ddH₂O. Mix powder ingredients together, then add to 900 mL ddH₂O in a large erlenmyer flask and mix until fully dissolved. Add ddH₂O to final volume.

Artificial Sea Water-Yeast/Tryptone-Pyruvate (ASW-YT-P)

Per 1 L: 20.0 g NaCl, 6.0 g MgSO₄·7H₂O, 3.0 g MgCl₂·6H₂O, 5.0 g Bacteriological Yeast Extract, 5.0 g Tryptone, 1.0 g NH₄SO₄, 0.2 g NaHCO₃, 0.3 g CaCl₂·2H₂O, 0.5 g KCl, 0.42 g KH₂PO₄, 50 mg NaBr, 20 mg SrCl₂·6H₂O, 10 mg Fe(NH₄)₂(SO₄)₃·6H₂O, 5.0 mL Wolfe's Trace Minerals, 1 L boiled ddH₂O, 5.0 g C₃H₃NaO₃ (optional: ASW-YT-P). Mix powder ingredients

together. In anaerobic chamber, mix powder ingredients with 900 mL boiled ddH₂O. Add ddH₂O to final volume. Aliquot into sealable serum bottles, then autoclave bottles containing media Liquid Cycle for 20 min sterilization time.

***T. kodakarensis* Solid Media**

Rich Plates: In 1, 100 mL serum bottle: 50 mL 2x ASW, 500 µL Wolfe's Trace Minerals, 0.5 g Bacteriological Yeast Extract, 0.5 g Tryptone. In 1, 100 mL serum bottle: 50 ml M18Ω H₂O, 1.0 g Gelzan. Seal each bottle separately, autoclave Liquid cycle 20 min.

Additives: In 1, 1.7 mL Eppendorf microcentrifuge tube: 200 µL 1 M Polysulfide Solution, 100 µL KOD vitamins, 100 µL 1.0 M Agm-SO₄ (for genetic finals). In the anaerobic chamber, pipette additives into serum bottle containing the 2xASW mixture. Swirl to mix, then pour 2xASW bottle into the serum bottle containing gelzan. Briefly swirl to mix, then pour into 4 glass petri plates. Allow to cool before use with cells.

Liquid Culture: For 100 mL: 100 mL ASW-YT or ASW-YT-P (aliquoted and sterilized from bulk batch), 0.2 g S°, 100 µL 1.0 M Agm-SO₄ (for genetic finals). In the anaerobic chamber, add S° and Agm-SO₄ to ASW-YT/P in 100 mL serum bottle. The bottle is then ready for inoculation using a liquid starter or from a colony scraped from a plate.

KOD Vitamin Mix

Per 1 L: 0.2 g niacin, 0.08 g biotin, 0.2 g pantothenate, 0.2 g lipoic acid, 0.08 g folic acid, 0.2 g P-aminobenzoic acid, 0.2 g thiamine, 0.2 g riboflavin, 0.2 g pyridoxine, 0.2 g cobalamin. Note: This solution is light sensitive and should be protected. Mix powder ingredients, then add to 900 mL double-distilled water, adjust volume to 1 L.

Wolfe's Trace Minerals

Per 1 L: 0.5 g $\text{MnO}_4\text{SO}_4 \cdot \text{H}_2\text{O}$, 0.1 g $\text{CoCl}_2 \cdot 6\text{H}_2\text{O}$, 0.1 g $\text{ZnSO}_4 \cdot 7\text{H}_2\text{O}$, 0.01 g $\text{CuSO}_4 \cdot 5\text{H}_2\text{O}$, 0.01 g $\text{AlK}(\text{SO}_4)_2 \cdot 12\text{H}_2\text{O}$, 0.01 g H_3BO_4 , 0.01 g $\text{Na}_2\text{MoO}_4 \cdot 2\text{H}_2\text{O}$, ~900 mL double-distilled water, Mix powder ingredients together, then add to water in 1 L bottle. Mix until fully dissolved, then autoclave liquid cycle for 20 minute sterilization.

Transformation of *T. kodakarensis*

100 mL of anaerobic ASW-YT-S+ was inoculated with 1 mL of fresh liquid culture in the anaerobic chamber. 100 mL culture was then grown overnight (12-13hrs) in a 85°C water bath. After growth, the culture was transferred to sterile centrifuge tubes in the anaerobic chamber, and then centrifuged at 9605 xg for 10 min at 4°C. After spinning, supernatant was decanted and discarded, the remaining cell pellet was resuspended in 3 mL sterile 0.8xASW. Cell suspension was then divided into 3, 1.7 mL Eppendorf microcentrifuge tubes, and incubated on ice for 30 min. After incubation, 200 µL of cell suspension was added to 1-3 µg of plasmid prepared from *E.coli*. The mixture was then incubated on ice for 1 h, then heat shocked at 85°C for 45 s, incubated on ice for another 5 min, then spread onto 2, rich media plates in a 10%/90% division. Plates were then placed in an anaerobic cylinder with a gas capture packet, the cylinder sealed, and the plates incubated at 85°C for 2-3 days or until growth occurred. After successful growth, transformant colonies were picked from solid media, resuspended in 10 µL sterile 0.8xASW and spotted onto plates containing selective media (+/- Agm) using a 1:10 dilution for 5 spots. Spot plates were then incubated at 85°C in an anaerobic cylinder with a gas capture packet for 3-5 days.

Preparation of *T. kodakarensis* low-quality genomic DNA

1 mL of liquid culture was harvested at 20,000 xg for 5 min. Supernatant was snapped out of tube, the tube spun 30 s at 20,000 xg, and remaining supernatant removed using a pipette. Cell pellet was resuspended in 100 μ L, 10 mM Tris HCl pH 8.0, 50 μ L Phenol/Chloroform/Isoamyl Alcohol (PCI) 25:24:1 (v:v:v) was added to the suspension and mixed by pipetting. Mixture was then spun at 20,000 xg for 10 min. 50 μ L of top aqueous layer of spun contents were added to 50 μ L of 10 mM Tris HCl pH 8.0 in a new Eppendorf tube and mixed by pipetting. 100 μ L of 100% isopropanol was added to the mixture, which was then centrifuged at 20,000 xg for 30 min. After centrifugation, supernatant was carefully removed by pipetting, and resultant DNA pellet dried at 37°C for 30 min. Once dried, the DNA pellet was reconstituted in 30 μ L of 10 mM Tris HCl pH 8.0, and stored at -20°C for later use.

Preparation of *T. kodakarensis* high-quality genomic DNA

100 mL of liquid culture was divided into two 50 mL conicals and pelleted at 3220 xg for 25 min. Supernatant was decanted and pellet resuspended in 2 mL of 2.0 mM Tris HCl pH 8.0, 5 mM EDTA, 10% sucrose. The resuspension was divided equally between 4, 1.7 mL Eppendorf tubes (~500 μ L each). 110 μ L of 10% SDS was added to each tube, then the tube was vortexed for 30 s. Next, 20 μ L of 100 mg/mL Proteinase K was added to the tubes, the tubes vortexed 10 s, and then incubated at 55-60°C for 1 hr on a dry bath. The tubes were inversion mixed every 20 min during this incubation. Afterwards, 120 μ L of 5M NaCl was added to each tube, and then shake-mixed by hand. The mixture was then incubated on ice for at least 10 min, then spun at 20,000 xg for 10 min at 4°C. Supernatant was transferred to a new 1.7 mL Eppendorf tube, and an equal volume of 100% isopropanol was added to the tube. The tubes were then spun at 20,000 xg for 30 min at 4°C. The supernatant was carefully decanted from the tubes, the tubes spun

again at 20,000 xg for 30 s at 4°C and the supernatant carefully decanted again. The remaining pellet was dried at 40°C for 10 min on a dry bath. 125 µL of 10 mM Tris HCl pH 8.0 was added to each tube and the pellet gently resuspended, along with 2 µL of RNase A. The mixture was incubated at 37°C for 1 hr on a dry bath. Each tube was then combined into a single 1.7 mL Eppendorf tube, then 200 µL of 24:25:1 phenol/chloroform/isoamyl alcohol was added and mixed by hand shaking. The tube was spun at 20,000 xg for 10 min. The top clear aqueous layer was removed to a new 1.7 mL Eppendorf tube. A 0.1x volume (~20 µL) of 3 M NaOAc pH 5.2 was added to the tubes, then a 0.7x volume (~154 µL) of 100% isopropanol was added and mixed via pipette. The tube was spun at 20,000 xg for 30 min at 4°C. The supernatant was carefully decanted, the tube spun again at 20,000 xg for 30 s at 4°C, and the supernatant carefully decanted again. The remaining pellet was dried at 40°C on a dry bath for 30 min. The dry pellet was resuspended in 30 µL of 10 mM Tris HCl pH 8.0, incubated at 37°C on a dry bath for at least 20 min, pipette mixed, and then quantified via fluorometry.

Diagnostic PCR

For a total reaction volume of 50 µL per sample: 1U of Phusion DNAP, 200 µM of dNTPS, 1X HF buffer (NEB), 0.5 µM forward and reverse primers, and ~250 ng of gDNA and amplified using the PCR protocol of 98°C for min, and the 35 cycles of 98°C for 10 s, 60°C for 30 s, 72°C for 30 s/kb. The samples were then run on a 1% agarose gel using gel electrophoresis at 120V for 35 min in 1X TBE (89 mM Tris, 89 mM boric acid, 2 mM EDTA), stained for 10 min in 0.5 µg/mL ethidium bromide and imaged.

Use of MinION “Tagmentation” kit for whole-genome sequencingThe library prep for whole genome sequencing was prepared with high-quality genomic DNA isolated from *T. kodakarensis* according to Oxford Nanopore guidelines.

Whole genome sequencing data analysis pipeline

Whole genome sequencing data analysis was completed using native MinIon alignment functions, as well as the open-source analysis tools available on Galaxy. Alignment files generated by the MinIon were uploaded to Galaxy and merged using SamTools Merge. Next, the merged sequencing file was run through the Medaka Variant Pipeline. The resultant .bam, .bai, and .vcf files along with the accompanying reference genome were uploaded to the Integrative Genome Viewer for final analysis.

Construction of pTS700-Tether constructs

The pTS700-Tether constructs were made using synthesized oligonucleotides encoding for the partial upstream sequence from either Tk2089 (Tether I) or Tk2093 (Tether II), the entire TK2012 sequence and associated N- or C-terminal (Tether II/Tether I) HA/6xHis tag, and partial downstream sequence from either TK089/MBH-J (Tether I) or TK2093/MBH-N (Tether II). These oligonucleotides were used as Quikchange PCR primers in a Quikchange PCR reaction with pTS700-TK2089A (Tether I) or pTS700-TK2093A (Tether II), according to Agilent Quikchange PCR protocol. The constructed plasmid was transformed into Stellar cells which were then plated onto solid LB+Amp media and incubated at 37°C for 12 hrs. Colonies from this plate were resuspended in ddH₂O and then diluted 1:10 in ddH₂O and spotted onto solid LB+Amp media and incubated at 37°C for 12 hrs.

Colony PCR

Colonies from spot plates were picked and vigorously resuspended in 10 uL ddH₂O. The following master mix was added to the cell lysate: For a total reaction volume of 50 µL per sample: 1U of Phusion DNAP, 200 µM of dNTPS, 1X HF buffer (NEB), 0.5 µM forward and reverse primers, and ~250 ng of gDNA and amplified using the PCR protocol of 98°C for min,

and the 35 cycles of 98°C for 10 s, 60°C for 30 s, 72°C for 30 s/kb. The samples were then run on a 1% agarose gel using gel electrophoresis at 120V for 35 min in 1X TBE (89 mM Tris, 89 mM boric acid, 2 mM EDTA), stained for 10 min in 0.5 µg/mL ethidium bromide and imaged.

Transformation of *E. coli* cells

100 µL of BL-21 competent *E. coli* cells were thawed on ice for 20 min, and 2 µL of ~100 µg/mL pQE-80L-Fd1/Fd2/Fd3 plasmid was added to the cells. The cells incubated on ice for 30 min, heat shocked at 42°C for 45 s, and then rested on ice for 5 min. Using a P1000, cells were dispensed via pipetting and then spread onto LB/amp (100 µg /mL) plates and incubated overnight at 37°C.

Isolation of plasmid DNA from *E. coli* cells (All buffers from Zymogen Plasmid Miniprep kit)

10 mL of liquid culture was spun down in 1.7 mL increments in 2, 1.7 mL Eppendorf tubes at 20,000 xg for 5 min. Supernatant was snapped out of tubes. The remaining pellet was resuspended in 200 µL P1 buffer and vortexed 30 s. 200 µL of P2 buffer was added, the tubes vortexed for 5 s, shaken vigorously, then incubated at room temperature for 1-2 min. 400 µL of P3 buffer was added and mixed via pipette until the solution was opaque and yellow. The tubes were spun at 20,000 xg for 7 min. The supernatant was transferred to a plasmid prep column in a collection tube. The columns were spun at 20,000 xg for 30 s. 400 µL of Plasmid Wash Buffer was added to the columns, which were then spun at 20,000 xg for 1 min. The flowthrough was discarded, then the columns were dried by spinning at 20,000 xg for 1 min. The columns were then transferred to 1.7 mL Eppendorf tubes. 16 µL of 10 mM Tris HCl pH 8.0 was added to the column and incubated for 5 min at room temperature before being spun at 20,000 xg for 1 min.

The previous step was repeated for a final flowthrough volume of 32 μ L. The isolated plasmid was then quantitated via fluorometry.

Western blotting for tether strain confirmation

100 mL cultures of TS559, Δ 2012, 2012D, Tether I, and Tether II were grown to an OD₆₀₀ ~0.3. Cultures were harvested at 10,000 xg for 15 min at 4°C. Cell pellets were resuspended in 3 mL of 10 mM Tris HCl pH 8.0, 1% SDS, 10% glycerol (Lysis Buffer) and transferred to a 15 mL plastic conical. Tubes were then frozen at -20°C for 1 hr. Frozen tubes were thawed at 85°C for 5-10 min, then quantitated for protein content via Qubit Protein Assay. Equal protein contents of cell lysates (28.6 μ g/5 μ g) were loaded into a 4-20% polyacrylamide stain-free gel (Criterion) and resolved at 170 V for 35 min. Resolved protein was transferred onto PVDF turboblot membrane (Criterion), and blocked for 2 hrs at room temperature with 5% non-fat dry milk (Blocking agent). The blocking agent was drained off the membrane, and the membrane washed twice quickly with ddH₂O. A 1:5000 dilution of anti-HA mouse antibody in 1x TBST was added to the membrane and incubated overnight with rocking at 4°C. Membrane was then washed 3 times in 1x TBST, rocking at room temperature in 10 min intervals. A 1:2000 dilution of anti-mouse goat antibody in 1x TBST was added to the membrane and incubated 2 hrs at room temperature on a rocker. The membrane was washed 2 times in alkaline phosphatase wash buffer, rocking at room temperature in 15 minute increments. The membrane was drained, and 2 mL of NBT/BCIP (Thermo) was added to the membrane and was allowed to develop for 5-10 minutes.

Gas chromatography for H₂ gas detection:

H₂ headspace measurements were conducted on a Hewlett-Packard 5890 Series 2 gas chromatograph using argon as carrier gas at 20 psi through an Alltech Hayesep Q 80/100 (8' x

1/8" x 0.85" SS) and thermal conductivity detector. Inlet temperature 110 °C; detector temperature 110 °C; oven temperature 40 °C. A standard curve of 50 µL to 500 µL of 100% H₂ gas in triplicate injections was used to calibrate the instrument. Culture headspaces were sampled in 250 µL single replicate injections from biological triplicate cultures. Data was collected using ChemStation software. Culturing techniques were identical to those used in the growth curve assay, with the exception that only final OD₆₀₀ was taken at 24 hours growth.

Data processing for gas chromatography

Raw data for H₂ headspace measurements was collected as area counts as reported by ChemStation. The area counts were averaged for each injection. A standard curve of 50 µL to 500 µL of 100% H₂ gas in triplicate injections was used to calibrate the instrument. The calculations for mmol H₂ gas were as follows:

$$x \text{ } \mu\text{L Hydrogen} \times \frac{0.08375 \text{ g}}{\mu\text{L Hydrogen}} \times \frac{\text{mol Hydrogen}}{2.016 \text{ g Hydrogen}} \times \frac{1000 \text{ mmol}}{1 \text{ mol}} = \text{mmoles Hydrogen injected}$$

The mmol quantities of each injection were averaged, then plotted as a function of the corresponding averaged area count. The data was fit to a linear equation, which was used to calculate total mmol output of the tested cultures.

Growth curve assays:

In the anaerobic chamber, 10 mL each of ASW-YT was pipetted into 60, 20 mL glass serum tubes, capped with virgin (previously unused) 20 mm rubber stoppers and sealed with 20 mm aluminum caps. The sealed tubes were then autoclaved for a liquid cycle, 20 minutes. In the anaerobic chamber, in sets of 4, the sterile tubes were opened using a decapper, 1 mM Agmatine sulfate was added to each tube, followed by 100 µL of the starter culture (Δ TK2012, TS 559, Tether1, Tether 2, TK2012D, TK2012QD, or TK2012M1). The tubes were then recapped with new, sterile virgin stoppers and sealed with aluminum caps. The inoculated tubes were placed

into an 85 °C water bath and cell density in each tube was measured at 600 nm once an hour for 25 hours.

Table 8: List of *T. kodakarensis* Strains

Name	Description
TS559 ⁸	<i>T. kodakarensis</i> strain encoding ΔTk2276; Tk0254::2276 ΔTk0149; ΔTk0664 Parental strain
Δ2012 ⁷	<i>T. kodakarensis</i> strain encoding ΔTk2276; Tk0254::2276 ΔTk0149; ΔTk0664; ΔTk2012 Strain lacking native Fd3 locus
Tether I	<i>T. kodakarensis</i> strain encoding ΔTk2276; Tk0254::2276 ΔTk0149; ΔTk0664; ΔTk2012; Tk2012::2089 Strain encoding tethered Fd3 to MBH-J
Tether II	<i>T. kodakarensis</i> strain encoding ΔTk2276; Tk0254::2276 ΔTk0149; ΔTk0664; ΔTk2012; Tk2093::2012 Strain encoding tethered Fd3 to MBH-N
2012D	<i>T. kodakarensis</i> strain encoding ΔTk2276; Tk0254::2276 ΔTk0149; ΔTk0664; 6xHis-HATk2012 Strain encoding an N-Terminally tagged 6xHis-HA Fd3
2012QD	<i>T. kodakarensis</i> strain encoding ΔTk2276; Tk0254::2276 ΔTk0149; ΔTk0664; pHmtb 6xHis-HATk2012 Strain encoding a constitutively overexpressed N-terminally tagged 6xHis-HA Fd3

Table 9: List of Primers used in pTS700¹⁰ Vector Construction

Name	Sequence (5'-3')	Description
700F ⁹	CGCCGCAATAGCGGTCGTCGTCATGTTCC C	Primer encoding for upstream region of

		pTS700 multiple cloning site
700R ⁹	AACAATTTACACAGGAAACAGCTATGACC	Primer encoding for downstream region of pTS700 multiple cloning site
2012:2089 gblock	GCTCAGGAGAGACCACACAGGCCTGCTC ACTGACTACGCGAGCTACCTGGTGATAA CGACGGCCTTCGTGCTGGGGGTGCTGCTG ATATGGGGATGAAGGGTTTTCCGCGAGA GCTCTGCCGAGGTGGTAGCTGATGCATC ACCATCACCATCACTACCCATACGACGTT CCGGACTACGCAGCCGATGTAAAGGCTC CCGTCATCGGGAGGGACGCTCTCGGGAG AGAGGTTAAGGACCTAAGCGTTATTCCG TGGTGGGGGGTTGATAGAAAGGAGATAG AGTGGTATCCAAAGATAAACTACAGCGT CTGCGCCCGCTGTGGCCTTTGCTTTATAA CCTGTGGACGGAGGGTCTTCGACTGGGA CACCGAAGAGGGAAAGCCCGTTGTTGCG AGGCCCTACAACCTGCATGGTTGGTTGCA ACACTTGTGCAATCCTCTGCCCATGTAAC GCCATAGAGTTCCACCAAAGGAGTACG TTAAGAAGCTCGTCATAGAGCACGGGAT CATAAGAAAGGCCTTTGAGATAACAAAG CCCCTGACGAAAAAGAAGGAAGAAAGC ACGAACGGAGCTGAGAGCGTGTTCAATC CTGGCGGAGGCGGAGGCATGGCGATAAC AGTTCCCGCCAACCAAAACGGGCAGAAA TCAAATCCATCGGAGCGCGAGAGGCTCG AAAAGAGAATAGCCCAGCTCTGCAGGTT CCTTGGAAGTCGCCCTGGGTATTCCACG TAAACAGCGGC	Synthesized oligonucleotide encoding for 154 bp upstream sequence from Tk2089, Tk2012 in entirety, a HA/6xHis tag, and 154 Tk2089
2093:2012 gblock	CCACGACGACAGGTTTATCCCTCTGAAGC CTGAAAAAGTCGAGGAGATAAAGAGGA AGCTGGAAGAGCAGAAGAAGGCCAAAG AGGCCGCGAAGAAGGAGAAGGAAGGGA AGGCAGGCCGAGGCGGAGGCATGGCCG ATGTAAAGGCTCCCGTCATCGGGAGGGA CGCTCTCGGGAGAGAGGTTAAGGACCTA AGCGTTATTCCGTGGTGGGGGGTTGATA GAAAGGAGATAGAGTGGTATCCAAAGAT AAACTACAGCGTCTGCGCCCGCTGTGGC CTTTGCTTTATAACCTGTGGACGGAGGGT CTTCGACTGGGACACCGAAGAGGGAAAG	Synthesized oligonucleotide encoding for 154 bp of Tk2093, a HA/6xHis tag, Tk2012 in entirety, and 154 downstream sequence from Tk2093

	<pre> CCCGTTGTTGCGAGGCCCTACAACCTGCAT GGTTGGTTGCAACACTTGTGCAATCCTCT GCCCATGTAACGCCATAGAGTTCCCACC AAAGGAGTACGTTAAGAAGCTCGTCATA GAGCACGGGATCATAAGAAAGGCCTTTG AGATAACAAAGCCCCTGACGAAAAAGAA GGAAGAAAGCACGAACGGAGCTGAGAG CGTGTTCAATCCTTACCCATACGACGTTT CGGACTACGCACATCACCATCACCATCA CTGATTACGCCGTCACCTTTACTTTTATTC CATACTGTTCAACGCTGAAGCCCATGAG CTCAGCCTCGCCCTTGAGCCTCTGGTAAT GGGCCCACTCTACGTTGGCAAGGTATTG GTAGACCTTTCTGGCCTCCTCGTTCTCCG TTATTGAGGCG </pre>	
--	---	--

Table 10: List of Primers used in Tether I Strain Construction

Name	Sequence (5'-3')	Description
700FMPB	GTTGCAAGCGCCGAGATAACCGTCAAGGA	Primer encoding for upstream region of pTS700 multiple cloning site, sequence-adjusted to bring melting temp closer to other primers
700RMPB	GGCTCGTATGTTGTGTGGAATTGTGAGCGG	Primer encoding for downstream region of pTS700 multiple cloning site, sequence-adjusted to bring melting temp

		closer to other primers
0012088	ATCATAATCTTCGCCTGCATAACC	Upstream primer from Tk2089
0022090	GGAGAATGAGTGAAGCTAATCCCAT	Downstream primer from Tk2089
001036	AACGGTACAACGTACATCTACAGC	Forward primer for control gene
0020036	GGTGA ACTCTTACGACGTTGTGATA	Reverse primer for control gene
0022088	GGAGAATGAGTGAAGCTAATCCCAT	Internal primer to Tk2089
0022009	GCTGTAGTTTATCTTTGGATAACCAC	Internal primer to Tk2012

Table 11: List of Primers used in Tether II Strain Construction

Name	Sequence (5'-3')	Description
700FMPB	GTTGCAAGCGCCGAGATAAACCGTCAAGGA	Primer encoding for upstream region of pTS700 multiple cloning site, sequence-adjusted to bring melting temp closer to other primers
700RMPB	GGCTCGTATGTTGTGTGGAATTGTGAGCGG	Primer encoding for downstream region of pTS700 multiple cloning site, sequence-adjusted to bring melting temp

		closer to other primers
0012092	TTTCAGGGACACAGCAGTGATAAGC	Upstream primer from Tk2093
0022095	GGTGTAGTCTGGATCACTCAGATT	Downstream primer from Tk2093
0010036	AACGGTACAACGTACATCTACAGC	Forward primer for control gene
0020036	GGTGAACTCTTACGACGTTGTGATA	Reverse primer for control gene
0022093	CGTGAGATAAACCCCTTTTGAGCTC	Internal primer to Tk2093
0012013	CTTTCTTCCTTCTTTTTCGTCAGG	Internal primer to Tk2012
0012095	GAAAAAGTCGAGGAGATAAAGAGG	Internal primer to Tk2093

REFERENCES

1. Aslam, M., Horiuchi, A., Simons, J. & Jha, S. Engineering of the Hyperthermophilic Archaeon *Thermococcus kodakarensis* for. *Applied and Environmental Microbiology* **83**, 1–16 (2017).
2. De Vos, W. M., Kengen, S. W. M., Voorhorst, W. G. B. & Van der Oost, J. Sugar utilization and its control in hyperthermophiles. *Extremophiles* **2**, 201–205 (1998).
3. Matsubara, K., Yokooji, Y., Atomi, H. & Imanaka, T. Biochemical and genetic characterization of the three metabolic routes in *Thermococcus kodakarensis* linking glyceraldehyde 3-phosphate and 3-phosphoglycerate. *Molecular Microbiology* **81**, 1300–1312 (2011).
4. Simons, J. R., Beppu, H., Imanaka, T., Kanai, T. & Atomi, H. Effects of high-level expression of A1-ATPase on H₂ production in *Thermococcus kodakarensis*. *Journal of Bioscience and Bioengineering* **130**, 149–158 (2020).
5. Kanai, T. *et al.* Overproduction of the membrane-bound [NiFe]-hydrogenase in *Thermococcus kodakarensis* and its effect on hydrogen production. *Frontiers in Microbiology* **6**, 1–11 (2015).
6. Hallenbeck, P. C. Fermentative hydrogen production: Principles, progress, and prognosis. *International Journal of Hydrogen Energy* **34**, 7379–7389 (2009).
7. Schut, G. J., Boyd, E. S., Peters, J. W. & Adams, M. W. W. The modular respiratory complexes involved in hydrogen and sulfur metabolism by heterotrophic hyperthermophilic archaea and their evolutionary implications. *FEMS Microbiology Reviews* **37**, 182–203 (2013).

8. Burkhart, B. W., Febvre, H. P. & Santangelo, T. J. Distinct physiological roles of the three ferredoxins encoded in the hyperthermophilic archaeon *thermococcus kodakarensis*. *mBio* **10**, 1-17 (2019).
9. Santangelo, T. J., Čuboňová, L. & Reeve, J. N. Deletion of alternative pathways for reductant recycling in *Thermococcus kodakarensis* increases hydrogen production. *Molecular Microbiology* **81**, 897–911 (2011).
10. Fukui, T. *et al.* Complete genome sequence of the hyperthermophilic archaeon *Thermococcus kodakaraensis* KOD1 and comparison with *Pyrococcus* genomes. *Genome Research* **15**, 352–363 (2005).
11. Atomi, H., Sato, T. & Kanai, T. Application of hyperthermophiles and their enzymes. *Current opinion in biotechnology* **22**, 618–26 (2011).
12. Straub, C. T. *et al.* Biotechnology of extremely thermophilic archaea. *FEMS Microbiology Reviews* **42**, 543–578 (2018).
13. Yu, H. *et al.* Structure of an Ancient Respiratory System. *Cell* **173**, 1636-1649 (2018).